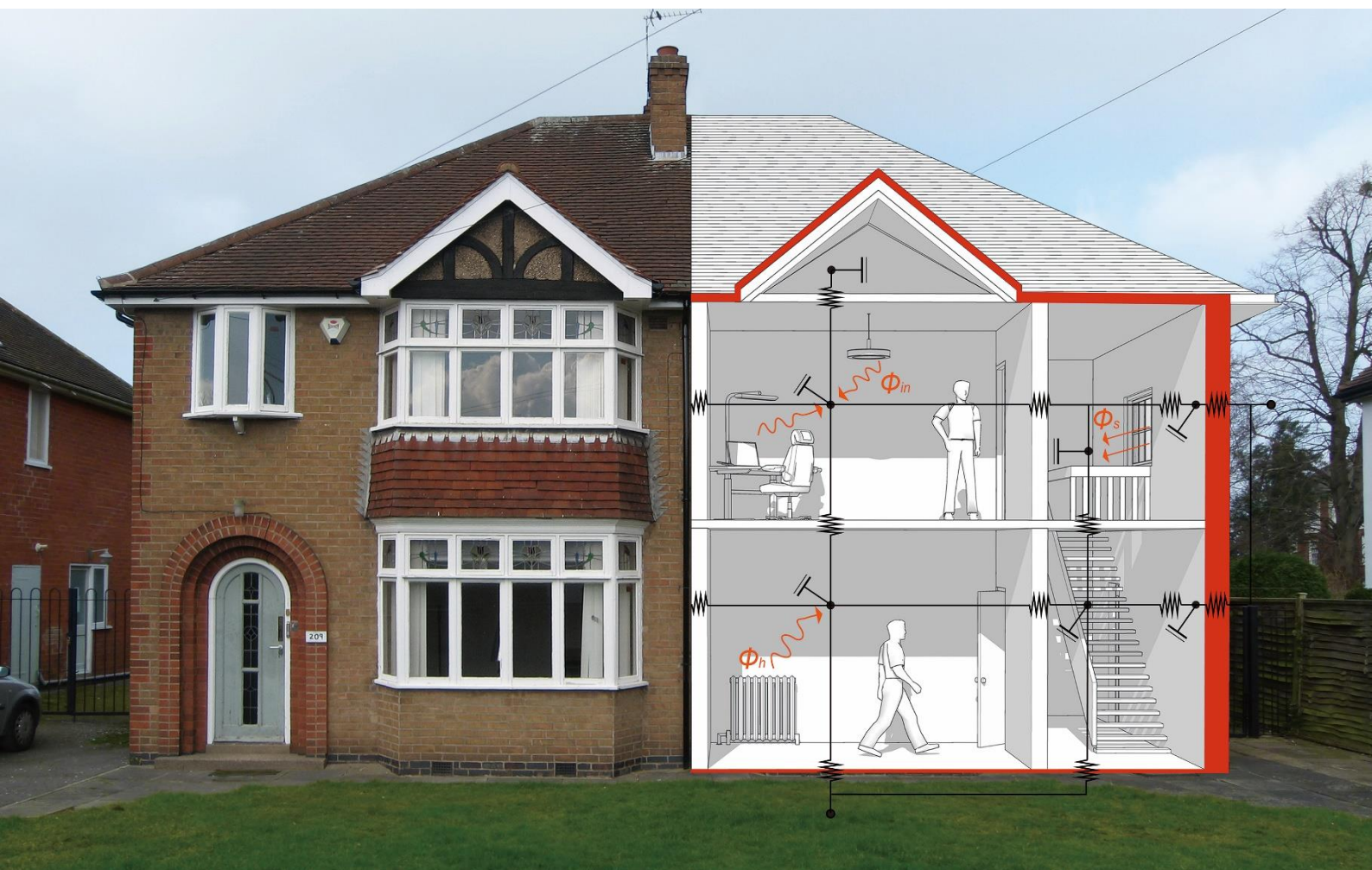


# Building energy performance assessment based on in-situ measurements

## Physical parameter identification

August 2021



© Copyright KU Leuven, Belgium 2021

All property rights, including copyright, are vested in KU Leuven, Belgium, Operating Agent for EBC Annex 71, on behalf of the Contracting Parties of the International Energy Agency Implementing Agreement for a Programme of Research and Development on Energy in Buildings and Communities.

In particular, no part of this publication may be reproduced, stored in a retrieval system or transmitted in any form or by any means, electronic, mechanical, photocopying, recording or otherwise, without the prior written permission of KU Leuven.

Published by KU Leuven, Belgium

Disclaimer Notice: This publication has been compiled with reasonable skill and care. However, neither KU Leuven, nor the Contracting Parties of the International Energy Agency's Implementing Agreement for a Programme of Research and Development on Energy in Buildings and Communities, nor their agents make any representation as to the adequacy or accuracy of the information contained herein, or as to its suitability for any particular application, and accept no responsibility or liability arising out of the use of this publication. The information contained herein does not supersede the requirements given in any national codes, regulations or standards, and should not be regarded as a substitute for the need to obtain specific professional advice for any particular application. EBC is a Technology Collaboration Programme (TCP) of the IEA. Views, findings and publications of the EBC TCP do not necessarily represent the views or policies of the IEA Secretariat or of all its individual member countries.

ISBN 9789075741094]

Participating countries in the EBC: Australia, Austria, Belgium, Brazil, Canada, P.R. China, Czech Republic, Denmark, Finland, France, Germany, Ireland, Italy, Japan, Republic of Korea, the Netherlands, New Zealand, Norway, Portugal, Singapore, Spain, Sweden, Switzerland, Turkey, United Kingdom and the United States of America.

Additional copies of this report may be obtained from: EBC Executive Committee Support Services Unit (ESSU), C/o AECOM Ltd, The Colmore Building, Colmore Circus Queensway, Birmingham B4 6AT, United Kingdom

[www.iea-ebc.org](http://www.iea-ebc.org)

[essu@iea-ebc.org](mailto:essu@iea-ebc.org)

Cover picture: drawing of Xiang Zhang (Jason) (KU Leuven, Belgium) on a picture of the Loughborough test houses (Loughborough University, UK)

# Building energy performance assessment based on in-situ measurements

---

## Physical parameter identification

August 2021

### Main Authors

Geert Bauwens, KU Leuven, Belgium, [geert.bauwens@kuleuven.be](mailto:geert.bauwens@kuleuven.be)

Katia Ritosa, KU Leuven, Belgium, [katia.ritosa@kuleuven.be](mailto:katia.ritosa@kuleuven.be)

Staf Roels, KU Leuven, Belgium, [staf.roels@kuleuven.be](mailto:staf.roels@kuleuven.be)

### Contributing Authors

Jade Deltour, BBRI, Belgium

Gabrielle Masy, UCLouvain, Belgium

Geert Bauwens, Katia Ritosa, Staf Roels, Marieline Senave, Xiang Zhang, KU Leuven, Belgium

Christoffer Rasmussen, DTU, Denmark

Simon Rouchier, Université Savoie Mont-Blanc, France

Kristian Skeie, NTNU, Norway

Twan Rovers, Christian Struck, Saxion Hogeschool Enschede, The Netherlands

Chris Gorse, Adam Hardy, Leeds Beckett University, United Kingdom

Frances Hollick, UCL, United Kingdom

David Allinson, Loughborough University, United Kingdom



# Preface

## The International Energy Agency

The International Energy Agency (IEA) was established in 1974 within the framework of the Organisation for Economic Co-operation and Development (OECD) to implement an international energy programme. A basic aim of the IEA is to foster international cooperation among the 30 IEA participating countries and to increase energy security through energy research, development and demonstration in the fields of technologies for energy efficiency and renewable energy sources.

## The IEA Energy in Buildings and Communities Programme

The IEA co-ordinates international energy research and development (R&D) activities through a comprehensive portfolio of Technology Collaboration Programmes (TCPs). The mission of the IEA Energy in Buildings and Communities (IEA EBC) TCP is to support the acceleration of the transformation of the built environment towards more energy efficient and sustainable buildings and communities, by the development and dissemination of knowledge, technologies and processes and other solutions through international collaborative research and open innovation. (Until 2013, the IEA EBC Programme was known as the IEA Energy Conservation in Buildings and Community Systems Programme, ECBCS.)

The high priority research themes in the EBC Strategic Plan 2019-2024 are based on research drivers, national programmes within the EBC participating countries, the Future Buildings Forum (FBF) Think Tank Workshop held in Singapore in October 2017 and a Strategy Planning Workshop held at the EBC Executive Committee Meeting in November 2017. The research themes represent a collective input of the Executive Committee members and Operating Agents to exploit technological and other opportunities to save energy in the buildings sector, and to remove technical obstacles to market penetration of new energy technologies, systems and processes. Future EBC collaborative research and innovation work should have its focus on these themes.

At the Strategy Planning Workshop in 2017, some 40 research themes were developed. From those 40 themes, 10 themes of special high priority have been extracted, taking into consideration a score that was given to each theme at the workshop. The 10 high priority themes can be separated in two types namely 'Objectives' and 'Means'. These two groups are distinguished for a better understanding of the different themes.

Objectives: The strategic objectives of the EBC TCP are as follows:

- reinforcing the technical and economic basis for refurbishment of existing buildings, including financing, engagement of stakeholders and promotion of co-benefits;
- improvement of planning, construction and management processes to reduce the performance gap between design stage assessments and real-world operation;
- the creation of 'low tech', robust and affordable technologies;
- the further development of energy efficient cooling in hot and humid, or dry climates, avoiding mechanical cooling if possible;– the creation of holistic solution sets for district level systems taking into account energy grids, overall performance, business models, engagement of stakeholders, and transport energy system implications.

Means: The strategic objectives of the EBC TCP will be achieved by the means listed below:

- the creation of tools for supporting design and construction through to operations and maintenance, including building energy standards and life cycle analysis (LCA);
- benefitting from 'living labs' to provide experience of and overcome barriers to adoption of energy efficiency measures;
- improving smart control of building services technical installations, including occupant and operator interfaces;
- addressing data issues in buildings, including non-intrusive and secure data collection;
- the development of building information modelling (BIM) as a game changer, from design and construction through to operations and maintenance.

The themes in both groups can be the subject for new Annexes, but what distinguishes them is that the 'objectives' themes are final goals or solutions (or part of) for an energy efficient built environment, while the 'means' themes are instruments or enablers to reach such a goal. These themes are explained in more detail in the EBC Strategic Plan 2019-2024.

## The Executive Committee

Overall control of the IEA EBC Programme is maintained by an Executive Committee, which not only monitors existing projects, but also identifies new strategic areas in which collaborative efforts may be beneficial. As the Programme is based on a contract with the IEA, the projects are legally established as Annexes to the IEA EBC Implementing Agreement. At the present time, the following projects have been initiated by the IEA EBC Executive Committee, with completed projects identified by (\*) and joint projects with the IEA Solar Heating and Cooling Technology Collaboration Programme by (☼):

Annex 1: Load Energy Determination of Buildings (\*)

Annex 2: Ekistics and Advanced Community Energy Systems (\*)

Annex 3: Energy Conservation in Residential Buildings (\*)

Annex 4: Glasgow Commercial Building Monitoring (\*)

Annex 5: Air Infiltration and Ventilation Centre

Annex 6: Energy Systems and Design of Communities (\*)

Annex 7: Local Government Energy Planning (\*)

Annex 8: Inhabitants Behaviour with Regard to Ventilation (\*)

Annex 9: Minimum Ventilation Rates (\*)

Annex 10: Building HVAC System Simulation (\*)

Annex 11: Energy Auditing (\*)

Annex 12: Windows and Fenestration (\*)

Annex 13: Energy Management in Hospitals (\*)

Annex 14: Condensation and Energy (\*)

Annex 15: Energy Efficiency in Schools (\*)

Annex 16: BEMS 1- User Interfaces and System Integration (\*)

Annex 17: BEMS 2- Evaluation and Emulation Techniques (\*)

Annex 18: Demand Controlled Ventilation Systems (\*)

Annex 19: Low Slope Roof Systems (\*)

Annex 20: Air Flow Patterns within Buildings (\*)

Annex 21: Thermal Modelling (\*)

Annex 22: Energy Efficient Communities (\*)

Annex 23: Multi Zone Air Flow Modelling (COMIS) (\*)

Annex 24: Heat, Air and Moisture Transfer in Envelopes (\*)

Annex 25: Real time HVAC Simulation (\*)

Annex 26: Energy Efficient Ventilation of Large Enclosures (\*)

Annex 27: Evaluation and Demonstration of Domestic Ventilation Systems (\*)

Annex 28: Low Energy Cooling Systems (\*)

Annex 29: ☼ Daylight in Buildings (\*)

Annex 30: Bringing Simulation to Application (\*)

Annex 31: Energy-Related Environmental Impact of Buildings (\*)

Annex 32: Integral Building Envelope Performance Assessment (\*)

Annex 33: Advanced Local Energy Planning (\*)

Annex 34: Computer-Aided Evaluation of HVAC System Performance (\*)

Annex 35: Design of Energy Efficient Hybrid Ventilation (HYBVENT) (\*)

Annex 36: Retrofitting of Educational Buildings (\*)

Annex 37: Low Exergy Systems for Heating and Cooling of Buildings (LowEx) (\*)

Annex 38: ☼ Solar Sustainable Housing (\*)

Annex 39: High Performance Insulation Systems (\*)

Annex 40: Building Commissioning to Improve Energy Performance (\*)

Annex 41: Whole Building Heat, Air and Moisture Response (MOIST-ENG) (\*)

Annex 42: The Simulation of Building-Integrated Fuel Cell and Other Cogeneration Systems (FC+COGEN-SIM) (\*)

Annex 43: ☼ Testing and Validation of Building Energy Simulation Tools (\*)

Annex 44: Integrating Environmentally Responsive Elements in Buildings (\*)

Annex 45: Energy Efficient Electric Lighting for Buildings (\*)

Annex 46: Holistic Assessment Tool-kit on Energy Efficient Retrofit Measures for Government Buildings (EnERGo) (\*)

Annex 47: Cost-Effective Commissioning for Existing and Low Energy Buildings (\*)

Annex 48: Heat Pumping and Reversible Air Conditioning (\*)

Annex 49: Low Exergy Systems for High Performance Buildings and Communities (\*)

Annex 50: Prefabricated Systems for Low Energy Renovation of Residential Buildings (\*)

Annex 51: Energy Efficient Communities (\*)

Annex 52: ☼ Towards Net Zero Energy Solar Buildings (\*)

Annex 53: Total Energy Use in Buildings: Analysis and Evaluation Methods (\*)

Annex 54: Integration of Micro-Generation and Related Energy Technologies in Buildings (\*)

Annex 55: Reliability of Energy Efficient Building Retrofitting - Probability Assessment of Performance and Cost (RAP-RETRO) (\*)

Annex 56: Cost Effective Energy and CO<sub>2</sub> Emissions Optimization in Building Renovation (\*)

Annex 57: Evaluation of Embodied Energy and CO<sub>2</sub> Equivalent Emissions for Building Construction (\*)

Annex 58: Reliable Building Energy Performance Characterisation Based on Full Scale Dynamic Measurements (\*)

Annex 59: High Temperature Cooling and Low Temperature Heating in Buildings (\*)

Annex 60: New Generation Computational Tools for Building and Community Energy Systems (\*)

Annex 61: Business and Technical Concepts for Deep Energy Retrofit of Public Buildings (\*)

Annex 62: Ventilative Cooling (\*)

Annex 63: Implementation of Energy Strategies in Communities (\*)

Annex 64: LowEx Communities - Optimised Performance of Energy Supply Systems with Exergy Principles (\*)

Annex 65: Long-Term Performance of Super-Insulating Materials in Building Components and Systems (\*)

Annex 66: Definition and Simulation of Occupant Behavior in Buildings (\*)

Annex 67: Energy Flexible Buildings (\*)

Annex 68: Indoor Air Quality Design and Control in Low Energy Residential Buildings (\*)

Annex 69: Strategy and Practice of Adaptive Thermal Comfort in Low Energy Buildings

Annex 70: Energy Epidemiology: Analysis of Real Building Energy Use at Scale

Annex 71: Building Energy Performance Assessment Based on In-situ Measurements

Annex 72: Assessing Life Cycle Related Environmental Impacts Caused by Buildings

Annex 73: Towards Net Zero Energy Resilient Public Communities

Annex 74: Competition and Living Lab Platform

Annex 75: Cost-effective Building Renovation at District Level Combining Energy Efficiency and Renewables

Annex 76: ☼ Deep Renovation of Historic Buildings Towards Lowest Possible Energy Demand and CO<sub>2</sub> Emissions

Annex 77: ☼ Integrated Solutions for Daylight and Electric Lighting

Annex 78: Supplementing Ventilation with Gas-phase Air Cleaning, Implementation and Energy Implications

Annex 79: Occupant-Centric Building Design and Operation

Annex 80: Resilient Cooling

Annex 81: Data-Driven Smart Buildings

Annex 82: Energy Flexible Buildings Towards Resilient Low Carbon Energy Systems

Annex 83: Positive Energy Districts

Annex 84: Demand Management of Buildings in Thermal Networks

Annex 85: Indirect Evaporative Cooling

Annex 86: Energy Efficient Indoor Air Quality Management in Residential Buildings

Working Group - Energy Efficiency in Educational Buildings (\*)

Working Group - Indicators of Energy Efficiency in Cold Climate Buildings (\*)

Working Group - Annex 36 Extension: The Energy Concept Adviser (\*)

Working Group - HVAC Energy Calculation Methodologies for Non-residential Buildings (\*)

Working Group - Cities and Communities

Working Group – Building Energy Codes

## IEA EBC Annex 71: Building energy performance assessment based on in-situ measurements Annex 71 in general

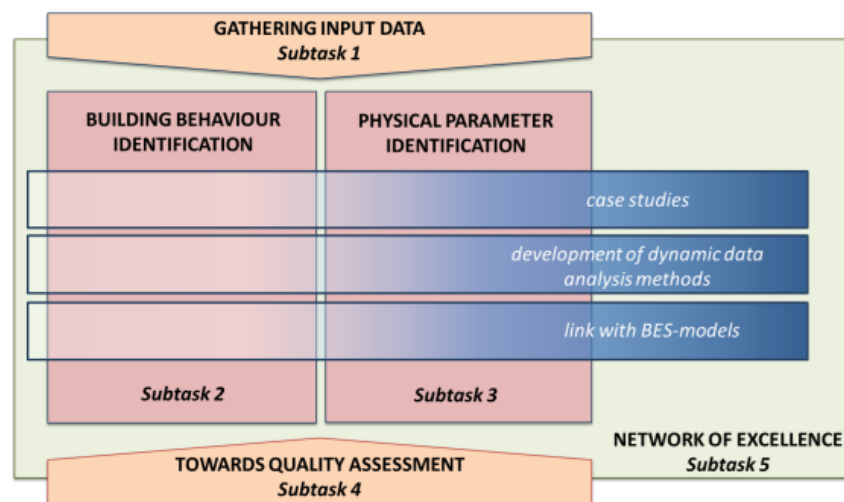
Decreasing the energy use in buildings can only be achieved by an accurate characterization of the as-built energy performance of buildings. This is mainly for two reasons. First of all, despite the ever more stringent energy legislation for new and renovated buildings, monitoring the actual energy performances reveals in many cases a significant performance gap compared to the theoretically designed targets. Secondly, the increasing need for integration of renewable energy stresses on the existing energy systems. This can be remedied by using intelligent systems and energy grids that are aware of the actual status of the buildings.

Within IEA EBC Annex 58, a first step was taken to characterize the actual energy performance of buildings based on full scale dynamic measurements. The onsite assessment methods applied within this project mainly focused on the thermal performance of the building fabric. By investigating the possibilities and limitations of black and grey box system identification models, guidelines were developed on how to assess the overall heat transfer coefficient of a building starting from dynamic measured data instead of static co-heating tests. Notwithstanding Annex 58 showed that onsite quality checks are feasible, the project highlighted at the same time the need of non-intrusive methods. Annex 71 progressed with the achievements of IEA EBC Annex 58, but aimed to make the step towards monitoring in-use buildings. The IEA EBC Annex 71 project focused on the **development of replicable methodologies embedded in a statistical and building physical framework to characterize and assess the actual energy performance of buildings starting from on board monitored data of in-use buildings.**

## Structure of the project

The IEA EBC Annex 71-project was limited to residential buildings, for which the development of characterisation methods as well as of quality assurance methods have been explored. Characterisation methods aim to translate the (dynamic) behaviour of a building into a simplified model that can inform predictive control, fault detection, optimisation of district energy systems,... Within Annex 71 we referred to this as building behaviour identification. Quality assurance methods aim to pinpoint some of the most relevant actual building performance metrics. This part is referred to as physical parameter identification.

A reliable characterisation and quality assurance is strongly dependent on the availability and quality of the input data. At the same time, the expected quality and reliability of the outcome will be determined by the required accuracy to perform a quality assurance. As a result, the analysis of potential methods was steered by both the possibilities and limitations of the available input data as well as by the requested outcome to perform real quality checks. Therefore, the research project was organised as illustrated in the figure below and five subtasks were defined:



**Subtask 1** investigated the possibilities and limitations of common data bases and monitoring systems. This subtask is strongly related to subtasks 2 and 3 by linking the available input data – as much as possible based on existing (non-intrusive) monitoring systems and data bases – to the accuracy of the predicted outcome. A state of the art survey of existing methods, their costs, timeframe and typical accuracy was made. In a second part the step from monitoring to current on board measuring methods was reviewed. Finally, the application of an on-site measured heat transfer coefficient within the global energy efficiency framework was proposed.

**Subtask 2** focused on the development of dynamic data analysis methods suitable for describing the energy dynamics of buildings. Based on in-situ monitored data, prediction models were applied and optimised that can be used in model predictive control, fault detection, and design, control and optimisation of district energy systems,... Necessary data acquisition, development of methodologies and accuracy and reliability of the building behaviour identification models was investigated.

The focus of **Subtask 3** was on development of dynamic data analysis methods suitable for physical parameter identification of buildings. Contrary to Subtask 2, in which the identified parameters do not necessarily have a physical meaning (or do not correspond to the actual value), parameter identification aims to characterize the actual physical parameter. Subtask 3 hence investigated which methodologies are most suitable to determine the actual energy performance indicators of buildings, such as the overall heat loss coefficient, solar aperture,... As in subtask 2, the focus was on methodologies that can be used on occupied buildings, making use of (limited) monitored data.

**Subtask 4** investigated to what extent the methodologies developed in ST2 and ST3 can be used in a quality assessment framework. A large survey was performed amongst possible stakeholders on interest and expectations of quality assessment methods based on in-situ measured data. The main focus was on the determination of the actual heat loss coefficient of a building in an easy, cheap and reliable way, so that it can replace the calculated design value in energy performance certifications. That way, subtask 4 made the link between the annex-participants and certification bodies, government, practitioners in the field. At the same time, subtask 4 gave the necessary boundary conditions (reliability, accuracy, cost,...) the methodologies have to fulfil to be applicable in real life quality checks.

**Subtask 5** continued the collaboration with DYNASTEE ([www.dynastee.info](http://www.dynastee.info)), started within Annex 58. This collaboration showed to be extremely fruitful in dissemination of the results, collecting and distributing research outcomes, and organizing conferences, workshops and training courses.

The **BES-validation exercise** investigated the reliability of common building energy simulation programs. There has been significant work undertaken in past IEA EBC Annexes on validation, particularly inter-program comparisons (e.g BESTEST) and empirical validation on test cells. In Annex 58, empirical validation was extended to full-scale buildings, namely the Twin Houses at Fraunhofer IBP's test site in Holzkirchen, Germany. In this research, the focus was on fabric performance with simple internal heat

gain schedules. The empirical validation undertaken in IEA Annex 71 extended the scope of the experiments in the Twin Houses by including underfloor heating systems and realistic occupancy schedules.

## Overview of the working meetings

The preparation and working phase of the project encompassed nine working meetings:

Meeting	Place, date	Attended by
Kick off meeting	Leuven, Belgium, October 2016	49 participants
Second preparation meeting	Loughborough, UK, April 2017	61 participants
First working meeting	Chambéry, France, October 2017	62 participants
Second working meeting	Brussels, Belgium, April 2018	56 participants
Third working meeting	Innsbruck, Austria, October 2018	55 participants
Fourth working meeting	Bilbao, Spain, April 2019	59 participants
Fifth working meeting	Rosenheim, Germany, October 2019	56 participants
Sixth working meeting	On-line meeting, April 2020	50 participants
Seventh working meeting	On-line meeting, October 2020	50 participants
Eighth working meeting	On-line meeting, April 2021	56 participants
Closing event	Salford, UK, September 2021	

During these meetings, working papers on different subjects related to full scale testing and data analysis were presented and discussed. Over the course of the Annex, different experiments on characterisation and quality assessment were undertaken, and several common exercises on data analysis methods were introduced and solved.

## Outcome of the project

The IEA EBC Annex 71-project worked closely together with the Dynastee-network ([www.dynastee.info](http://www.dynastee.info)). One of the deliverables of the Annex project was the enhancement of this network and promoting of actual building performance characterization based on full scale measurements and the appropriate data analysis techniques. This network of excellence on full scale testing and dynamic data analysis organizes on a regular basis events such as international workshops, annual training, with outputs that support organisations interested in full scale testing campaigns.

In addition to the network of excellence, the outcome of the Annex 71-project has been described in a set of reports, including:

IEA EBC Annex 71 – Building energy performance assessment based on in-situ measurements: challenges and general framework (joint report of Subtasks 1 and 4)

IEA EBC Annex 71 – Building energy performance assessment based on in-situ measurements: building behaviour identification (report of Subtask 2)

IEA EBC Annex 71 – Building energy performance assessment based on in-situ measurements: physical parameter identification (report of Subtask 3)

IEA EBC Annex 71 – Building energy performance assessment based on in-situ measurements: design, description and results of the validation of building energy simulation programs (report of the BES-validation exercise)

IEA EBC Annex 71- Building energy performance assessment based on in-situ measurements: project summary report

## List of participants and coregroup

In total 42 institutes from 11 countries participated in the IEA EBC Annex 71-project. The different participants are listed below:

- Austria: Max Blöchle, Austrian Institute of Technology  
A. Susanne Metzger, Vienna University of Technology  
Gabriel Rojas, University of Innsbruck
- Belgium: **Geert Bauwens, KU Leuven (subtask 3 co-leader)**  
**Hans Bloem, INIVE – Dynastee (subtask 5 co-leader)**  
Karel De Sloover, Belgian Building Research Institute  
Jade Deltour, Belgian Building Research Institute

Arash Erfani, KU Leuven  
Nicolas Heijmans, Belgian Building Research Institute  
Eline Himpe, Ghent University  
Evi Lambie, KU Leuven / EnergyVille  
Gabrielle Masy, UCLouvain

**Glenn Reynders, VITO EnergyVille (subtask 2 co-leader)**

**Katia Ritosa, KU Leuven (secretary)**

**Staf Roels, KU Leuven (operating agent)**

**Dirk Saelens, KU Leuven / EnergyVille (subtask 2 co-leader)**

**Marieline Senave, KU Leuven / EnergyVille (secretary)**

**Liesje Van Gelder, BCCA (subtask 4 leader)**

Matthias Van Hove, Ghent University

**Luk Vandaele, INIVE – Dynastee (subtask 5 co-leader)**

Xiang Zhang (Jason), KU Leuven

Denmark: Peder Bacher, Technical University of Denmark

Morten Brøgger, Danish Building Research Institute (SBI), Aalborg University

Christoffer Rasmussen, Technical University of Denmark

Kim B. Wittchen, Danish Building Research Institute (SBI), Aalborg University

Estonia: Anti Hamburg, Tallinn University of Technology

Tuule Mall Kull, Tallinn University of Technology

Karl-Villem Võsa, Tallinn University of Technology

France: Balsam Ajib, Ecole des Mines de Douai

Rémi Bouchie, CSTB

U Bramkamp, Groupe Atlantic

Antoine Caucheteux, Cerema

Lorena de Carvalho Araujo, CSTB

Tianyun Gao, CSTB

Jordan Gauvrit, Cerema

Christian Ghiaus, INSA Lyon

Myriam Humbert, Cerema/ DterOuest/ DLRB

Sarah Juricic, LOCIE, Université Savoie Mont-Blanc

Guillaume Pandraud, Saint-Gobain Isover

Simon Rouchier, Université Savoie Mont-Blanc

Simon Thebault, CSTB

Germany: Witta Ebel, Passive House Institute

Philippe Gorzalka , German Aerospace Center

Lucia Hanfstaengl, Rosenheim Technical University of Applied Sciences

**Matthias Kersken, Fraunhofer Institute for Building Physics IBP (BES validation co-leader)**

Michael Parzinger, Rosenheim Technical University of Applied Sciences

Jacob Schmiedt, German Aerospace Center

Uli Spindler, Rosenheim Technical University of Applied Sciences

Markus Wirnsberger , Rosenheim Technical University of Applied Sciences

Netherlands: Twan Rovers, Saxion Hogeschool Enschede

Marleen Spiekman, TNO

Christian Struck, Saxion Hogeschool Enschede

Norway: Arild Gustavsen, Research Centre on Zero Emission Buildings, Norwegian University of Science and Technology

Kristian Stenerud Skeie, Norwegian University of Science and Technology

Xingji Yu, Norwegian University of Science and Technology

Spain: Pablo Eguia, Vigo University

Aitor Erkoreka, University of the Basque Country (UPV/EHU)

Catalina Giraldo-Soto, University of the Basque Country

Enrique Granada, Vigo University

Hector Herrarda, CIEMAT

**Maria Jose Jimenez, CIEMAT (subtask 5 co-leader)**

Sandra Martínez Mariño, Vigo University

Gerard Mor Martinez, JRC / CIMNE

Irati Uriarte Perez de Nanclares, University of the Basque Country (UPV/EHU)

Switzerland: Chirag Deb, ETH Zurich

UK: David Allinson, Loughborough University

Zoe De Grussa, BBSA (ESSO)

Cliff Elwell, UCL Energy Institute

David Farmer, Leeds Beckett University

**Richard Fitton, University of Salford (subtask 1 leader)**

Martin Fletcher, Leeds Beckett University

Virginia Gori, UCL Energy Institute

Chris Gorse, Leeds Beckett University

Rajat Gupta, Oxford Brookes University

Adam Hardy, Leeds Beckett University

Ross Holleron, Knauf Insulation

Frances Hollick, UCL

**Richard Jack, Build Test Solutions (subtask 4 co-leader)**

Matthew Li, Loughborough University

Kevin Lomas, Loughborough University

Eirini Mantesi, Loughborough University

Behzad Sodagar, University of Lincoln

**Paul Strachan, University of Strathclyde (BES validation co-leader)**

# Table of content

<b>Preface</b>	<b>i</b>
<b>1. Introduction</b>	<b>11</b>
<b>2. Building Physical Framework</b>	<b>13</b>
<b>2.1. Introduction</b>	<b>13</b>
<b>2.2. Definition of the HTC and HTC<sub>tr</sub></b>	<b>13</b>
<b>2.3. Single zone heat balance</b>	<b>14</b>
2.3.1. Heat input by heating system	15
2.3.2. Internal heat gains	15
2.3.3. Solar heat gains	15
2.3.4. Latent heat gains/losses	16
2.3.5. Transmission heat gains/losses	16
2.3.6. Ventilation heat gains/losses	17
2.3.7. Loading unloading thermal mass	17
2.3.8. Conclusions	18
<b>2.4. From building physical framework to HTC</b>	<b>18</b>
2.4.1. Common simplifications of the heat balance equations	18
2.4.2. Towards the assessment of HTC and HTC <sub>tr</sub>	19
<b>3. Statistical modelling approaches</b>	<b>21</b>
<b>3.1. Static methods to determine HTC</b>	<b>21</b>
3.1.1. Average Method	21
3.1.2. Linear Regression Analysis	21
3.1.3. Energy Signature Method	23
<b>3.2. Dynamic methods to determine HTC and HTC<sub>tr</sub></b>	<b>24</b>
3.2.1. White-box tuning	24
3.2.2. ARX- and ARMAX-modelling	24
3.2.3. State space models	25
<b>4. Determining the input variables</b>	<b>27</b>
<b>4.1. Solar gains</b>	<b>27</b>
4.1.1. Ignore solar gains	27
4.1.2. Constant solar transmittance	27
4.1.3. Constant solar transmittance for each cardinal direction	27
4.1.4. Spline based solar transmittance	28
4.1.5. Using diffuse and beam irradiation separately	28
<b>4.2. Heat input</b>	<b>29</b>
4.2.1. Measurement taken before the generator, common for SH+DHW	29
4.2.2. Measurement taken before the generators, separate for SH and DHW	30
4.2.3. Measurement taken after the generator, common for SH+DHW	30
4.2.4. Measurement taken after the generator for SH	30
<b>4.3. Infiltration heat loss and ventilation heat loss</b>	<b>30</b>
4.3.1. Simplified infiltration models	31
4.3.2. Accounting for mechanical ventilation in the estimation of HTC	32
4.3.3. Splitting the HTC into HTC <sub>tr</sub> and HTC <sub>inf</sub>	32
<b>4.4. Occupant and appliance heat gains</b>	<b>33</b>
4.4.1. Lighting and appliance heat gains	33
4.4.2. Using standardized occupancy profiles from the ISO 17772-1 standard.	33
4.4.3. Using measurements of relative humidity (RH) to determine presence.	33
4.4.4. Using measurements of CO <sub>2</sub> to determine presence.	34

4.4.5.	Estimating the metabolic heat input using a CO <sub>2</sub> balance.	34
<b>4.5.</b>	<b>Weather data</b>	<b>34</b>
4.5.1.	Preprocessing	36
<b>4.6.</b>	<b>Indoor temperature</b>	<b>36</b>
4.6.1.	No measured data available	37
4.6.2.	One sensor in the main living room	38
4.6.3.	Measurements in all different heating zones	38
4.6.4.	Detailed measurements in all rooms	38
<b>4.7.</b>	<b>Conclusions</b>	<b>38</b>
<b>5.</b>	<b>Case studies</b>	<b>40</b>
<b>5.1.</b>	<b>Twin Test Houses</b>	<b>40</b>
<b>5.2.</b>	<b>Loughborough Matched Pair Test Houses</b>	<b>42</b>
<b>5.3.</b>	<b>Gainsborough Test House</b>	<b>43</b>
<b>5.4.</b>	<b>Uccle Test House</b>	<b>45</b>
<b>6.</b>	<b>Exploration of inputs</b>	<b>48</b>
<b>6.1.</b>	<b>Solar gains</b>	<b>48</b>
6.1.1.	Twin Test Houses	48
6.1.2.	Gainsborough	49
6.1.3.	Loughborough	50
6.1.4.	Uccle	50
6.1.5.	Conclusion	51
<b>6.2.</b>	<b>Heat input</b>	<b>51</b>
6.2.1.	Twin Test Houses	51
6.2.2.	Gainsborough	53
6.2.3.	Loughborough	56
6.2.4.	Uccle	56
6.2.5.	Conclusion	57
<b>6.3.</b>	<b>Infiltration heat loss and ventilation heat loss</b>	<b>57</b>
6.3.1.	Twin Test Houses	58
6.3.2.	Gainsborough	58
<b>6.4.</b>	<b>Occupant and appliance heat gain</b>	<b>59</b>
6.4.1.	Gainsborough	59
6.4.2.	Uccle	60
6.4.3.	Conclusion	60
<b>6.5.</b>	<b>Weather data</b>	<b>61</b>
<b>6.6.</b>	<b>Indoor temperature</b>	<b>63</b>
6.6.1.	Twin Test Houses	63
6.6.2.	Gainsborough	66
6.6.3.	Loughborough	67
6.6.4.	Conclusion	68
<b>6.7.</b>	<b>Conclusions</b>	<b>68</b>
<b>7.</b>	<b>Discussion of results</b>	<b>70</b>
<b>7.1.</b>	<b>Twin Test Houses</b>	<b>70</b>
<b>7.2.</b>	<b>Loughborough</b>	<b>72</b>
<b>7.3.</b>	<b>Gainsborough</b>	<b>72</b>
<b>7.4.</b>	<b>Uccle</b>	<b>74</b>

<b>7.5. Guidelines</b>	<b>75</b>
<b>8. Towards real-life applications</b>	<b>78</b>
<b>8.1. SMETER test cases</b>	<b>78</b>
<b>8.2. Datasets</b>	<b>79</b>
8.2.1. Measurements	79
8.2.2. Preprocessing	79
<b>8.3. Assumptions</b>	<b>80</b>
<b>8.4. Results</b>	<b>81</b>
<b>8.5. Investigation of the assumptions</b>	<b>85</b>
8.5.1. Impact of the choice of period	85
8.5.2. Impact of electrical appliances gains	87
8.5.3. Impact of DHW splitting	88
8.5.4. Impact of temperature averaging	89
8.5.5. Impact of weather data availability on HTC estimation	91
<b>8.6. Conclusions</b>	<b>92</b>
<b>9. Conclusion</b>	<b>94</b>
<b>10. References</b>	<b>96</b>
<b>11. Annex: Common Exercises</b>	<b>100</b>



# Abbreviations

List of frequently used abbreviations

---

Abbreviation	Meaning
AIM-2	Alberta Air Infiltration Model
ARX	Autoregressive with Exogenous Inputs
AVG	Average Method
BES	Building Energy Simulation
CI	Confidence interval
DHW	Domestic hot water
EN	European Norm
EPBD	Energy Performance of Buildings Directive
ES	Energy Signature Method
GB	Grey-box Modelling (in the context of this report same as State-space Modelling)
GBORO	Gainsborough Test House
HP	Heat pump
HR	Heat recovery
IEA EBC	Energy in Buildings and Communities Programme of the International Energy Agency
LBORO	Loughborough Matched Pair Test Houses
LR	Linear Regression
LR1	Linear Regression Approach 1, forced through zero
LR2	Linear Regression Approach 2, forced through zero
LR3	Linear Regression Approach 3
MLR	Multiple Linear Regression
SD	Standard deviation
SH	Space heating
SS	State-space Modelling (in the context of this subtask same as Grey-box Modelling)
Twin N2	Twin Test House N2
Twin O5	Twin Test House O5
Uccle	Uccle Test House
UFH	Underfloor heating
U-value	Thermal transmittance of a building element

---



# Definitions

Explanation of frequently used definitions:

**B-splines:** B-spline is piecewise polynomial, where the  $m^{\text{th}}$  order B-splines signify series of polynomials of degree  $m-1$ . The key feature of B-splines is that the point-wise sum of infinitely B-spline series for the entire range of interest is always equal to one.

**Building Energy Simulation (BES):** computer modelling based on building physics, used in the evaluation of energy and environmental aspects of building performance.

**Building thermal envelope:** defined in ISO EN 52016 as “*total area of all elements of a building that enclose thermally conditioned spaces through which thermal energy is transferred, directly or indirectly, to or from the external environment*”.

**g-value (Total Solar Energy Transmittance):** The total energy transmittance of a glazing, indicates the proportion of the incident radiation which is transmitted by the glazing, based on EN 410:2011.

**HTC (Heat Transfer Coefficient):** defined in ISO 13789 as the “*heat flow rate divided by temperature difference between two environments*”. It represents the steady-state aggregate total fabric and ventilation heat transfer from the entire thermal envelope in Watts per kelvin of temperature difference ( $\Delta T$ ) between the internal and external environments, and is expressed in Watts/Kelvin (W/K) (BSI, 2017). In this document, HTC typically refers to the fabric heat transfer by conduction and air infiltration, unless explicitly stated otherwise.

**Solar aperture (solar transmittance, gA value):** The solar transmittance of an observed transparent building element as a function of window properties, window orientation, shading obstacles, and other variables which are infeasible to observe alone.

**Test case:** In the context of this Annex a test case is a dwelling subjected to (extensive) monitoring campaigns in order to get detailed measurement data which are used in HTC assessment.

**Thermal zone:** defined in ISO EN 52016 as “*internal environment with assumed sufficiently uniform thermal conditions to enable a thermal balance calculation*”. In the zoning procedure neighbouring spaces with similar services and comfort settings are merged in thermal zones. A dwelling is often treated as a two-zone building, consisting of a day and night zone.

**U-value:** U-value, also known as thermal transmittance, is defined in ISO 7345 as the “*heat flow rate in the steady state divided by area and by the temperature difference between the surroundings on both sides of a flat uniform system*” in unit  $W/(m^2 \cdot K)$ .



## List of symbols

Explanation of frequently used symbols:

Symbol	Description	Unit
$C$	Heat capacity	J/K
$c_a$	Specific heat capacity of air	J/kgK
$C_i$	Heat capacity of the indoor air in the observed dwelling	J/K
$C_{i,eff}$	Effective averaged heat capacity of the dwelling	J/K
$C_m$	Thermal mass of the dwelling	J/K
$g$	Total energy transmittance or g-value of the glazing	-
$G_a$	Ventilation air flow rate	kg/s
$gA$	Solar aperture	m <sup>2</sup>
HTC	Heat transfer coefficient	W/K
$HTC_{inf}$	Heat transfer coefficient due to infiltration	W/K
$HTC_{tr}$	Heat transfer coefficient due to transmission	W/K
$H_{vent}$	Heat gains/losses due to ventilation	W/K
$I_{sol}$	Global solar irradiation	W/m <sup>2</sup>
$I_{sol,dif}$	Diffuse solar irradiation	W/m <sup>2</sup>
$I_{sol,dir}$	Direct solar irradiation	W/m <sup>2</sup>
$\eta_{HR}$	Heat recovery efficiency	%
RH	Relative (air) humidity	%
$\theta$	Temperature	K or °C
$\theta_e$	Outdoor air temperature	K or °C
$\theta_i$	Indoor air temperature	K or °C
$\theta_{sup}$	Ventilation air supply temperature	K or °C
$\Phi$	Heat flow rate	W
$\Phi_h$	Heat input by the heating system	W
$\Phi_{inf}$	Infiltration heat exchange	W
$\Phi_{int}$	Internal heat gains from occupants and appliances	W
$\Phi_l$	Latent heat exchange due to moisture loading and unloading of interior objects and building parts	W
$\Phi_m$	Heat exchange when loading/unloading thermal mass of interior objects and building parts	W

---

$\Phi_{sol}$	Solar heat gains through transparent fabric parts	W
$\Phi_{tr}$	Transmission heat exchange towards adjacent, towards neighbouring buildings and towards the external environment taking into account solar radiation and long wave heat exchange at the exterior surfaces	W
$\Phi_v$	Heat exchange due to mechanical ventilation	W

---

# 1. Introduction

In Subtask 3 'Physical Parameter Identification' of the IEA EBC Annex 71 project we investigated methodologies to identify, in a way that is reproducible and repeatable, the performance of the fabric and systems of residential buildings that are in use, and for which we have limited monitoring data available. This is different from Subtask 2, as the identified performance indicators directly reflect actual physical parameters. To achieve the above, we apply statistical methods that are based on physical background knowledge.

The physical background is elaborated in Chapter 2. A complete heat balance is constructed as an umbrella that serves to encapsulate the different simplified models that are applied in this subtask. This reference allows us the clear pinpointing of the physical phenomena that are lumped into the estimated parameters, and to evaluate the impact of the model simplification on reliability.

The underlying pursuit that we set ourselves is to assess the building's Heat Transfer Coefficient (HTC). In Chapter 3 methods to determine HTC are established and further developed. Methods can be static, e.g. linear regression or energy signature, or dynamic, using e.g. ARX or stochastic state-space models. But they all consider simplified models of the investigated building. They also all use statistical modelling techniques to assess uncertainty and determine how accurate are the obtained performance indicators, and how confident we can be about them.

In Chapter 4 we review the different input parameters and corresponding statistical modelling approaches used to identify the simplified models from (limited) on site measured data. Although focus is on HTC, some methods identify additional physically relevant parameters, such as the solar aperture, efficiency of heating systems, airtightness, etc. Four case studies have been selected and investigated in detail in this subtask. They consist of residential buildings that are in-use (by actual users or artificial users, i.e. automated heating and window opening). All of them are extensively monitored, and solid reference performance indicators are available. Moreover, in two of them intrusive well-controlled tests (e.g. co-heating tests) were performed. In Chapter 5 we will briefly introduce them, and refer the reader to more detailed instruction documents and data sources.

Chapter 6 explores the impact of the approaches that were outlined in Chapter 4 on the estimated physical parameters, and the related uncertainty. We zoom in on each significant term in the overarching heat balance laid out in Chapter 2, and apply different approaches that best represent these terms in a simplified way. The different approaches are tested on the four case studies. From this, we distil quality procedures and clear guidelines for building parameter identification.

Chapter 7 turns things around and focuses on obtaining optimal results for the case studies. For each case study, we apply the best possible approach to model those terms that prove most significant. For instance, for one particular case study, a combination of a beta-splines approach to model solar gains, and an explicit model of internal gains might prove optimal.

In Chapter 8 we make the step towards real life applications. Realistic measurement campaigns of five houses, with no additional energy usage monitoring other than smart meters, have been provided via the Technical Evaluation of SMETER Technologies (TEST) project, phase 2 of the UK. Only the raw data was provided and the target value (the reference value of the HTC) was unknown when performing the analysis. This offered the possibility to perform a blind test and validate the assumptions and guidelines develop in the previous chapters.

Finally, we summarise the overall general conclusions of the IEA EBC Annex 71 work on physical parameter identification in Chapter 9.



## 2. Building Physical Framework

### 2.1. Introduction

In this chapter we want to develop a solid building physical framework, that describes the dynamic thermal behaviour of a building and the corresponding physical phenomena. To do so, we model buildings as dynamic thermal systems, consisting of a distributed set of thermal nodes, with temperatures that vary in time and which are steered by the temperature and spatial distribution of surrounding thermal nodes. The thermal behaviour of the building can then be described by a system of differential equations, which defines how the thermal nodes are linked. Thermal nodes can represent an indoor air temperature, a temperature inside the building fabric, the temperature of a neighbouring zone, or the temperature attained by heaters, amongst others. If we want to exactly describe a building's thermal behaviour, we need to discern an infinite number of nodes. The building's heat balance can then be written as an infinite system of differential equations that apply the first law of thermodynamics: conservation of energy:

$$\text{For } j=1,2,\dots \infty: \sum \Phi_j = C_j \frac{\partial \theta_j}{\partial t} \quad (1.1)$$

where  $\sum \Phi_j$  represents the sum of heat flow rates towards temperature node  $j$  and  $C_j$  denotes the heat capacity and  $\theta_j$  the temperature of the node. To simplify the problem, we will often lump different nodes into one thermal node. For instance, the outdoor environment, which might slightly differ along the building envelope, typically will be presented by one external air temperature node at  $\theta_e$ .

The framework developed in this chapter should provide us with the necessary theoretical tools to confidently assess assumptions and simplifications in our statistical models. Models that are appropriate to deduce the overall heat transfer coefficient of a building based on limited data. Moreover, the framework should help us to interpret the reliability and uncertainty of the estimated parameters. This chapter derives the dynamic heat balance equation and interactions at play for the case studies described in Chapter 4. Nonetheless, the developed framework is generally applicable and where necessary generalisations are made towards other building types, heating systems and usage.

### 2.2. Definition of the HTC and HTCtr

The aim of this research is to assess the actual thermal performance of a building envelope. The building fabric of interest is bounded by the coloured lines in Figure 1.

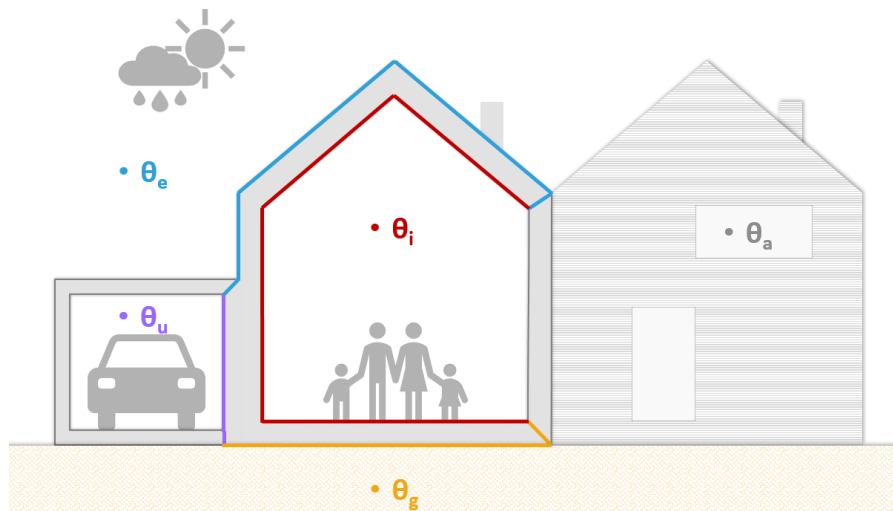


Figure 1. Cross section of a dwelling. The part of the building envelope which we want to characterize the thermal performance of is outlined in colour. It is on one side (red lines) bounded by surfaces enclosing the interior environment at temperature  $\theta_i$ . The blue lines, on the other side, depict the surface area in contact with the external environment, which is represented by the temperature node  $\theta_e$ . Finally, the envelope's surfaces exchanging heat with unconditioned spaces at temperature  $\theta_u$  and the ground at  $\theta_g$  are coloured in respectively purple and orange.

It separates the indoor environment at temperature  $\theta_i$  from (1) the external environment, defined by among other things the external temperature  $\theta_e$ , solar and sky radiation and precipitation; (2) unconditioned spaces as for example garages or cellars at a temperature  $\theta_u$ ; and (3) the soil mass underneath the building, represented by the ground temperature  $\theta_g$ . This part of the building envelope hence determines how the indoor temperature is affected by changes in these boundary conditions. The indoor temperature is furthermore affected by the temperature of the adjacent building  $\theta_a$ , which we will have to try to eliminate to assess the performance indicator of interest.

In the Annex 71 project we will characterise the thermal performance of this building fabric by a so-called 'overall heat transfer coefficient' (in short 'HTC'). The HTC accounts for both transmission and infiltration heat gains and losses:

$$\text{HTC} = \text{HTC}_{\text{tr}} + \text{HTC}_{\text{inf}} = \text{HTC}_{\text{tr}} + \frac{\Phi_{\text{inf}}}{(\theta_e - \theta_i)} = \text{HTC}_{\text{tr}} + (H_{\text{inf}}^e + H_{\text{inf}}^u) \quad (2.1)$$

where  $\Phi_{\text{inf}}$  stands for the infiltration losses (or gains) [W] (note that intentional ventilation is not included in the HTC) and  $H_{\text{inf}}^e$  and  $H_{\text{inf}}^u$  stand for the heat transfer coefficient by infiltration through the building parts in contact with the external and unconditioned spaces respectively [W/K].  $\text{HTC}_{\text{tr}}$  stands for the transmission heat gains and losses from inside through the building fabric to the external environment ('e'), ground ('g') and unconditioned spaces ('u') and can be written as the sum of the respective transmission heat transfer coefficients  $H_{\text{tr}}$  [W/K]:

$$\text{HTC}_{\text{tr}} = H_{\text{tr}}^e + H_{\text{tr}}^g + H_{\text{tr}}^u \quad (2.2)$$

The transmission heat transfer coefficient to the external environment,  $H_{\text{tr}}^e$ , embeds the heat transfer by transmission through the  $n_e$  building elements,  $p_e$  linear thermal bridges and  $q_e$  point thermal bridges separating the internal from the external environment (Eq. 2.3). Hereby,  $U_i$  and  $A_i$  respectively correspond to the building elements' thermal transmittance [W/m<sup>2</sup>K] and surface area [m<sup>2</sup>],  $\psi$  is the linear thermal transmittance [W/mK] of the linear thermal bridges with length  $L$  [m] and  $\chi$  represents the thermal transmittance of the point thermal bridges in W/m<sup>2</sup>K.  $H_{\text{tr}}^g$  and  $H_{\text{tr}}^u$  follow similar equations (Eqs. 2.4 and 2.5), but they include an extra temperature difference factor that accounts for the fact that the elements thermally interact with an environment at a temperature different from  $\theta_e$ .

$$H_{\text{tr}}^e = \sum_{j=1}^{n_e} U_j A_j + \sum_{k=1}^{p_e} \Psi_k L_k + \sum_{l=1}^{q_e} X_l A_l \quad (2.3)$$

$$H_{\text{tr}}^g = \left( \sum_{j=1}^{n_g} U_j A_j + \sum_{k=1}^{p_g} \Psi_k L_k + \sum_{l=1}^{q_g} X_l A_l \right) \cdot \frac{(\theta_g - \theta_i)}{(\theta_e - \theta_i)} \quad (2.4)$$

$$H_{\text{tr}}^u = \left( \sum_{j=1}^{n_u} U_j A_j + \sum_{k=1}^{p_u} \Psi_k L_k + \sum_{l=1}^{q_u} X_l A_l \right) \cdot \frac{(\theta_u - \theta_i)}{(\theta_e - \theta_i)} \quad (2.5)$$

### 2.3. Single zone heat balance

The total volume  $V$  of a building – the volume encapsulated by the HTC – can be considered as consisting of  $n$  subvolumes ( $V = \sum V_j$ ). Each subvolume  $j$  is simplified to a thermal node of uniform temperature  $\theta_j$ . Thermal nodes exchange heat with adjacent subvolumes, neighbouring buildings and outdoors by heat conduction and enthalpy flows.

The overall heat balance of the thermal node of subvolume  $j$  can be written as:

$$C_j \frac{\partial \theta_j}{\partial t} = \Phi_h + \Phi_{\text{int}} + \Phi_{\text{sol}} + \Phi_l + \Phi_{\text{tr}} + \Phi_v + \Phi_m \quad (2.6)$$

with  $C_j$  heat capacity of volume air,  $\Phi_h$  the heat input by the heating system,  $\Phi_{\text{int}}$  the internal heat gains,  $\Phi_{\text{sol}}$  solar heat gains through transparent fabric parts,  $\Phi_l$  latent heat exchange due to moisture loading and unloading of interior objects and building parts,  $\Phi_{\text{tr}}$  the transmission heat exchange towards adjacent zones of our building, towards neighbouring buildings and towards the external environment taking into account solar radiation and long wave heat exchange at the exterior surface,  $\Phi_v$  the ventilation and infiltration heat exchange and  $\Phi_m$  the heat exchange when loading/unloading thermal mass of interior objects and building parts.

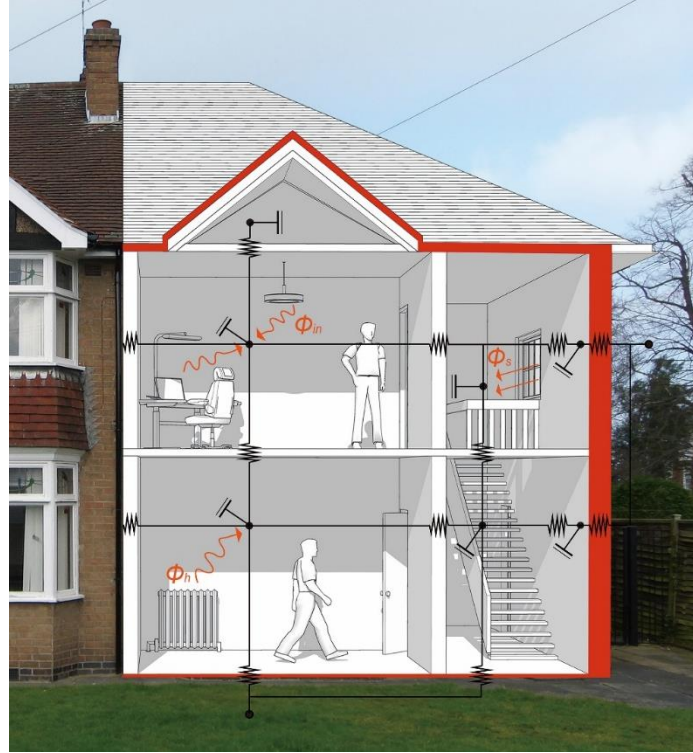


Figure 2. Heat balance at the level of the building zones. In this model the building zones are replaced by thermal nodes at different temperatures  $\theta_j$ , connected by heat flows.

### 2.3.1. Heat input by heating system

At certain time steps, a heating system might inject a heating power into the zone. Heating of the thermal node is mostly indirect. Often the heating system is associated with a certain thermal mass that will be loaded during and unloaded after heating hours. If we assume the heating system in the building zone at one uniform temperature, we can model the heating as a subsystem by making a distinction between the heating power  $\Phi_{h,h}$  supplied to the heating system with capacity  $C_h$  and at a temperature  $\theta_h$ . The heating power  $\Phi_{h,h}$  hence serves to heat the heater, which in turns exchanges heat not only with the internal zone at  $\theta_i$ , but also with surrounding surfaces:

$$C_h \frac{\partial \theta_h}{\partial t} = \Phi_{h,h} + \frac{1}{r_{h,i}} (\theta_i - \theta_h) + \sum \frac{1}{r_{h,si}} (\theta_{si} - \theta_h) \quad (2.7)$$

with  $C_h$  the heat capacity of the heater and  $r_{h,i}$  and  $r_{h,si}$  specific resistances (K/W) between heater at temperature  $\theta_h$  and indoor air temperature  $\theta_i$ , and between  $\theta_h$  and indoor surface temperatures  $\theta_{si}$ .

The heating power injected into the building zone  $\Phi_h$  corresponds then to:

$$\Phi_h = \frac{1}{r_{h,i}} (\theta_h - \theta_i) \quad (2.8)$$

### 2.3.2. Internal heat gains

Along with the intended heat input by the heating system, internal heat gains due to the presence of inhabitants, water heat gains (storage, pipework,..), the use of appliances, lights, etc. may be present. The internal heat gains can be written as:

$$\Phi_{int} = \sum \Phi_{inhab} + \Phi_{water} + \Phi_{appliances} + \Phi_{lighting} + \dots \quad (2.9)$$

### 2.3.3. Solar heat gains

Solar heat gains can be described as

$$\Phi_{sol} = \left( \sum_{j=1}^k g_j(\beta_j) A_j(\text{azel}) \right) I_{sol,dir} + \left( \sum_{j=1}^k g_j(\beta_j) A_j(\text{azel}) \right) I_{sol,dif} \quad (2.10)$$

in which  $I_{sol,dir}$  denotes the direct solar radiation and  $I_{sol,dif}$  the diffuse solar radiation, measured along the sun vector,  $azel$  the angle between a vector aligned with the sun beams and a vector aligned with an on-site horizontal plane.  $g_j(\beta_j)$  represents the total solar energy transmittance or g-value of the glazing. It expresses the portion of solar radiation that passes through the window surface, directly or indirectly. It is dependent on the properties of the transparent component and on the angle of incidence  $\beta_j$ ; the angle between the sun vector and the normal vector to the transparent component  $j$ . The surface areas  $A_j(azel)$  seen by the sun are dependent on its position in the celestial sphere, the orientation of the transparent component  $j$  and shading provided by surrounding buildings and trees amongst others.

The solar heat gains described above focus on transparent components of the building envelope. Aside from this, other thermal dynamics due to solar radiation will play a role. For instance, outdoor surface temperatures of opaque envelope parts will rise when irradiated by the sun. As a result, local transmission heat losses are reduced or even turned into heat gains. This will be accounted for in Section 2.3.5.

### 2.3.4. Latent heat gains/losses

Latent heat flows  $\Phi_l$  arise due to hygroscopic loading and unloading of furnishing and building fabric parts. For newly built dwellings in particular, the evaporation of built-in moisture demands a significant amount of latent heat. The latent heat exchange can be described as:

$$\Phi_l = h(G_{si} + G_{cond/evap}) \quad (2.11)$$

with  $h$  (J/kg) the latent heat of evaporation and  $G_{si}$  (kg/s) the moisture exchange rate between room air and all hygroscopic materials and  $G_{cond/evap}$  the condensation/evaporation rate at e.g. window surfaces.

### 2.3.5. Transmission heat gains/losses

Transmission heat losses (or gains) are of core interest in the determination of the  $HTC_{tr}$  (and HTC). However,  $\Phi_{tr}$  in Eq. 2.6. not only comprises transmission losses (or gains) to the outdoor, ground and (neighbouring) unconditioned spaces, but also losses (or gains) to neighbouring (conditioned) zones and adjacent buildings. Therefore, we will split  $\Phi_{tr}$  into five parts:

$$\Phi_{tr} = \Phi_{tr}^e + \Phi_{tr}^g + \Phi_{tr}^u + \Phi_{tr}^n + \Phi_{tr}^{adj} \quad (2.12)$$

with  $\Phi_{tr}^e$  heat losses from the considered indoor zone to the external,  $\Phi_{tr}^g$  heat losses from the considered zone towards the ground,  $\Phi_{tr}^u$  heat losses from the considered zone to unconditioned spaces,  $\Phi_{tr}^n$  heat losses to neighbouring zones of the same dwelling and finally  $\Phi_{tr}^{adj}$  heat losses to adjacent buildings.

Linking  $\Phi_{tr}^e$ ,  $\Phi_{tr}^g$  and  $\Phi_{tr}^u$  to the  $HTC_{tr}$  is not as straightforward as it seems. Transmission heat losses as implemented in e.g. the EPBD-regulation are written as a function of the indoor and ambient temperatures, while actual transmission heat flows through the fabric are driven by the surface temperature gradients across them. As illustrated in Figure 3, the outdoor surface temperature of opaque and transparent fabric parts  $\theta_{se}$ , can differ significantly from the outdoor air temperature  $\theta_e$ . Surface temperatures of opaque fabric parts (and to a lesser extent of transparent parts) rise when struck by short-wave solar radiation. Similarly, surface temperatures of opaque and transparent parts typically drop at night due to long-wave radiative exchange with sky and surroundings. They are also influenced by latent heat gains due to condensing water vapour or rain water uptake, or latent heat losses due to evaporating moisture, or again, water uptake. For instance, when moisture evaporates at the external fabric surface, it locally lowers surface temperature  $\theta_{se}$ . Similarly, indoor surface temperatures are also influenced by inputs other than  $\theta_i$ , such as solar gains, long-wave radiative heat exchange to other interior surfaces, or latent heat. Therefore, we could link  $\theta_i$  with the indoor surface temperatures  $\theta_{si}^e$ ,  $\theta_{si}^n$ ,  $\theta_{si}^{adj}$ ,  $\theta_{si}^g$ .

$$\Phi_{tr} = \frac{1}{r_i^e} (\theta_{si}^e - \theta_i) + \frac{1}{r_i^g} (\theta_{si}^g - \theta_i) + \frac{1}{r_i^u} (\theta_{si}^u - \theta_i) + \frac{1}{r_i^n} (\theta_{si}^n - \theta_i) + \frac{1}{r_i^{adj}} (\theta_{si}^{adj} - \theta_i) \quad (2.13)$$

in which the special thermal resistances  $r_i$  (K/W) reflect the combined resistance to convective and radiative heat exchange. Similarly, we could link the surface temperatures at the other side of the building fabric with the external conditions that inform them. In between both surface temperatures we could define several nodes within the building fabric to couple indoor and outdoor surface temperatures. This, though, would quickly expand our system of equations significantly. Moreover, the equations would describe the dynamic heat balance only locally at building fabric parts. Typically, different fabric parts are present in one dwelling, that are situated and oriented differently, that can be irradiated or shaded and this differently at inside or outside surfaces.

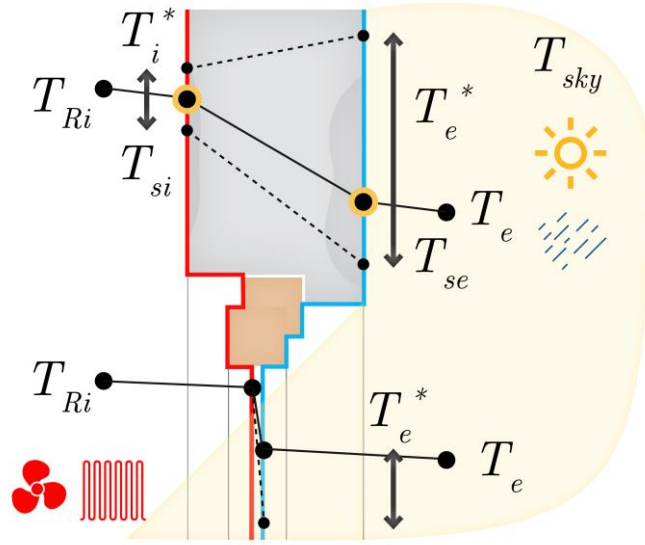


Figure 3. Solar radiation and long wave heat exchanges with surrounding surfaces and the sky pushes outdoor and, to a lesser degree, indoor surface temperatures of opaque and transparent building parts above or below air temperatures. Figure from [Bauwens, 2015].

It is therefore impractical to further elaborate the equations at play. Instead, we keep the equations generic but ensure that they provide sufficient theoretical accuracy to sensibly interpret scenarios in practice and fully capture the thermal link between  $\theta_i$  and boundary conditions  $\theta_e$ ,  $\theta_g$ ,  $\theta_u$ ,  $\theta_n$  and  $\theta_{adj}$ . Only then we can extract the actual characteristics of the building envelope and deduce the  $HTC_{tr}$ .

### 2.3.6. Ventilation heat gains/losses

A distinction needs to be made between the intended replacement of the indoor air by fresh supply air, the so-called ventilation, and the uncontrolled mass transfer due to infiltration:

$$\Phi_v = \Phi_{vent} + \Phi_{inf} \quad (2.14)$$

The intended part can be realised via natural ventilation due to wind pressure differences and thermal stack effects along the building envelope or via mechanical ventilation.  $\Phi_{vent}$  comprises air exchange with outdoors and neighbouring zones. While studies identify air exchanges between cojoined buildings, the impact is generally limited by purposely restricted flow paths and is not included here. Hence,  $\Phi_{vent}$  consists of three parts:

$$\Phi_{vent} = \Phi_{vent}^e + \Phi_{vent}^u + \Phi_{vent}^n \quad (2.15)$$

with  $\Phi_{vent}^e$  heat gains/losses due to ventilation from the considered indoor zone to the ambient,  $\Phi_{vent}^u$  heat gains/losses from the considered zone to an unconditioned neighbouring zone of the same dwelling and  $\Phi_{vent}^n$  heat gains/losses from the considered zone to a conditioned neighbouring zone of the same dwelling. Eq. 2.15. can be rewritten as:

$$\Phi_{vent} = (1 - \eta_{HR})c_a G_{a,vent}^e (\theta_e - \theta_i) + c_a G_{a,vent}^u (\theta_u - \theta_i) + c_a G_{a,vent}^n (\theta_n - \theta_i) \quad (2.16)$$

with  $\eta_{HR}$  the heat recovery efficiency (zero without),  $c_a$  the specific heat capacity of air and  $G_a$  the air flow rate in kg/s.

Infiltration losses arise along air leakage paths in the building components, thereby providing again a direct connection between  $\theta_i$  and  $\theta_e$ ,  $\theta_i$  and  $\theta_n$ , and  $\theta_i$  and  $\theta_u$ . When infiltration flows pass through a building component some heat recovery occurs, while exfiltration flows will temper the transmission losses. Combined, the two effects are so small that they are commonly neglected and the infiltration losses are approximated by

$$\Phi_{inf} = c_a G_{a,inf}^e (\theta_e - \theta_i) + c_a G_{a,inf}^u (\theta_u - \theta_i) + c_a G_{a,inf}^n (\theta_n - \theta_i) \quad (2.17)$$

### 2.3.7. Loading unloading thermal mass

The last term in Eq. 2.6. describes the loading and unloading of the thermal mass available in the subvolume. The indoor air of the subvolume has limited capacity of his own, but can appeal to available thermal capacity of indoor walls,

floors, furniture and other objects contained within the building envelope. If we merge this capacity in a fictitious thermal tank with capacity  $C_m$ , at a homogeneous temperature  $\theta_m$ , we can simplify the loading and unloading term as:

$$\Phi_m = C_m \frac{\partial \theta_m}{\partial t} = \frac{1}{r_{i,m}} (\theta_i - \theta_m) \quad (2.18)$$

### 2.3.8. Conclusions

In this section, we developed the general dynamic heat balance equation at subvolume level. The heat balance was written as a system of differential equations. In the next sections, we will use this framework as a blueprint, and deduce from it simplified thermal models that are suitable to determine the  $HTC_{tr}$  and  $HTC$  starting from on-site measured data.

## 2.4. From building physical framework to HTC

### 2.4.1. Common simplifications of the heat balance equations

Elaborating the different terms in the heat balance equation of each zone as illustrated in Section 2.3, allows the rewriting of Eq. 2.6. Unfortunately writing out the different terms often introduces new unknowns in the equation. At the building level this results in a set of  $n$  equations, often with more than  $n$  unknowns. To be able to solve the system of equations we either have to perform an unacceptable amount of measurements or we have to simplify the system.

Limiting the number of thermal zones

A significant step to simplify the problem is by aggregating zones with similar heating patterns and set points. Often a dwelling is treated as a two-zone building, consisting of a day and night zone. The day zone aggregates all living spaces, the night zone all bedrooms.

Further simplification of the problem is achieved by treating the building as one heated zone. Doing so, the set of  $n$  equations reduces to one averaged heat balance equation

$$C_i \frac{\partial \theta_i}{\partial t} = \Phi_h + \Phi_{int} + \Phi_{sol} + \Phi_l + \Phi_{tr} + \Phi_v + \Phi_m \quad (2.19)$$

with  $C_i$  the heat capacity and  $\theta_i$  a representative averaged indoor temperature of the dwelling.

Introducing an effective thermal capacity

In a further simplification, the loading and unloading of interior objects and building surfaces is included in an effective thermal mass of the building node.

$$C_{i,eff} \frac{\partial \theta_i}{\partial t} = \Phi_h + \Phi_{int} + \Phi_{sol} + \Phi_l + \Phi_{tr} + \Phi_v \quad (2.20)$$

with  $C_{i,eff}$  the effective averaged heat capacity of the dwelling.

Neglecting latent heat effects

Latent heat effects can take a significant share in the heat balance of newly built dwellings. Specifically, the drying out of built-in moisture can strongly increase the energy use. But a few months after erection, latent heat effects become much smaller and limited to the hygric loading and unloading of finishing materials and objects in the building and sometimes condensation/evaporation effects. These phenomena typically take a much smaller share in the overall heat balance, and it is rather common to neglect them, further simplifying the heat balance equation to:

$$C_{i,eff} \frac{\partial \theta_i}{\partial t} = \Phi_h + \Phi_{int} + \Phi_{sol} + \Phi_{tr} + \Phi_v \quad (2.21)$$

Combining infiltration and transmission heat losses

Since infiltration losses are linked to indoor-outdoor temperature differences, as is often assumed for transmission losses,  $\Phi_{inf}$  is often combined with  $\Phi_{tr}$  in one global term:

$$C_{i,eff} \frac{\partial \theta_i}{\partial t} = \Phi_h + \Phi_{int} + \Phi_{sol} + \Phi_{vent} + \tilde{\Phi}_{tr} \quad (2.22)$$

#### 2.4.2. Towards the assessment of HTC and HTC<sub>tr</sub>

Rewriting Eq. 2.12 in function of the transmission heat transfer coefficients  $H_{tr}$  [W/K], adopting a single-zone approach, yields:

$$\Phi_{tr} = (H_{tr}^e + H_{tr}^g + H_{tr}^u + H_{tr}^{adj})(\theta_e - \theta_i) \quad (2.23)$$

Hence, the  $HTC_{tr}$  (Eq. 2.2) can be linked to  $\Phi_{tr}$ ,  $\theta_i$  and  $\theta_e$  as:

$$\Phi_{tr} - H_{tr}^{adj}(\theta_e - \theta_i) = \mathbf{HTC}_{tr}(\theta_e - \theta_i) \quad (2.24)$$

where the second term at the left hand side corresponds to the transmission heat losses to an adjacent dwelling.

Since the HTC additionally incorporates the infiltration heat losses/gains to the ambient and unconditioned spaces, it can be expressed as:

$$\left( \Phi_{tr} - H_{tr}^{adj}(\theta_e - \theta_i) \right) + \left( \Phi_v - (H_{vent}^e + H_{vent}^u)(\theta_e - \theta_i) \right) = \mathbf{HTC}(\theta_e - \theta_i) \quad (2.25)$$

Which equals:

$$\left( \tilde{\Phi}_{tr} - H_{tr}^{adj}(\theta_e - \theta_i) \right) = \mathbf{HTC}(\theta_e - \theta_i) \quad (2.26)$$

Equation (2.26) links the HTC of a dwelling with its heat balance, for instance as simplified written in Equation (2.22). In the next chapter we will take a look at the different statistical tools at hand to solve the equation. In chapter 4 we will go in detail on the different terms in Equation (2.22) that we have to quantify as inputs to the equation in order to determine the HTC starting from in-situ measured data.



## 3. Statistical modelling approaches

In this chapter we give a general overview of the different statistical methods that can be used to determine the HTC of a building starting from on site measured data. We make a distinction between static methods (section 3.1) and dynamic methods (section 3.2). In the next chapter we will review the different inputs needed in the models, and how to deal with them in practical situations.

### 3.1. Static methods to determine HTC

Often, the energy consumption data of buildings in use are only collected on low frequencies (e.g. weekly, monthly or even yearly basis, e.g. for billing purposes). Although we might lose accuracy, when combined with other data such as climatic boundary conditions and (averaged) indoor temperatures, these data might still yield sufficient information to assess the overall HTC. The dynamic behaviour, though, needs to be neglected and Eq. 2.22. further simplifies to

$$C_{i,\text{eff}} \frac{\partial \theta_i}{\partial t} = \Phi_h + \Phi_{\text{int}} + \Phi_{\text{sol}} + \tilde{\Phi}_{\text{tr}} + \Phi_{\text{vent}} = 0 \quad (3.1)$$

This final simplification is applied in the first three statistical methods discussed below: the Average Method (section 3.1.1), Linear Regression (section 3.1.2) and the Energy Signature Method (section 3.1.3).

#### 3.1.1. Average Method

Under steady state conditions Eqs. 2.26 and 3.1 can be combined into:

$$\left( \tilde{\Phi}_{\text{tr}} - H_{\text{tr}}^{\text{adj}} (\theta_e - \theta_i) \right) = \text{HTC} (\theta_e - \theta_i) = - \left( \Phi_h + \Phi_{\text{int}} + \Phi_{\text{sol}} + \Phi_{\text{vent}} + \Phi_{\text{tr}}^{\text{adj}} \right) \quad (3.2)$$

And therefore:

$$\text{HTC} = \frac{\Phi_h + \Phi_{\text{int}} + \Phi_{\text{sol}} + \Phi_{\text{vent}} + \Phi_{\text{tr}}^{\text{adj}}}{(\theta_i - \theta_e)} \quad (3.3)$$

The Average Method is described in [ISO 9869, 2014] as a simple method to determine the U-value of homogenous building elements based on on-site heat flux and environmental temperature measurements. Given the analogy between the definition of the HTC in Eq. 3.3 and that of the U-value, the Average Method should also be applicable on a whole building scale to determine the HTC.

As demonstrated in Eq. 3.4, the method presumes that the division of the mean heat flow rate by the mean internal-external temperature difference asymptotically converges to the HTC as the average is taken over a sufficiently long period.

$$\text{HTC} = \frac{\sum_{j=1}^n (\Phi_{h,j} + \Phi_{\text{int},j} + \Phi_{\text{sol},j} + \Phi_{\text{vent},j} + \Phi_{\text{tr},j}^{\text{adj}})}{\sum_{j=1}^n (\theta_{i,j} - \theta_{e,j})} \quad (3.4)$$

where  $j$  corresponds to the individual measurement points.

To ensure that the steady-state conditions are met, the heat content of the building fabric should, on average, remain constant throughout the experiment, and direct solar radiation should be avoided.

#### 3.1.2. Linear Regression Analysis

The goal of linear regression (LR) analysis is to determine a linear relationship between a dependent variable  $y$  and one (simple LR, Eq. 3.5) or more (multiple LR, Eq. 3.6) independent variables  $x$ .

$$y = ax + b + \varepsilon_t \quad (3.5)$$

$$y = a_1 x_1 + a_2 x_2 + b + \varepsilon_t \quad (3.6)$$

Where we assume  $\varepsilon_t$  is a sequence of mutually uncorrelated, identically distributed random variables with zero mean and constant variance (Madsen, 2008).

The three different LR approaches that can be applied to characterize the HTC will be discussed and visualised below.

### Approach 1

The heat balance in Eq. (3.7) can be translated into a simple linear regression model with the sum of the heat flow rates ( $\sum_1 \Phi$ ) as the independent variable and the indoor-outdoor temperature difference ( $\Delta\theta_{ie}$ ) as the dependent variable (Eq. 3.8). When the measurement data is plotted against these two variables, the slope of the fitted regression line yields the HTC, as illustrated in the left graph on Figure 4. Typically the intercept is forced to be zero (as in Eqs. 3.7 and 3.8). This introduces a small bias but makes the assessment significantly more robust.

$$\Phi_h + \Phi_{int} + \Phi_{sol} + \Phi_{vent} + \Phi_{tr}^{adj} = HTC(\theta_i - \theta_e) \quad (3.7)$$

$$\sum_1 \Phi = HTC \cdot \Delta\theta_{ie} \quad (3.8)$$

### Approach 2

Identifying a multiple linear regression model, with the incident solar radiation as second independent variable, on the monitoring data, makes it possible to additionally assess a solar aperture coefficient, see Equations. (3.9) and (3.10). Note, that this solar aperture coefficient represents a lumped gA-value. As can be seen from the right graph on Figure 4 the identified MLR model will take the form of a 3D-plane through the point cloud of measurement data.

$$\Phi_h + \Phi_{int} + \Phi_{vent} + \Phi_{tr}^{adj} = HTC(\theta_i - \theta_e) - \Phi_{sol} = HTC(\theta_i - \theta_e) - gA \cdot I_{sol} \quad (3.9)$$

$$\sum_2 \Phi = HLC \Delta\theta_{ie} - gA \cdot I_{sol} \quad (3.10)$$

### Approach 3

An estimate for  $gA_l$  can also be obtained using simple linear regression. After all, Equation (3.10) can be rewritten as:

$$\frac{\sum_2 \Phi}{\Delta\theta_{ie}} = -gA \frac{I_{sol}}{\Delta\theta_{ie}} + HTC \quad (3.11)$$

This single linear regression analysis performed using Equation (3.11) is visualised in Figure 5: the intersection of the regression line with the y-axis determines the HTC, while the slope of the regression line yields an indication of the solar aperture.

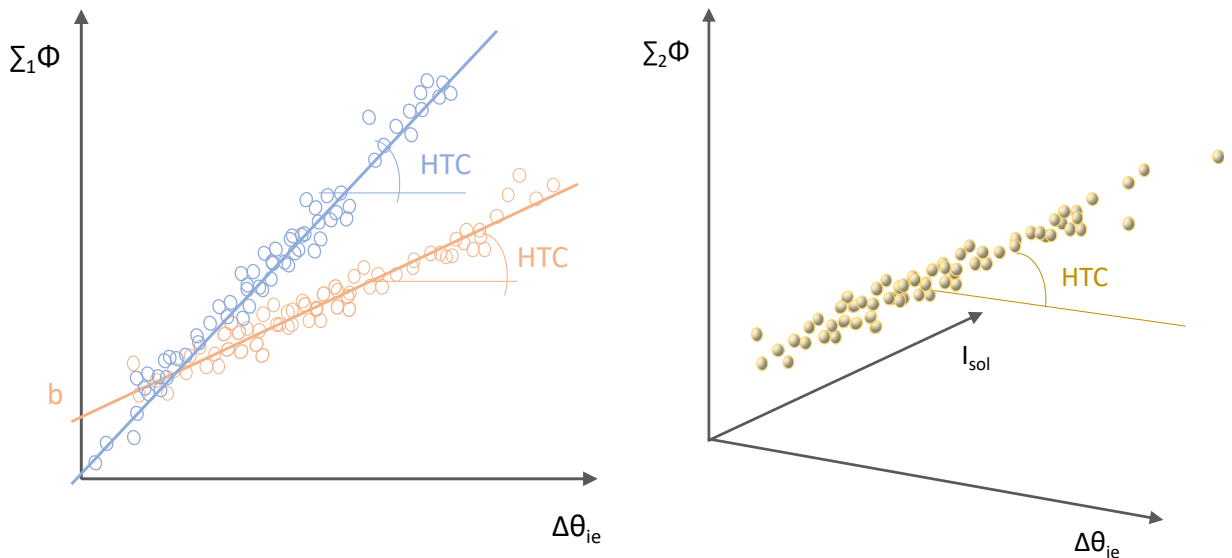


Figure 4. Identifying a Simple or Multiple Linear Regression model on monitoring data in order to assess respectively the HTC (Approach 1, left figure) or the HTC and a solar aperture coefficient (Approach 2, right figure).

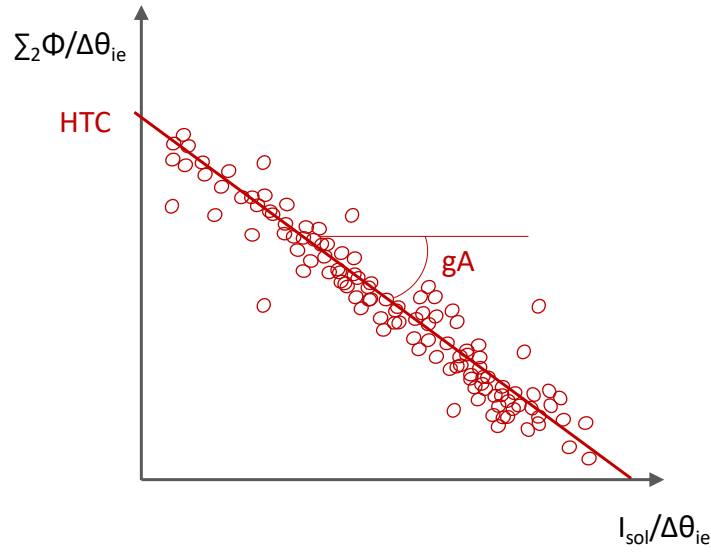


Figure 5. Approach 3 allows to estimate both the HTC and the solar aperture coefficient using a simple linear regression model.

### 3.1.3. Energy Signature Method

The energy signature method relates the energy use of a dwelling to the environmental parameters, typically the outdoor temperatures. This method can be considered as a special case of linear regression analysis, which also starts from the quasi-stationary equation:

$$\begin{aligned} 0 &= \Phi_h + \Phi_{int} + \Phi_{sol} + \Phi_{vent} + \tilde{\Phi}_{tr} \\ &= \Phi_h + \Phi_{int} + \Phi_{sol} + \Phi_{vent} + \Phi_{tr}^{adj} + HTC(\theta_e - \theta_i) \end{aligned} \quad (3.12)$$

where the HTC accounts for both transmission and infiltration heat losses.

Next, the internal and solar heat gains, intended ventilation losses and transmission losses to adjacent buildings are related to a so-called 'base temperature'  $\theta_b$ ; the outdoor temperature for which the building at  $\theta_i$  is in thermal balance with its environment.

$$\Phi_{int} + \Phi_{sol} + \Phi_{vent} + \Phi_{tr}^{adj} = HTC(\theta_i - \theta_b) \quad (3.13)$$

The indoor temperature is assumed to be quasi-constant, so that heating only is needed when the outdoor temperature is lower than this base temperature. The power for heating the building is then:

$$\Phi_h = HTC(\theta_b - \theta_e)\delta \quad (3.13)$$

with  $\delta=1$  if the outdoor temperature is lower than the base temperature ( $\theta_e < \theta_b$ ) and  $\delta=0$  otherwise.

Plotting the monitored energy consumption as a function of the outdoor temperature typically results in a cloud of data. By performing simple linear regression on this data cloud, the global heat loss coefficient HTC and base temperature  $\theta_b$  can be obtained, as shown in Figure 6.

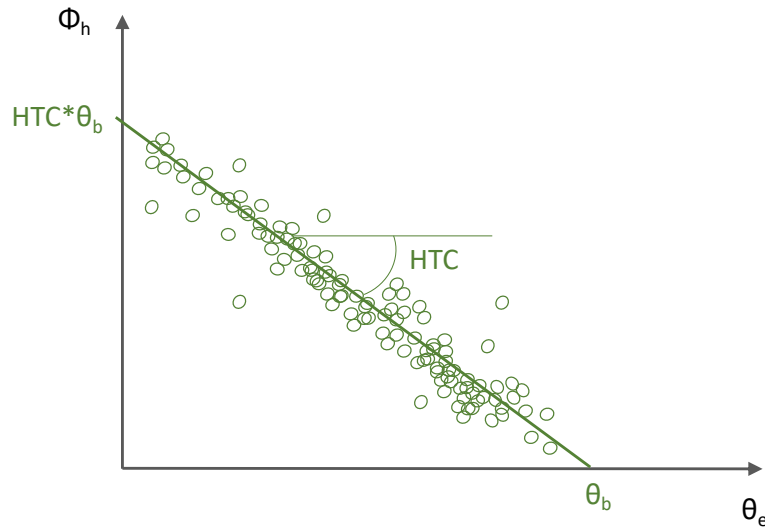


Figure 6. By applying the Energy Signature Method, which is a special version of Linear Regression Analysis, an estimate for the HTC and base temperature  $\theta_b$  can be obtained.

A more elaborated description of the method and its limitations can be found in [Janssens, 2016].

## 3.2. Dynamic methods to determine HTC and HTCtr

### 3.2.1. White-box tuning

Whole Building Energy Simulation (BES) models are nowadays commonly applied to optimise buildings and their energy systems. These BES-models, or so-called white box models, are mainly used in the design phase of new – to be erected – buildings to predict performances and compare design options. In principle, BES-models can also be used to determine the actual physical parameters of an existing building by calibrating the model to on-site measured data. But, although the models try to incorporate all physical phenomena as precisely as possible, they still simplify the full complexity of a building and its many independent interacting variables. Therefore, within the IEA EBC Annex 71-project, white box models were not used to deduce physical parameters from on-site measured data. Instead, the question was how reliable the models are in real world building operation. To answer this question, a detailed empirical validation exercise was performed on a full scale test building to verify the model predictive accuracy of BES-models for real life applications including heating systems and (synthetic) users. All details on this validation exercise can be found in [Kersken and Strachan, 2021].

### 3.2.2. ARX- and ARMAX-modelling

Compared to the methods described in Section 3.1, ARX and ARMAX -models include the dynamics of the data. In the abbreviation, AR stands for AutoRegressive: the current output is related to the previous values of the output; MA (Moving Average) refers to the noise model used, and X refers to the fact that eXternal inputs are used: the system relies not only on the current input value, but also on the history of the input. To apply AR(MA)X-models to assess the HTC of a building, the building is considered as a linear time invariant (LTI) system. For identifying LTI-systems AR(MA)X-models are a standard methodology. The most common ARX-model structure is the simple linear difference equation which relates the current output at time  $t$  to a finite number of past outputs and inputs. For the estimation of the overall heat transfer coefficient, the interior temperature could for instance be taken as output and the outdoor temperature and heat gains as inputs. This would correspond to a multiple input, single output ARX-model, represented as:

$$\varphi(B) \cdot \theta_{i;t} = \omega_h(B) \cdot (\Phi_{h;t} + \Phi_{int;t} + \Phi_{sol;t} + \Phi_{vent;t}) + \omega_e(B) \cdot \theta_{e;t} + \varepsilon_t \quad (3.13)$$

With  $\varphi(B)$  and  $\omega_{h/e}(B)$  back shift operators to take past observations into account. ARX and ARMAX models have among others been applied by Norlén [1994], and were further developed by Jimenez and Heras [2005] for modelling the heat dynamics of buildings and building components. A main problem when applying AR(MA)X-models is first of all

the selection and validation of the model, but then also the extraction of physical information from the model parameters. In an ARX-model, each individual parameter lacks a direct physical meaning. However, steady-state physical parameters can be obtained by calculating the stationary gain of the transfer function from each input to the output. We refer to [Madsen et al., 2016], in which the principles of ARX modelling are extensively described.

An important step in ARX-modelling is to select a suitable model with the appropriate orders of input and output polynomials. Madsen et al. [2016] showed that by stepwise increasing the model order until most significant autocorrelation and cross correlation are removed, a reliable modelling of both stationary and dynamic properties of buildings is feasible.

### 3.2.3. State space models

A final methodology to characterise the HTC of a building is the use of state space models or so-called grey-box models. State space models consisting of simple resistance/capacitance schemes can be used to model the thermal dynamics of a building as a linear time-invariant system, represented as a series of stochastic first-order differential equations (SDEs). Most often a suitable model is identified with a forward model selection approach and the parameters are estimated with the support of statistical tools (e.g. the maximum likelihood technique). In this approach the analysis starts with fitting the simplest feasible model on the basis of physical knowledge, which is then stepwise extended until the loglikelihood no longer increases significantly compared to the previous model and the residuals (the difference between the measured and predicted output) correspond to white noise. Both the initial model and possible extended models are treated as candidate models, which are based on different simplifications of the building's thermal behaviour. Thus, defining those candidate models requires – in contrast to the ARMAX-model – some prior physical knowledge. But, the benefit is that the parameters involved in them have direct physical interpretations. That is why state space models are often referred to as grey-box models. Figure 7 shows as an example of a two-state grey-box model for a one zone building, taking into account heat input by the heater and solar radiation, capacities of the interior and walls, and (conductive) heat flow through the walls.

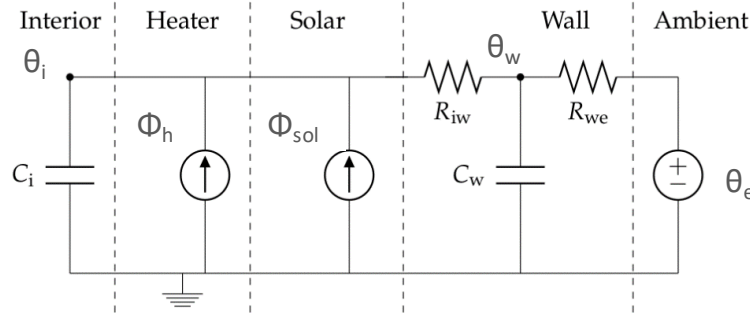


Figure 7. Example of a two-state grey box model applied to characterise the dynamic thermal response of a building.

The two-state grey-box model, visualized in Figure 7, is mathematically represented as two coupled stochastic differential equations:

$$d\theta_i = \frac{1}{C_i} \left( \frac{1}{R_{iw}} (\theta_w - \theta_i) + \Phi_{sol} + \Phi_h \right) dt + \sigma_i d\omega_i(t) \quad (3.14)$$

$$d\theta_w = \frac{1}{C_w} \left( \frac{1}{R_{iw}} (\theta_i - \theta_w) + \frac{1}{R_{we}} (\theta_e - \theta_w) \right) dt + \sigma_w d\omega_w(t) \quad (3.15)$$

and the discrete-time measurement equation is:

$$\theta_{r,t_k} = \theta_i(t_k) + \epsilon_{t_k} \quad (3.16)$$

For more details, we refer to [Madsen et al., 2016], in which the principles of state space modelling are extensively described.



## 4. Determining the input variables

To apply the different statistical methods presented in the previous chapter, we have to determine several input parameters starting from the (limited) on site measured data. In real life applications, several input parameters are not explicitly measured: internal heat gains, infiltration losses, net heat input, solar heat gains, among others. The building physical framework (Chapter 2) and the description of the statistical models (Chapter 3) clearly illustrate that a reliable estimate of the HTC can only be achieved if we are able to determine these input parameters as precisely as possible. Therefore, we revert in this chapter to the (simplified) single zone heat balance

$$C_{i,\text{eff}} \frac{\partial \theta_i}{\partial t} = \Phi_h + \Phi_{\text{int}} + \Phi_{\text{sol}} + \Phi_{\text{tr}} + \Phi_{\text{vent}} + \Phi_{\text{inf}} \quad (4.1)$$

and address successively the different terms and how we can optimise their determination in practical applications. That way, clear guidelines for building parameter identification can be established.

### 4.1. Solar gains

One way to include the solar gains in the single zone heat balance equation for a specific point in time is

$$\Phi_{\text{sol},t} = gA \cdot I_{\text{sol},t} \quad (4.2)$$

where  $\Phi_{\text{sol}}$  is the solar gain,  $gA$  is the solar transmittance (or solar aperture),  $I_{\text{sol}}$  is the global solar irradiation, and the subscript  $t$  represents the time. Note that, compared to Equation (2.10) no distinction is made between direct and diffuse solar radiation and that solar transmittance through all windows is lumped in one solar transmittance  $gA$ . The latter is a function of among others window properties, window orientation, and shading obstacles, information that is costly to collect. Therefore, statistical methods typically rely on simplified methods for estimating solar gains. .

In the following sections, different model formulations of solar gains are described. The first approach neglects solar gains entirely, while the fourth approach models the solar transmittance as a non-linear phenomenon which is affected by window properties and distribution, building geometry, surroundings shading obstacles, etc.

#### 4.1.1. Ignore solar gains

In the first approach solar gains are ignored entirely, in other words:

$$\Phi_{\text{sol},t} = 0 \quad (4.3)$$

Using this approach, the solar gains term in Equation 4.1 will disappear. Consequently, the estimated HTC will be underestimated as heat demand of the building appears to be lower than it actually is.

#### 4.1.2. Constant solar transmittance

In this approach the solar transmittance is treated as constant. With that, the solar transmittance is independent of the sun position. Instead, the average solar transmittance over the course of the day and year is considered. In practice it means that a fixed percentage of the solar irradiation ends up as a contribution to the heat balance – independent of the sun position. This is of course a simplification of reality but might serve as a sufficient model for some buildings.

$$\Phi_{\text{sol},t} = gA \cdot I_{\text{sol},t} \quad (4.4)$$

Note the solar transmittance  $gA$  here is without time index, and therefore treated as constant. This method is identical to what is typically found in the literature, such as in grey-box modeling [Madsen et al., 2016; Jiménez et al., 2008]. The approach is often used in the average and linear regression methods.

#### 4.1.3. Constant solar transmittance for each cardinal direction

As the solar transmittance is not constant over the course of the day, Approach 3 extends the previous approach by considering a constant solar transmittance for each cardinal direction: north, south east and west. The formulation can be expressed as

$$\Phi_{\text{sol},t} = gA^* \cdot I_{\text{sol},t}^* \quad (4.5)$$

where  $I_{sol,t}^*$  is a  $n$ -by-4 matrix with  $n$  being the number of observations, and  $\eta^*$  is a 1-by-4 vector with the four solar transmittances in each direction.

$$I_{sol,t}^* = [I_{sol,t}^{(north)} \quad I_{sol,t}^{(south)} \quad I_{sol,t}^{(east)} \quad I_{sol,t}^{(west)}]_{n \times 4} \quad (4.6)$$

$$(gA^*)^T = [gA^{(north)} \quad gA^{(south)} \quad gA^{(east)} \quad gA^{(west)}]_{1 \times 4} \quad (4.7)$$

Furthermore, the inner parts of  $I_{g,t}^*$  is defined as

$$I_{sol,t}^{(north)} = \begin{cases} I_{sol,t} & \text{for } \gamma_t > 315^\circ \mid \gamma_t \leq 45^\circ \\ 0 & \text{otherwise} \end{cases} \quad (4.8)$$

$$I_{sol,t}^{(south)} = \begin{cases} I_{sol,t} & \text{for } 135^\circ > \gamma_t \geq 225^\circ \\ 0 & \text{otherwise} \end{cases} \quad (4.9)$$

$$I_{sol,t}^{(east)} = \begin{cases} I_{sol,t} & \text{for } 45^\circ > \gamma_t \geq 135^\circ \\ 0 & \text{otherwise} \end{cases} \quad (4.10)$$

$$I_{sol,t}^{(west)} = \begin{cases} I_{sol,t} & \text{for } 225^\circ > \gamma_t \geq 315^\circ \\ 0 & \text{otherwise} \end{cases} \quad (4.11)$$

where  $\gamma_t$  is the azimuth angle of the sun at time  $t$ , and  $\gamma = 0$  corresponds to the north.

#### 4.1.4. Spline based solar transmittance

The fourth approach relies on B-splines. Here the functional relation between the solar transmittance and the sun position (specifically the azimuth angle,  $\gamma$ ) is estimated. The B-spline allows to approach non-linear relationships with a linear model. This is done by transforming a variable—in this case the azimuth angle—into a number of basis splines which ultimately is used as model input in place of the original variable.

$$\gamma_t \xrightarrow{\text{transform}} S(\gamma_t) \quad (4.12)$$

where  $\gamma_t$  is a vector of length  $n$  containing the azimuth angles,  $S(\gamma_t)$  is a  $n$ -by- $m$  matrix with  $m$  being the number of basis splines that  $\gamma_t$  is transformed into. This way the non-linear operations are carried out prior to the model fitting, and the solar gain can now be expressed by

$$\Phi_{sol,t} = S(\gamma_t) \cdot gA \cdot I_{sol,t} \quad (4.13)$$

Where  $gA$  now is a vector containing one parameter for each of the  $m$  basis splines. More information on this approach can be found in [Rasmussen et al., 2020].

#### 4.1.5. Using diffuse and beam irradiation separately

For Approach 3 and 4 (Sections 4.1.3 and 4.1.4) solar radiation is treated as directional, i.e. the solar transmittance is dependent on the sun position. To refine Approach 3 and 4 diffuse and direct irradiation can be treated separately. This is done by estimating the solar gain related to beam irradiation as already shown in Approach 3 and 4 with the only exception that the global irradiation ( $I_{sol,t}$ ) is replaced with the beam irradiation ( $I_{b,t}$ ). Additionally, the solar gain contribution from the diffuse omnidirectional irradiation ( $I_{d,t}$ ) can be estimated as constant proportion of the diffuse solar irradiation.

As an example, Approach 3 can be extended to

$$\Phi_{sol,t} = I_{b,t}^* \cdot gA_b^* + I_{d,t} \cdot gA_d \quad (4.14)$$

and Approach 4 can be extended to

$$\Phi_{sol,t} = S(\gamma_t) \cdot gA_b \cdot I_{b,t} + gA_d \cdot I_{d,t} \quad (4.15)$$

Examples of this approach can be found in [Rasmussen et al., 2020; Zhang et al., 2021].

In this report Approach 5 in Section 6.1 refers to Equation 4.14.

## 4.2. Heat input

In this section, the objective is to list different approaches that can be used to model the heat input into the house. Evidently, the heat input is among the most significant heat balance contributions, especially during the heating season. Measurements of the net heat input to the individual zones of the building are commonly not available. Moreover, often only gross energy use measurements before the heat generator are available, and it is unclear which part is used to produce space heating (SH), and which part is used to produce domestic hot water (DHW). In this section different model formulations, and different input packages are considered to evaluate the impact on the assessment of HTC. A visual representation of the investigated approaches is shown in Figure 8.

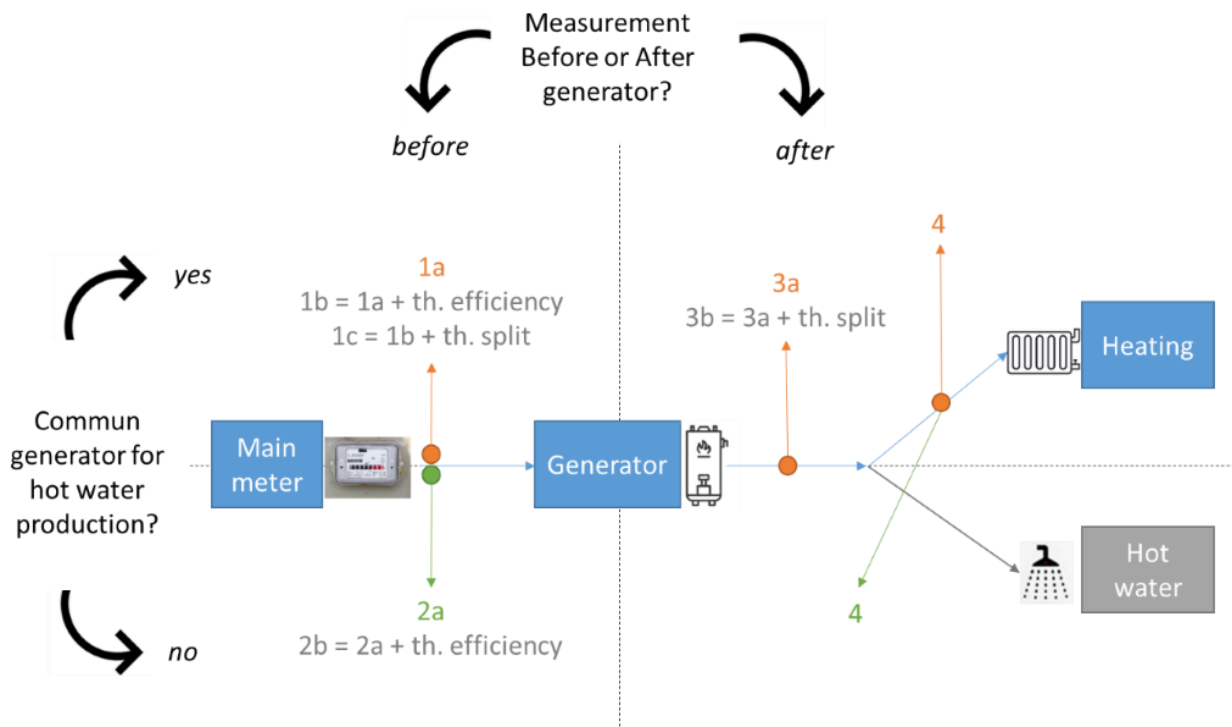


Figure 8. Nomenclature of the heat input accuracy for different production and measurement scenarios

To investigate the impact of the inputs we have available, and the assumptions we make to approach the actual situation, we consider four approaches, going from less (group 1) to more (group 4) accurate:

- Approach 1: Measurement taken before the generator, common for SH+DHW
- Approach 2: Measurement taken before the generators, separate for SH and DHW
- Approach 3: Measurement taken after the generator, common for SH+DHW
- Approach 4: Measurement taken after the generator for SH

### 4.2.1. Measurement taken before the generator, common for SH+DHW

In this approach, we consider measurements taken before the generator, and the generator provides for both space heating and domestic hot water. Based on knowledge of the heating system and experience, we can assume a theoretical efficiency of the generator and a theoretical split between SH and DHW. Three scenarios can be discerned:

- No theoretical generator efficiency used (accuracy 1a)
- Theoretical generator efficiency used (accuracy 1b)
- Theoretical generator efficiency and theoretical split DH and DHW (accuracy 1c)

Splitting SH and DHW is not straightforward. Moreover, part of the drained DHW might provide useful heat gains. A step further from a theoretical split of the DHW consumption is the application of different statistical methods designed to perform this separation. Those methods usually rely on the identification of patterns in the data or perform as filters and detect peaks in consumption. The method used in this work is the *Non-parametric method for separating domestic hot water heating spikes and space heating* [Bacher et al., 2016]. This method is also applicable in case when a

common measurement is taken for SH and DHW after the generator. The drawback of this approach is that it can be used only in cases where SH and DHW are generated instantaneously by the boiler because the existence of buffers and DHW tanks affects the dynamic of the SH and DHW demand.

#### 4.2.2. Measurement taken before the generators, separate for SH and DHW

With two separate generators for SH and DHW, two scenarios remain:

- No theoretical generator efficiency used (accuracy 2a)
- Theoretical generator efficiency used (accuracy 2b)

#### 4.2.3. Measurement taken after the generator, common for SH+DHW

With measurements of the *net* heating energy use for both SH and DHW, we can discern two scenarios:

- No theoretical split DH and DHW (accuracy 3a)
- Theoretical split DH and DHW (accuracy 3b)

#### 4.2.4. Measurement taken after the generator for SH

With separate measurements of the *net* heating energy use for SH and DHW, this is the most accurate approach possible. In accuracy 4, we need not make assumptions about the generator efficiency nor about the split between SH and DHW.

### 4.3. Infiltration heat loss and ventilation heat loss

In the Building Physical Framework (see Chapter 2) and the corresponding simplified heat balance equation (4.1), a distinction is made between the heat gain (or loss) caused by an intended air change by mechanical ventilation  $\Phi_{vent}$ , and by the uncontrolled infiltration heat exchange  $\Phi_{inf}$ . The latter might also include natural ventilation. When looking at ventilation and infiltration we investigate two questions:

1. Mechanical ventilation: if we explicitly include the heat exchange from mechanical ventilation in the models (e.g. linear regression, grey-box models), what is the effect on the estimation of HTC?
2. Infiltration: can we split HTC into  $HTC_{tr}$  and  $HTC_{inf}$ , and how?

The intentional ventilation heat exchange  $\Phi_{vent}$  comes from outdoor at temperature  $\theta_e$  with heat recovery efficiency  $\eta_{HR}$ ), adjacent unheated room at temperature  $\theta_u$ , and other neighbouring zones at temperature  $\theta_n$ :

$$\Phi_{vent} = (1 - \eta_{HR})c_a G_{a,vent}^e (\theta_e - \theta_i) + c_a G_{a,vent}^u (\theta_u - \theta_i) + c_a G_{a,vent}^n (\theta_n - \theta_i) \quad (4.16)$$

with  $\eta_{HR}$  the heat recovery efficiency (zero without),  $c_a$  the specific heat capacity of air and  $G_a$  the air flow rate in kg/s.

**Infiltration** gains/losses arise along leakage paths, and may come from separate flows. Often, however, it is considered that infiltration is only a direct exchange with the outdoor air:

$$\Phi_{inf} = c_a G_{a,inf}^e (\theta_e - \theta_i) \quad (4.17)$$

Following the hypotheses presented in section 2.4, the  $HTC$  and  $HTC_{tr}$  are defined in steady-state as:

$$\Phi_{tr} = HTC_{tr} (\theta_e - \theta_i) \quad (4.18)$$

$$\Phi_{tr} + \Phi_{inf} = HTC (\theta_e - \theta_i) \quad (4.19)$$

By incorporating the infiltration losses through the building fabric, the definition of the  $HTC_{tr}$  can be extended to the definition of the heat loss coefficient  $HTC$ :

$$HTC = HTC_{tr} + \frac{\Phi_{inf}}{\theta_e - \theta_i} = HTC_{tr} + H_{inf} \quad (4.20)$$

According to this definition, the  $HTC$  does not incorporate the heat exchange from controlled ventilation.

#### Balanced vs. unbalanced ventilation

When infiltration and mechanical ventilation air flow rates are combined, the solution is simple additivity assuming the ventilation system has balanced flow. Because a balanced ventilation system does not impact internal pressure or the

air flows through the envelope. In case of unbalanced systems, most commonly buildings with exhaust ventilation fans, they change the internal pressures and therefore need special consideration.

Ventilation heat loss can be calculated from measurements of supply temperature, indoor temperature and ventilation flow rate.

$$\Phi_{\text{vent}} = c_a G_{a,\text{vent}}^e \frac{(1 - \eta_{\text{HR}})(\theta_e - \theta_i)}{(\theta_{\text{sup}} - \theta_i)} \quad (4.21)$$

If the supply temperature is not known, it should be estimated using the efficiency of the heat recovery  $\eta_{\text{HR}}$ . If there is no HR then  $\eta_{\text{HR}} = 0$  and the supply temperature is the external temperature.

- In this case, the small temperature rise over fans can be considered included in the temperature efficiency of the HR (one can consider 90 % of the fan power to be converted into heat which typically lead to a 0.5-1 °C temperature rise over the supply fan, but lost on the exhaust side, assuming the exhaust fan is located after the HR-unit).
- Duct losses and short-circuiting of supply and extract (for example surrounding the outlet & inlet on the building facade) may also impact ventilation efficiency, supply temperature and ventilation heat exchange. This may explain higher heat recovery efficiency than expected when efficiency is estimated based on supply temperature, indoor and outdoor temperatures.
- Some ventilation units have a heating coils on the supply side in addition to heat recovery (and/or a pre-heating coil operated for frost-protection). On residential units the heating coil is rarely hydronic (as is more common in large buildings), more commonly it is direct electric heating. Ventilation heating should be considered in the energy balance to adhere to the building physical framework, and in this case the supply temperature or at least the supply heating set-point (and operation strategy) will be needed.
- It may also be relevant to know whether the ventilation unit and ductwork is located inside or outside of the heated building area (i.e. on an unheated attic, or basement).

With unbalanced (typically buildings with exhaust ventilation fans), the pressure changes can impact natural infiltration non-linearly and make it sub-additive. [Hurel et al., 2016] reviewed different approaches and proposed new sub-additive methods that are more robust across the full spectrum of air-tight to leaky buildings. In ESP-r's implementation of the AIM-2 model, the calculated natural infiltration air flow is adjusted subsequently by the Kiel-Wilson approach [Kiel and Wilson, 1987].

$$Q_t = \left( (Q_{\text{inf}})^{\frac{1}{n}} + (0.5Q_f)^{\frac{1}{n}} \right)^n + 0.5Q_f \quad (4.22)$$

Where the net air flow rate from outdoors  $Q_t$  is caused by the combined influence of natural infiltration  $Q_{\text{inf}}$  and the unbalanced portion of the mechanical ventilation  $Q_f$ .

#### 4.3.1. Simplified infiltration models

Many infiltration models for residential buildings have been developed based on statistical fits of infiltration data. Most empirical models rely on pressurization results (commonly obtained from blower door tests) and use flow theory and statistical techniques to fit data to common housing characteristics, but not all models are dependent on weather conditions. A review of applicable models for air infiltration calculations is given by Orme [1999].

By considering weather is the dominant driving force, infiltration flow can be assumed to be linearly dependent on the outside-inside temperature difference and/or wind-speed. According to Sherman & Grimsrud [1980], previous work at that time had been found to be quite accurate for the site where the data was taken.

The Alberta Air Infiltration Model (AIM-2) can be expressed on the convenient form below where the calculated potential specific infiltration flow rate  $Q_{\text{inf}}^*$  multiples with the infiltration coefficient  $C_{\text{inf}}$ . This flow coefficient can be estimated or obtained by using data from blower door pressurizations tests. AIM-2 uses a superposition technique where the infiltration flow rates due to wind and stack effects are added, and in addition an interaction term is introduced.

$$Q_{\text{inf}} = C_{\text{inf}} \left( (Q_s^*)^{\frac{1}{n}} + (Q_w^*)^{\frac{1}{n}} - 0.33(Q_w^* Q_s^*)^{\frac{1}{2n}} \right)^n \quad (4.23)$$

The power law models the relationship between the indoor–outdoor pressure difference and the airflow rate through the leaks in the building envelope. Infiltration rates due to stack and wind effects are calculated as

$$Q_s^* = C_s (\Delta P_s)^n = C_s \left( \frac{9.8 \text{Hpa} |T_e - T_i|}{T_i + 273.15} \right)^n \quad (4.24)$$

$$Q_w^* = C_w (\Delta P_w)^n = C_s (0.5U^2 \lambda_w^2 \rho_a)^n \quad (4.25)$$

Infiltration models are sensitive to parameters used for converting wind data measured at a weather station to the building site and for local wind shelter effects from typography and nearby buildings. This uncertainty can be reduced by wind measurements on site.

#### 4.3.2. Accounting for mechanical ventilation in the estimation of HTC

The heat exchange from mechanical ventilation may result from several supply air flows at different temperatures and flow rates. It can however be more simply expressed as:

$$\Phi_{\text{vent}} = c_a G_{a,\text{vent}}^e (1 - \eta_{\text{HR}})(\theta_e - \theta_i) \quad (4.26)$$

$$\Phi_{\text{vent}} = c_a G_{a,\text{vent}}^e (\theta_{\text{sup}} - \theta_i) \quad (4.27)$$

If the ventilation (mass or volumetric) flow rate is not directly measured, we can use the electricity consumption of the ventilation system instead. The volumetric flow rate  $Q$  ( $\text{m}^3/\text{s}$ ) relates to the static pressure  $\Delta p$  (Pa), the fan efficiency and the power of the ventilation system  $P_v$  (W) as:

$$\eta = \frac{Q\Delta p}{P_v} \quad (4.28)$$

If we assume that the static pressure drop of the ventilation system  $\Delta p$  is proportional to  $Q^2$ , this implies that the mass flow rate can be roughly considered proportional to the power of the ventilation system  $P_v$  with a 1/3 exponent:

$$\dot{m}_{\text{vent}} \propto P_v^{\frac{1}{3}} \quad (4.29)$$

**Summary:** measurements required to estimate  $\Phi_{\text{vent}}$

- Either the ventilation flow rate  $G_{a,\text{vent}}^e$  or the electricity consumption of the ventilation system  $E_v$  (kWh). In the latter case, an extra parameter will have to be identified.
- If the air supply temperature ( $^{\circ}\text{C}$ ) is not measured, the heat recovery efficiency HR should either be known or estimated.

We can then extend the linear regression and energy signature methods with an additional term. For instance, the “Linear Regression 2” approach (Section 3.1.2) with ventilation reads:

$$\Phi_h + \Phi_{\text{int}} + \Phi_{\text{vent}} = \text{HTC}(\theta_i - \theta_e) - gA_{\text{sol}} \quad (4.30)$$

Or, if the supply flow rate is not measured but the energy consumption of ventilation and the air supply temperature is measured:

$$\Phi_h + \Phi_{\text{int}} = \text{HTC}(\theta_i - \theta_e) - gA_{\text{sol}} - a_v E_v^{\frac{1}{3}} (\theta_{\text{sup}} - \theta_i) \quad (4.31)$$

#### 4.3.3. Splitting the HTC into $\text{HTC}_{\text{tr}}$ and $\text{HTC}_{\text{inf}}$

“Natural ventilation” includes air infiltration and air flow through open windows and doors. We are only interested in the infiltration part, which is part of HTC. Supposing air infiltration occurs at the ambient temperature with a total mass flow rate  $m_{\text{inf}}$ , the related heat flow is:

$$\Phi_{\text{inf}} = c_a G_{a,\text{inf}}^e (\theta_e - \theta_i) \quad (4.32)$$

And the  $\text{HTC}_{\text{inf}}$  coefficient is simply

$$\text{HTC}_{\text{inf}} = \frac{\Phi_{\text{inf}}}{(\theta_e - \theta_i)} = c_a G_{a,\text{inf}}^e \quad (4.33)$$

The infiltration air flow rate is driven by the outdoor-indoor temperature difference  $\Delta p$ , wind and buoyancy effects. If we suppose that:

- Stack effects are negligible in a relatively small building
- Wind predominantly follows one direction and has a variable speed  $V$

Then we can approximate the infiltration air flow rate linearly:

$$G_{a,\text{inf}}^e = a_1 \sqrt{\Delta p} + a_2 V \quad (4.34)$$

where the  $a_1$  and  $a_2$  coefficients can be estimated by linear regression along with the other parameters of the model. There is however an issue with this formulation: the amplitude of the pressure difference  $\Delta p$  that drive the air flow is usually too small to be measured.

Alternatively, the infiltration air flow rate or the total air flow rate (including mechanical ventilation) can be measured by a tracer gas method, or by using the  $\text{CO}_2$  concentration emitted by occupants (warning: this is not easy if the flow is variable).

If we wish to separate mechanical ventilation from unintended infiltration, two separate source terms  $\Phi_{vent}$  and  $\Phi_{inf}$  should be used in all models.

Supposing that the wind speed  $V$  and the outdoor-indoor pressure difference  $\Delta p$  are measured, the infiltration mass flow rate can be estimated by linear regression:

$$\Phi_h + \Phi_{int} + \Phi_{vent} = \text{HTC}(\theta_i - \theta_e) - gA_{I_{sol}} + \underbrace{c_a G_{a,inf}^e(\theta_i - \theta_e)}_{\Phi_{inf}} \quad (4.35)$$

$$\Phi_h + \Phi_{int} + \Phi_{vent} = \text{HTC}(\theta_i - \theta_e) - gA_{I_{sol}} + a_1 c_a \sqrt{\Delta p}(\theta_i - \theta_e) + a_2 c_a V(\theta_i - \theta_e) \quad (4.36)$$

By estimating  $a_1$  and  $a_2$  (for instance by linear regression), we can then compute the average mass flow rate and the  $H_{inf}$  coefficient using the formulas shown above.

#### 4.4. Occupant and appliance heat gains

The Building Physical Framework includes the internal heat gains ( $\Phi_{int}$ ) into the overall heat balance. The largest share of internal heat gains is typically attributed to the use of lighting and appliances and the presence of inhabitants, i.e. metabolic heat gains ( $\Phi_{inhab}$ ). Electric heating of DHW, dish washer and washing machine also introduce heat gains as the water is drained.

$$\Phi_{int} = \Phi_{lighting} + \Phi_{appliances} + \Phi_{inhab} \quad (4.37)$$

Whilst the first two term are straightforward to include by measuring the electricity consumption, accounting for the latter is more challenging due to its stochastic character. Lighting and appliance heat gains are added in Approach 1. Approaches 2 to 5 comprise four methods to determine metabolic heat gains ( $\Phi_{inhab}$ ).

##### 4.4.1. Lighting and appliance heat gains

This modelling approach accounts for heat gains due to lighting and house appliances, by including the electricity consumption as a term that yields heat gains.

##### 4.4.2. Using standardized occupancy profiles from the ISO 17772-1 standard.

Appendix N of the standard [ISO, 2017] provides default occupant schedules for a variety of buildings. The standardized usage factors (hourly values) are multiplied by the standardized occupant heat gains ( $2,8 \text{ W m}^{-2}$ ) and the net floor area of the building.

##### 4.4.3. Using measurements of relative humidity (RH) to determine presence.

In this modelling approach, metabolic heat gains are estimated based on RH measurements.

First, the measured relative humidity (RH) is converted to absolute humidity:

$$P_{vs} = e^{(C_1\tau + C_2\tau^{1.5} + C_3\tau^3 + C_4\tau^{3.5} + C_5\tau^4 + C_6\tau^{7.5}) \frac{T_C}{T}} \cdot P_C \quad (4.38)$$

In which  $P_{vs}$  is the saturated vapour pressure (Pa),  $C_1$  to  $C_6$  are constants ( $C_1 = -7.85951783$ ,  $C_2 = 1.84408259$ ,  $C_3 = -11.7866497$ ,  $C_4 = 22.6807411$ ,  $C_5 = -15.9618719$ ,  $C_6 = 1.80122502$ ),  $\tau$ :  $1 - (T/T_C)$ ,  $T$  the temperature in the building zone under consideration (K) and  $T_C$  and  $P_C$  the critical temperature (647.096 K) and pressure (22064 kPa).

The actual vapour pressure ( $P_w$ ) is calculated as follows:

$$P_w = \text{RH} \cdot P_{vs} \quad (4.39)$$

In which  $P_w$  is the actual vapour pressure (Pa) and RH th relative humidity (%). Finally, the absolute humidity (AH) in ( $\text{g/m}^3$ ) is calculated as:

$$AH = C \cdot \frac{P_w}{T} \quad (4.40)$$

with C: 2.16679 g K J<sup>-1</sup>

Second, based on the obtained absolute humidity time series the occupant presence is deduced. Third, metabolic heat gains ( $\Phi_m$ ) are calculated by multiplying occupant presence with a standardized metabolic heat rate of 2,8 W m<sup>-2</sup> [ISO, 2017] and the floor area of the room in question.

#### 4.4.4. Using measurements of CO<sub>2</sub> to determine presence.

If available, metabolic heat gains can also be estimated based on CO<sub>2</sub> measurements. First, the measured CO<sub>2</sub> concentration in ppm is converted to mg m<sup>-3</sup>, using the Ideal Gas Law:

$$C \left[ \frac{\text{mg}}{\text{m}^3} \right] = \frac{1}{1000} \cdot C[\text{ppm}] \cdot \frac{M_{\text{CO}_2} \left[ \frac{\text{g}}{\text{mol}} \right]}{R \left[ \frac{\text{J}}{\text{mol K}} \right] \cdot \frac{T[\text{K}]}{p[\text{Pa}]}} \quad (4.41)$$

In which C is the CO<sub>2</sub> concentration in the building zone under consideration, M<sub>CO<sub>2</sub></sub> the molecular weight of CO<sub>2</sub> (44.01 g mol<sup>-1</sup>), R the Ideal Gas Constant (8.314 J K<sup>-1</sup> mol<sup>-1</sup>), T the temperature in the building zone under consideration and P the atmospheric pressure. For the latter, one atmosphere (101,325 Pa) can be used in absence of on-site measurements.

Second, based on the obtained CO<sub>2</sub> concentration (mg m<sup>-3</sup>) time series the occupant presence is deduced. Third, metabolic heat gains ( $\Phi_m$ ) are calculated by multiplying occupant presence with a standardized metabolic heat rate of 2,8 W m<sup>-2</sup> [ISO, 2017] and the floor area of the room in question.

#### 4.4.5. Estimating the metabolic heat input using a CO<sub>2</sub> balance.

The CO<sub>2</sub> emission rate (E) can be estimated using the following formula [Batterman, 2017]:

$$V \frac{dC}{dt} = E + QC_R - QC \quad (4.42)$$

In which V is the volume (m<sup>3</sup>) of the building zone, C the CO<sub>2</sub> concentration in the building zone (mg/m<sup>3</sup>), C<sub>R</sub> the CO<sub>2</sub> concentration in the replacement air (mg/m<sup>3</sup>), E (mg/m<sup>3</sup>) the CO<sub>2</sub> emission rate and Q the air change rate (m<sup>3</sup>/s) of the building zone under consideration.

Whilst V is known, and the gradient dC/dt can be derived from the data, C<sub>R</sub> and Q need to be estimated.

The CO<sub>2</sub> concentration in the replacement air (C<sub>R</sub>) depends on the source of the air. If the replacement air originates from outdoors, this may be approximated by using C = 400 ppm. For T, the outdoor temperature is to be used for natural ventilation and infiltration. In case of a mechanical ventilation system, the supply temperature of the ventilation air can be used. If the replacement air originates from other building zones, a measured CO<sub>2</sub> concentration and temperature is necessary.

When the electricity consumption of a mechanical ventilation system is measured, the ventilation flow rate may be approximated using the power of the ventilation system (P<sub>v</sub>), with a 1/3 exponent (see Section 4.3). In the absence of (measurements of) a mechanical ventilation system, a standardized ventilation rate (0.5 l s<sup>-1</sup> m<sup>-2</sup>, ISO 17772-1) may be used. With all the other parameters known, the emission rate E can now be calculated. By dividing this emission rate by standardized figures on CO<sub>2</sub> respiration rates [Persily and de Jonge, 2017], the number of occupants can be calculated. The number of occupants can then be multiplied by standardized metabolic heat rates [ISO, 2004].

## 4.5. Weather data

Weather phenomena impact the thermal performance of buildings and are essential inputs describing boundary conditions and driving dynamics in building thermal energy characterization. Ideally, short-interval environmental data is observed at the building site at intervals corresponding to the modelling time-step, but on-site measurements are not always available. Furthermore, some elements are easier to measure than others (complexity due to cost, maintenance, etc.) making it relevant to consider what alternative weather data sources and strategies exist to represent local conditions.

On regional level, national weather centres are increasingly releasing detailed weather observations and climate information and making it easily available free-of-charge e.g. according to Open Geospatial Consortium standards [OGC, 2020]. In Europe, the INSPIRE directive is an initiative that aims to build a European spatial data infrastructure

to ease the access to public data through standardisation of data and APIs. The services under development cover more than meteorology, releasing spatial information to the public from sectors monitoring land use and land cover, terrain, buildings, constructions, and cadastral information. Moreover, the EU Copernicus Earth observation programme, has operated a policy of open data since its inception and the ECMWF (European Centre for Medium Range Weather Forecasts) is moving towards a policy of open data (ECMWF: <https://www.ecmwf.int/en/about/media-centre/news/2020/ecmwf-moves-towards-policy-open-data>). Regional developments like the above, represents opportunities to acquire localized information on building site specific surroundings and climatic conditions.

Climate reanalysis datasets and web-services combining model data with observations from remote sensing weather orbiting satellites or large-scale observational networks on the land surface are sailing up as alternatives to acquire data capturing weather phenomena that are not measured on-site. Climate reanalysis combines numerical weather prediction (NWP) models of the atmosphere and land surface with observations into a complete dataset on global or regional scale. Reanalyses in particular have the advantage of providing consistent data spanning back several decades, avoiding some of the common quality issues such as missing data, gaps or instrument drift, that can arise from maintaining an on-site weather station.

Climate reanalysis datasets with hourly resolution continuously updated in near real-time is a recent development, making data available up to recent date and spanning several decades back. Currently several operational reanalyses are in production, and those that cover the whole of Europe are summarised in Table 1. Other recent high-resolution regional reanalysis datasets for Europe include COSMO-REA6, NEWA and UERRA, spanning 1995-2017, 1989-2018 and 1961-2019 respectively.

Table 1. Operational reanalysis produced by ECMWF members (European Centre for Medium Range Weather Forecasts) available in the Copernicus C3S CDS (Climate Data Store).

	ERA5	ERA5-Land	CERRA and CERRA-land
Coverage	Global reanalysis	Global reanalysis (replay of land surface)	Regional reanalysis for Europe
Resolution	31 km	9 km on surface level	5.5 km on surface level
Timespan	1950 to present	1950 to present	1961 to present
NWP model	IFS cy41r2	IFS cy41r2	HARMONIE cy40.1h/42
Update frequency	3-5 days delay in ERA5T, or about three months delay for the monthly quality checked product.	Monthly quality checked product with a delay of about three months (Soon synchronized with ERA5T in ERA5-LandT).	Not available yet, in production (expected summer 2021).

Some of the most relevant weather variables in the ECMWF ERA5/CERRA reanalysis products are:

- 2t: External air temperature at 2 meters
- r2m: Relative humidity at 2 meters
- 10u, 10v: Wind speed ( $\sqrt{10u^2+10v^2}$ ) and wind direction at 10 m ( $\text{atan2}(10u,10v)+\pi$ )
- strd: Sky temperature from surface thermal radiation downwards:  $(\text{strd}/5.67e-8)^{0.25}-273.15\text{K}$
- stl3, stl4: Soil temperature at level 3 (28-100 cm) and level 4 (100-289 cm) below ground surface
- fdir: Total sky direct radiation at surface (equivalent to beam horizontal irradiance)
- ssrd: Surface solar radiation downwards (equivalent to global horizontal irradiance)
- ssr: Surface solar radiation to calculate surface broadband albedo ( $1-(\text{ssr}/\text{ssrd})$ )

In addition to the listed variables, surface model parameters like forecasted surface roughness, forecasted albedo, land cover, leaf area index, snow depth, density and coverage in the grid cell can be valuable for pre-processing. For example, the forecasted model surface roughness can be used in downscaling of the wind speed or in diagnostic models, or snow cover and depth can be used to estimate ground reflectance (see Section 4.5.1).

When it comes to solar radiation it is possible to use surface downwelling radiation from the reanalysis models, but other products based on remote sensing techniques exist with greater temporal and spatial resolution. Several studies have shown that reanalysis is accustomed to over estimation of solar radiation, while underestimation is observed in satellite methods [Babar et al., 2019]. Many historical radiation databases like SARAH and CM-SAF are produced from

processing images from geo-stationary weather satellites [PVGIS: <https://ec.europa.eu/jrc/en/PVGIS/docs/othersources>]. Operational services are also available in near real-time or real-time like the free to use Copernicus CAMS Radiation Service (CAMS-Rad) or HelioClim-3 and Solcast, two examples of commercial web-services providing both historical datasets and forecasts with uncertainty predictions.

#### 4.5.1. Preprocessing

Some weather variables may require pre-processing. Modelling techniques are commonly used to generate required items like solar irradiance or sky temperature estimations, filling gaps, reconstructing shorter time steps from hourly data, or adjusting data to account for urban effects [Crawley, 2019].

With knowledge of the surroundings, we can use simple relations to adapt the weather data to better fit local conditions. This may be particularly useful if observations are sourced from a site far away (or multiple sites), or working with gridded reanalysis data or forecasts, especially when variables are based on model grid cell averages that cover a larger geographic area with heterogenous characteristics. For air temperature, common relations are nearest neighbour selection, bilinear correlation and altitude corrections, or more sophisticated kriging techniques.

Wind speed is an element greatly influenced by local surroundings that is rarely measured on-site and subject to variation over small spatial and temporal scales. Commonly observations are sourced from airports or wind towers located in open landscape. Similarly, the ERA5 reanalysis surface wind speed at 10-meter represent potential wind speed in open grassland (surface roughness  $z_0=0.03$  meter). Power-law or log-law wind profile relations can be used to convert the wind speed from one site to another using boundary layer similarity theory [Skeie et al., 2021]. These conversion methods require surface roughness estimates. To include local wakes and canyon effects more advanced techniques are needed.

Many techniques exist to measure the combination of direct and diffuse solar radiation on a façade or on the horizontal (total sky irradiance) e.g. from high precision pyranometers to cheaper refence based PV-cells. In case direct (beam) irradiance or the diffuse component is not measured directly, solar separation models are useful to estimate the diffuse and direct part from global horizontal irradiance. A separation of direct and diffuse radiation (from the sky and surroundings) is needed to perform calculations of vertical irradiance on facades, or tilted roofs, and for detailed shading analysis. The most common separation models are derived empirically and utilizes a clear sky model as part of the transformation, together with a solar positioning algorithm.

Both physical models and data-driven techniques may benefit from knowing the solar azimuth and zenith angle which can be obtained as part of a pre-processing step and supplied in the inputs knowing the building position. In Section 6.5, from the acquired diffuse horizontal and beam normal irradiance, we used the Perez method [ISO 52010-1:2017] to calculate vertical unshaded irradiance for each façade orientation. The result was presented as a direction independent unshaded vertical diffuse irradiance (including uniform sky, horizon band and reflected radiation from flat ground) and the direct (beam and circumsolar) irradiance for each façade direction together with the solar positioning angles.

To estimate ground reflectance (albedo) for radiation calculations, one approach is to utilize surface variables from ERA5-Land and radiation quantities from the ERA5 atmospheric reanalysis. For the case study buildings (see Chapters 5 and 6), we first calculated the surface broadband albedo ( $1-(ssr/ssrd)$ ) when the sun is above the horizon from ERA5 data and used the forecasted surface albedo  $fal$  variable at night. This resulted in a ground reflectance of approximately 0.14 at daytime in winter. To account for increased reflectance when the ground is covered by snow we used the two factors: snow coverage in grid cell,  $snowc$ , and snow albedo,  $asn$ , from the ERA5-Land surface dataset. We scaled between the two by the following function:

$$\text{albedo} = \text{snowc} \cdot \text{asn} + (1 - \text{snowc}) \cdot \max(1 - (\text{ssr}/\text{ssrd}), \text{fal}) \quad (4.43)$$

Sky temperature, either sourced from atmospheric reanalysis or derived from empirical correlations of outdoor temperature and cloud cover, can also be used in surface resistance calculations, or indirectly included by substituting part of the outdoor temperature in an equivalent outdoor temperature (so-called sol-air temperature). We included the sky temperature calculated from the  $strd$  quantity in ERA5 for the cases were on-site measurements or observations of sky conditions were not available.

## 4.6. Indoor temperature

The static and dynamic methods presented in the Building Physical Framework are meant to characterize the HTC of a building considered as one single zone. Consequently, Equation (4.1) requires a representative global indoor temperature  $\theta_i$ , which is never directly measured and hence not available. Determination of the aggregated indoor

temperature is optimally based on measured data of each room within the building. Such an extensive data set is commonly not available and we have to keep in mind that even within one room local differences will occur for instance due to stratification. Figure 9 and Figure 10 illustrate this effect occurring in on of the case studies: the Twin test houses in Holzkirchen, Germany (see Section 5.1). The Holzkirchen N2 house is heated by electric radiators and suffers from significant stratification in all rooms, compared to the O5 house, which is identical to the N2 house, but heated with an underfloor heating system.

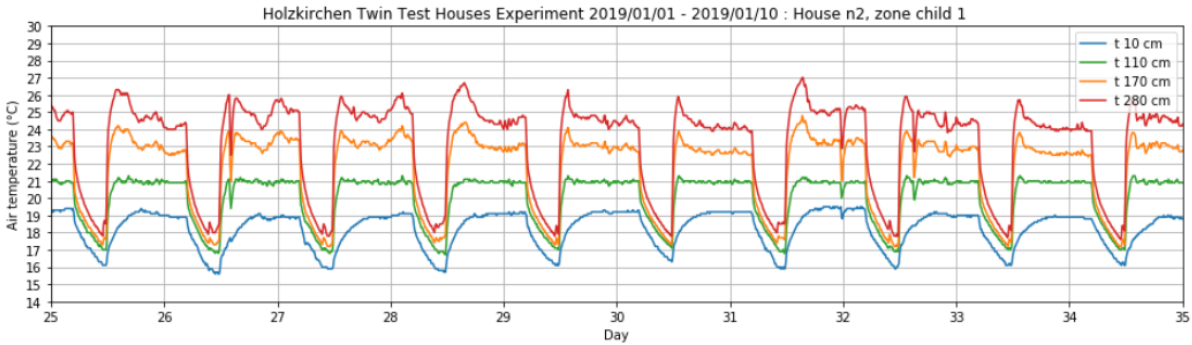


Figure 9. Room temperatures measured at different heights in bedroom 1 of Holzkirchen house N2, heated by electric radiators , from 2019/01/01 to 2019/01/10.

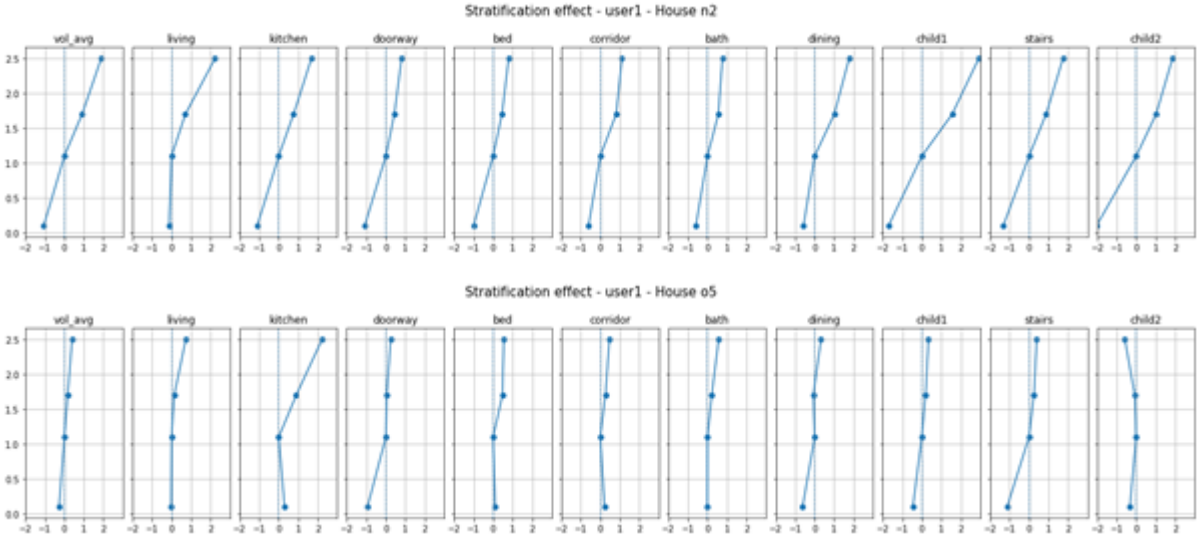


Figure 10. Average temperature difference with the temperature measured at 1.10 m height, over the room height, in house N2 (up) and O5 (down).

Figure 10 furthermore clearly demonstrates that the interior temperature within the house is not identical for the different room. Applying the single-zone heat balance equation hence requires an equivalent homogeneous indoor temperature. Different approaches to do so can be determined based on the available sensor setup. This section describes the most common ones. In this report the impact of the approach on the obtained HTC accuracy will be investigated for the case studies described in Chapter 5. A more detailed analysis on synthetic data has been performed by [Senave et al, 2020].

**4.6.1. No measured data available**

If no measured data is at hand, room temperatures can be assumed equal to constant values suggested in standards (e.g. national standards on EPBD-regulations). Alternatively, if available, the setpoint temperatures of the room thermostat could be used as global indoor temperature.

#### 4.6.2. One sensor in the main living room

If we have to rely on on-board measured data, often only the indoor temperature as measured by the room thermostat in the living room is available. This indoor temperature can be used as input for the single zone heat balance equation. However, as most dwellings typically maintain a significant lower temperature in the night zone of the dwelling, a second indoor temperature can be synthetically created based on the assumption that the night zone of a dwelling is always 2° Celsius lower than the living room temperature. This value of 2°C stems from the difference between the temperatures prescribed by the Belgian ('BE') Annexes to standard EN 12831-1 (heat load calculation) for a living room and bedroom. The measured and synthetic signal can then weighted according to the methods described in Section 4.6.4.

#### 4.6.3. Measurements in all different heating zones

Measured data of all rooms are seldomly available. If more than one measurement point is present, typically the living room and one of the sleeping rooms is monitored to get an idea of the indoor temperature in the main heating zones. In this case similar weighing methods can be used as when data of all rooms are available.

#### 4.6.4. Detailed measurements in all rooms

This is considered as the highest amount of measured data, as it assumes the air temperature to be measured in all rooms of the building. To determine the equivalent indoor temperature different weighing of the measured data can be applied:

- a) Simple arithmetic mean of the measured values  
In this case the global indoor temperature at each time step  $t$  is determined as the sum of all data points, divided by the number of sensors:

$$\theta_i^t = \frac{\sum_{j=1}^n \theta_{ij}^t}{n} \quad (4.44)$$

- b) Volume weighted mean of the measured values  
Instead of averaging the monitored temperatures, they can be weighted according to the volume  $V_j$  of each room  $j$ :

$$\theta_i^t = \frac{\sum_{j=1}^n V_j \theta_{ij}^t}{\sum_{j=1}^n V_j} \quad (4.45)$$

- c) Averaged weighted mean of the measured values

Weighing of the monitored temperatures can also be done according to the facade area  $A_j$  of each room  $j$ :

$$\theta_i^t = \frac{\sum_{j=1}^n A_j \theta_{ij}^t}{\sum_{j=1}^n A_j} \quad (4.46)$$

Equation (4.46) in essence assumes the HTC equally distributed over the facade area. It would be more correct, though also unfeasible, to weigh the global indoor temperature according to the share of the HTC for each room. Since this share is unknown (as is the HTC), a calculated value based on the construction information could be used.

## 4.7. Conclusions

The present chapter explored possible approaches to determine the different terms of the single zone heat balance equation in practical applications. Quantification approaches for infiltration and ventilation losses, heat input by solar gains, space heating and building use as well as the selection of indoor and outdoor conditions starting from limited available data were explored. In Chapter 6 we will investigate the impact of the different approaches on the determination of the HTC for each of the input terms separately. To that end, the different approaches are tested on four case studies which will be described in the next Chapter 5. In Chapter 7 we will combine the optimal approaches for each case study and compare the obtained results with their HTC reference values.



## 5. Case studies

In order to validate the statistical methods and modelling approaches presented in Chapters 3 and 4 extensive monitoring of in-use buildings is needed. Since detailed measurement campaigns require tailored experimental setups, which are often invasive and costly, only a limited number of testing facilities can provide the desired measurements. Therefore five testing facilities: two in the UK, two in Germany, and one in Belgium, were chosen as case studies in this project. All case studies in this work are single-family houses, an overview of general features of each testing facility is given in Table 2.

Table 2. Overview of the main characteristics of each test case. The reference HTC was estimated based on data collected during co-heating tests (Twin N2 and Twin O5, LBORO), PRBS tests (Uccle), and on a calculated design value (GBORO). The reference gA was calculated based on window areas and window pane g-values.

Case study	Type of house	Heating generator	Occupant	Weather data	Construction year	Renovated	Ref. HTC [W/K]	Ref. gA [m2]
Twin N2	Detached single-family house	Electrical heaters	Synthetic	On location	1980s	Yes	110	11.39
Twin O5	Detached single-family house	Air source heat pump	Synthetic	On location	1980s	Yes	106	10.21
Uccle	Semi-detached house	Gas boiler	Real	Free data base	2010	No	106	5.92
LBORO	Semi-detached single-family house	Gas boiler	Synthetic	Station 8 km away	1930s	No	375	5.3
GBORO	Terraced house	Gas boiler	Real	On location	2012	No	40	3.6

### 5.1. Twin Test Houses



47.874 °N, 11.728 °E Holzkirchen, Germany

The Twin houses, Twin N2 and Twin O5, are part of the testing facilities at Fraunhofer Institute for Building Physics in Holzkirchen, Germany. They are two almost identical, detached, single-family houses built for empirical validation experiments on full-scale buildings (see Figure 11). The houses were built in the 1980s but are regularly adapted to the prevailing energy standards. Since the two houses are structurally identical side-by-side on-site comparative measurements under the same outdoor conditions are possible. Detailed measurements of the outdoor conditions are provided by a weather station which is part of the institute's facilities.



Figure 11. Twin Test Houses: View from the East and South (source: Fraunhofer IBP).

The houses have three floors: cellar, ground floor and attic. The ground floor and the attic are part of the heated space, while the cellar, where the technical room in Twin O5 is located, is not heated. The floor plan of the houses is presented in Figure 12. The useful floor area amounts to 165.75 m<sup>2</sup>, and the indoor air volume is 364.15 m<sup>3</sup>. Apart from the measuring equipment, all rooms are unfurnished.

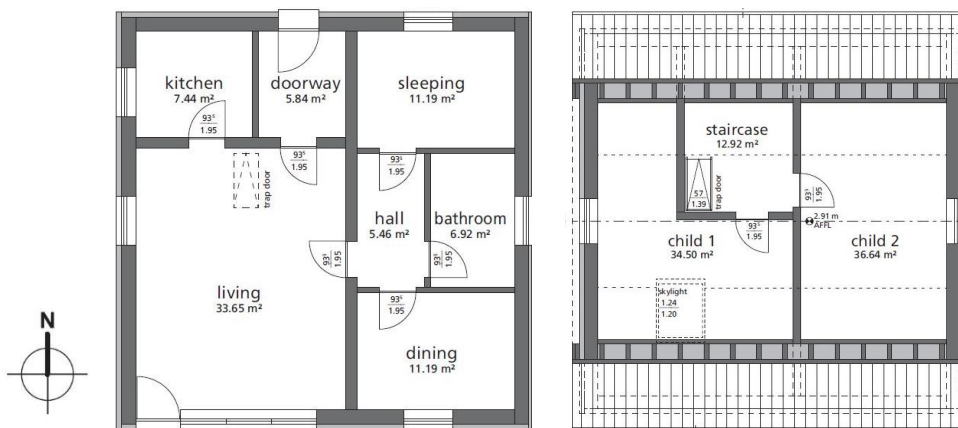


Figure 12. Twin Test Houses: Floor plans of the ground floor (left), and attic (right).

After the last adaptation of the Twin test houses, the U-values of opaque envelope components range between 0.2 and 0.3 W/m<sup>2</sup>K. While the windows have double glazing with low emissivity coating and argon fill with an U-value of 1.2 W/m<sup>2</sup>K for all windows in the façade. The buildings are essentially unshaded and all windows are equipped with roller blinds. The overall building's mean airtightness at 50 Pa pressure difference is 0.87 h<sup>-1</sup> for Twin N2 and 1.10 h<sup>-1</sup> for Twin O5. A mechanical ventilation system is installed in the houses and it operates based on a target constant air change rate of 0.6 h<sup>-1</sup>. The total supply and exhaust air volume for entire buildings are measured and precisely PLC controlled. After a co-heating test was carried out, reference HTC values were calculated for both houses. Based on the measurements collected during the co-heating test, for Twin O5 the reference HTC is 106 W/K, and for Twin N2 it is 110 W/K.

Both houses are occupied by “synthetic users”. The occupancy profiles used in this experiment are simulated profiles for a family with two children. A profile for the internal heat loads, caused by the occupants, their usage of appliances and artificial lighting has been derived from the occupancy profiles. The heat loads representing the synthetic occupants are injected into the rooms by electrical convectors and are provided as a separate measured input. For the testing period, a set temperature of 21 °C is chosen for occupied rooms in both houses, with 17 °C as the night-time setback temperature.

Within the scope of the Annex 71 measurements, the main difference between the houses is in the heating system. In Twin O5 the heat generator is an air-water heat pump coupled to a hydronic low-temperature underfloor heating. The underfloor heating is designed for a 35 °C supply temperature. The heating system consists of a 4.9 kW heat pump with an average COP of 2.40, and an additional 6 kW direct electric heating. The DHW demand is also supplied by the heat pump but there is no DHW circulation since DHW is drained directly out of the building. On the other hand, the

heat input for Twin N2 is generated by electrical heaters located in the indoor space. Seven electrical heaters, with the nominal power of 2 kW, are allocated in each room except for the hall, doorway and staircase. No DHW demand is foreseen for this test house.

More details about the Twin Test Houses can be found in the experimental specifications of the BES-validation exercise [Kersken and Strachan, 2021].

## 5.2. Loughborough Matched Pair Test Houses

 52.771 °N, 1.224 °W      Loughborough, UK

The Matched Pair Test Houses are a testing facility operated by the Building Energy Research Group, in the School of Architecture, Building and Civil Engineering at Loughborough University. They are a pair of adjoining, almost identical, semi-detached, single-family houses (see Figure 13). The houses were built as private homes in the 1930s. They have the same geometry (mirrored about the party wall), construction and heating systems. At the time that the data were collected, they had not been significantly altered since construction: single glazing, uninsulated cavity walls, and no loft or floor insulation. A relatively new, gas-fired, hydronic, central heating system with distribution pipework and wall mounted radiators provided the space heating. Data from the left-hand house (as viewed from the front) were used for this study.



Figure 13. Loughborough Matched Pair Test Houses: view from the South (source: Loughborough University).

The houses have two floors and the floor plan is presented in Figure 14. The useful floor area amounts to 91.2 m<sup>2</sup>, and the indoor air volume is 240 m<sup>3</sup>. Synthetic occupancy equipment was used to represent heat gains from people, lights and appliances. The profile was based on a family of two working adults with two school-aged children. Apart from the equipment for measurement and synthetic occupancy, all rooms were unfurnished. There was no mechanical ventilation.

The U-values were approximately: brick cavity external walls 1.5 W/m<sup>2</sup>K, suspended timber ground floor 0.6 W/m<sup>2</sup>K, uninsulated pitched roof with tiles 2.3 W/m<sup>2</sup>K, and single glazed windows with wooden frames 4.8 W/m<sup>2</sup>K. The measured air permeability was 21.5 h<sup>-1</sup> at a pressure of 50 Pa. The HTC estimated based on a co-heating test was 382 W/K with an estimated 95% confidence interval of +/-10%.

All data were collected during research work that is detailed in Beizae et al. [2015] and Beizae [2016].

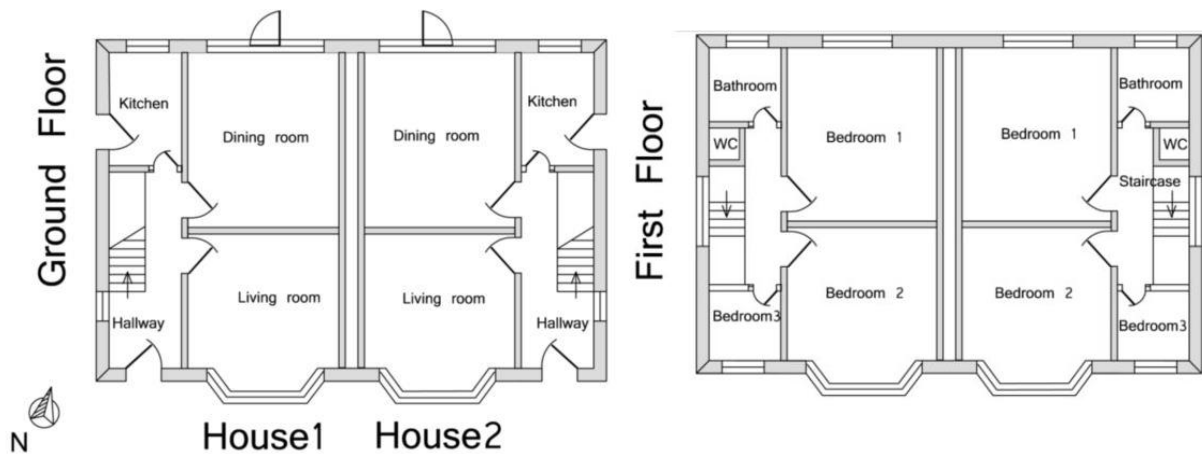


Figure 14. Loughborough Matched Pair Test Houses: floor plans.

### 5.3. Gainsborough Test House

 53.4 °N, 0.77 °E Gainsborough, UK

This case object comprises a south-facing end-of-terrace social housing dwelling (see Figure 15). The house has two floors with a total floor area of 67 m<sup>2</sup> and a building volume of 192.68 m<sup>3</sup>. The living room, kitchen, toilet and entrance hall are located on the ground floor. Two bedrooms and a bathroom are situated on the first floor. A small technical room is located on the landing of the first floor.



Figure 15. Gainsborough Test House: view from the South (source: [Sodagar & Starkey, 2016]).

In Table 3, the main construction elements are specified. Air leakage tests in July 2012 and August 2014 revealed an air permeability of the dwelling of 2.12 m<sup>3</sup> h<sup>-1</sup> m<sup>-2</sup> and 3.65 m<sup>3</sup> h<sup>-1</sup> m<sup>-2</sup> at a pressure of 50 Pa, respectively.

Space heating and domestic hot water (DHW) production are provided by a Potterton Promax combination boiler with a manufacturer's quoted efficiency of 91%. Space heating is controlled using two room thermostats, in the hall and

bedroom 1. The total gas consumption of the heating system is monitored with volumetric gas meters. Ventilation is provided using a 'Lo-Carbon Astra' mechanical ventilation system with heat recovery (MVHR) from Vent-Axia. The system is equipped with a monitoring system that registers temperature and relative humidity of supply and return air, as well as the electricity consumption of the ventilation unit. From March 2013, the building is inhabited by one adult and two children.

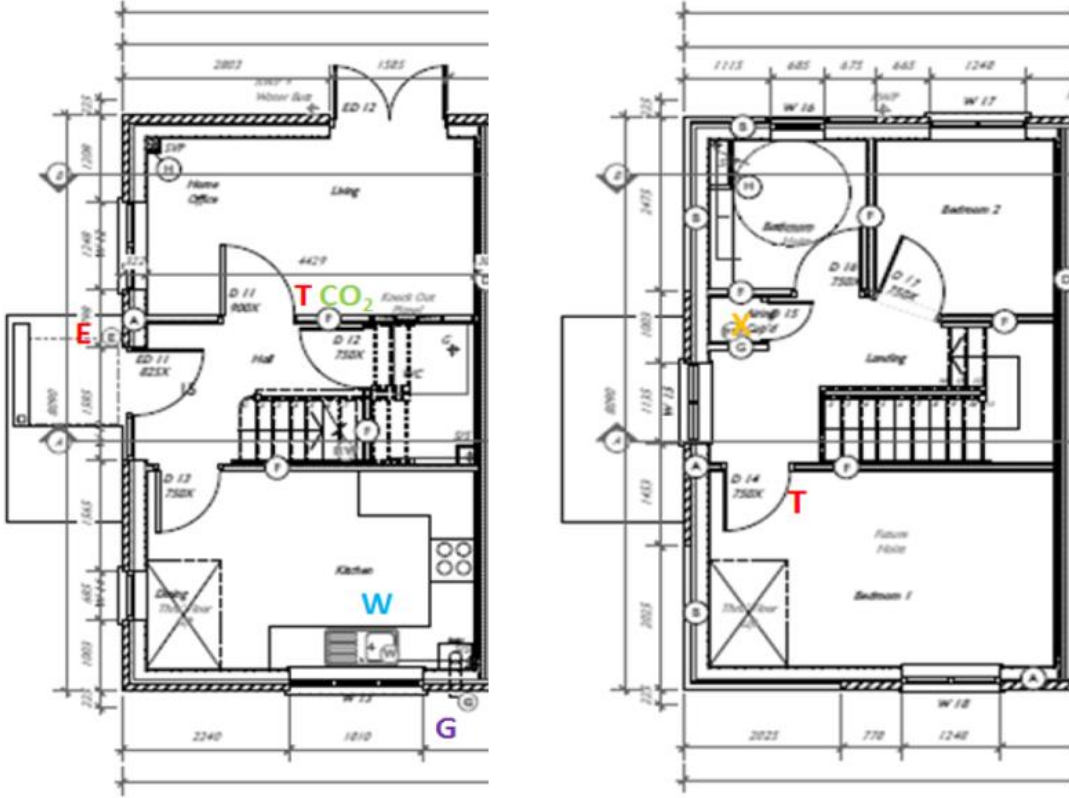


Figure 16. Gainsborough test house: floor plans of the ground floor (left) and first floor (right).

Table 3. Gainsborough test house: Specification of main construction elements [Sodagar & Starkey, 2016]

Element	Characteristics	Area (m <sup>2</sup> )	Target U-value (W m <sup>-2</sup> K <sup>-1</sup> )
Ground floor	Proprietary suspended concrete beam and block with 20mm of insulation	33.62	0.11
External walls	142mm Structural Insulated Panels (SIPs) finished in brick or render clad.	76.15	0.12
Roof	Single ply roofing membrane fixed to 142mm Structural Insulated Panels (SIPs) and 50mm rigid insulation.	33.62	0.11
Door	Munster EcoClad timber board effect with triple glazed side screen	1.89	1.20
Windows	Munster EcoClad triple glazed windows.	15.66	1.15
		(S: 6.24, E: 3.63, W: 5.79)	

## 5.4. Uccle Test House



50.79 °N, 4.37 °E Brussels, Belgium

The Uccle Test House is a high insulated semi-detached house located in Brussels. The house shares a partition wall with the neighboring house south (Figure 17). It was built in 2010 and is occupied by a couple with a regular guest. The house has received bonuses as part of the "BatEx" certification process. Within the framework of this certification, a one-year monitoring was carried out in 2016 during occupancy.

Internal temperature, relative humidity, and CO<sub>2</sub> were measured in the bathroom, living room and guest room. Gas consumption was recorded for heating, hot water, and cooking. Measurements of the outdoor conditions were downloaded from free access data base. More details about the monitoring is available in [Deltour et al, 2020].

The rooms in the house are connected via an open staircase over 4 floors including one floor that is partly underground (Figure 18). All thermal bridges were optimized and calculated according to the Passive House certification. The overall external loss surface amounts to 521.9 m<sup>2</sup> and the airtightness is 0.52 h<sup>-1</sup> measured at 50 Pa pressure difference (n50). Therefore, the calculated theoretical reference value of HTC is 94.2 W/K. The heated floor area of the house is 153.7 m<sup>2</sup>, and the interior volume is 400.4 m<sup>3</sup>. The building is East-West oriented and located in an urban location, resulting in mostly shaded windows during winter period.



Figure 17. Uccle Test House: East façade and cross-section (source: Atelier d'architecture Gérard Bedoret).

Heating is provided by a single heating system, a gas insert, located in the living room, with maximum power of 9 kW and theoretical efficiency of 85%. Domestic hot water (DHW) is provided by an instant gas water heater combined with a thermal solar panel (2 m<sup>2</sup>) for the bathroom and an electric storage water heater of 10 litres located in the garage, used for the kitchen and the wash basin in the WC at the first floor. Ventilation is provided by a balanced mechanical system with heat recovery. The system has a theoretical efficiency of 84%.

An adapted co-heating was performed in February 2019 [Deltour et al, 2020], the resulting HTC was around 106.3 W/K. This value can be selected as a reference. The difference between the theoretical value (94.2 W/K) and the adapted co-heating value (106.3W/K) should be mainly due to heat exchange with the party wall that would contribute around 13% of the losses (instead of 0% in the theoretical calculation).

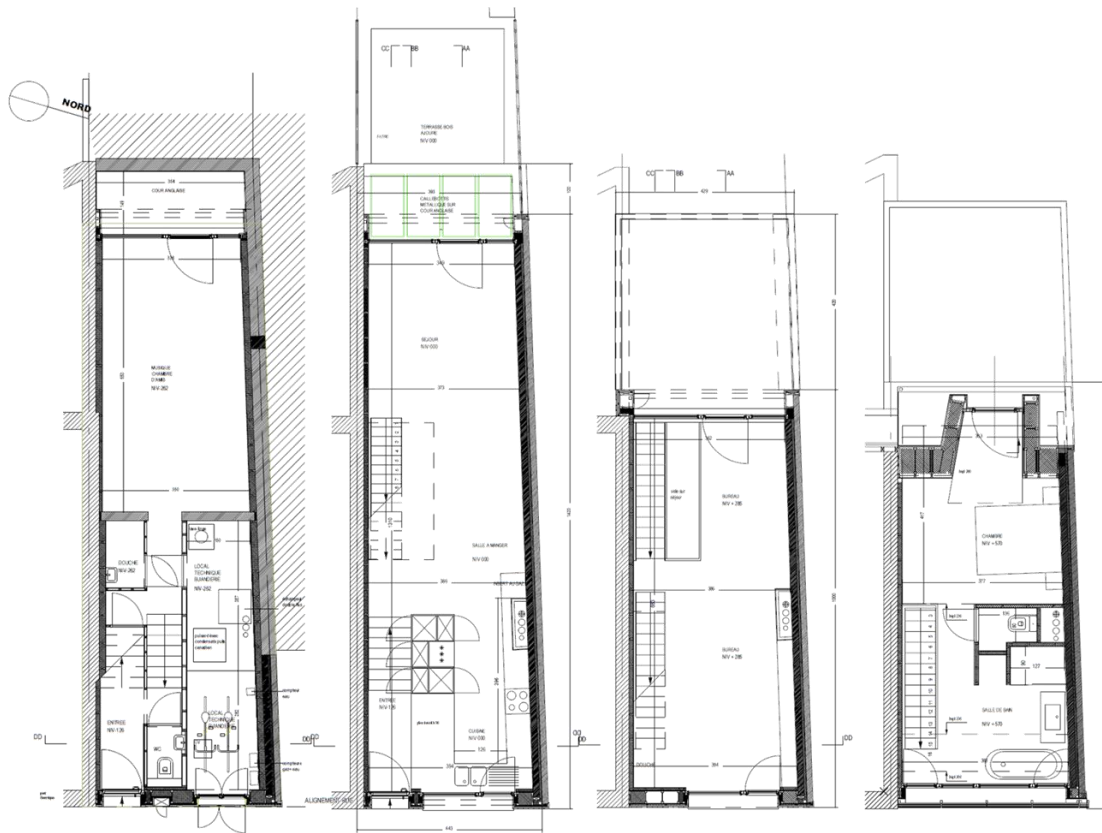


Figure 18. Uccle Test House: Floor plans from the left to the right: semi-buried floor (guest room), ground floor (living room), first floor (office), second floor (bath and bed rooms).



## 6. Exploration of inputs

With the building physical framework in the back of our mind, and the statistical modelling approaches and potential input variables under our belt, we are ready to look at the actual impact of our modelling choices on the estimated physical parameters, and the related uncertainty. The different approaches are tested on the four case studies detailed in the previous Chapter. From this, we distill quality procedures and clear guidelines for building parameter identification. For each input variable, we zoom in on each significant term in the overarching heat balance laid out in Chapter 2, and apply the modelling approaches described in Chapter 4. During this time, basic assumptions are made with regard to the other terms:

- Solar gains: horizontal global solar irradiation, with calculated constant solar aperture values as in Table 2
- Heat input: depending on the test case, one of the approaches for heat input was selected based on the installed system. Mostly, the most precise available measurements without additional theoretical assumptions were used.
- Infiltration and ventilation heat loss: ignored
- Occupant and appliance heat gain: ignored
- Weather data: local air temperature and horizontal global solar irradiation
- Indoor temperature: living room, except for the Twin test houses for which a volume averaged indoor temperature was used as basic assumption.

We depict the obtained results in multi-panel plots. Each of these plots collects the model type (e.g. linear regression model LR1, or ARX model) in separate columns. In each panel plot, the modelling approaches are grouped side-by-side, numbered as they are in Chapter 4. The estimated heat loss coefficients and the standard deviation (95% confidence interval) are represented as points and error bars, respectively. All models are validated based on the state-of-the-art described in the IEA EBC Annex 58 statistical guidelines report. For some modelling approaches, more than one result can be plotted, as more participants independently applied them.

In this Chapter, we focus on the impact of individual approaches on the HTC-estimate. Hence, although a reference value was calculated for the different case studies, it is not included in the charts, as it should not serve as gauge to evaluate results.

### 6.1. Solar gains

The overall heat balance for a single zone building can be expressed as in Equation 4.1. To investigate the influence of solar irradiation on the thermal balance, the following simplification is made:

$$\underbrace{C_{i,eff} \frac{\partial \theta_i}{\partial t}}_{\substack{\text{only in} \\ \text{dynamic models}}} = \underbrace{\Phi_h}_{\substack{\text{always} \\ \text{included}}} + \underbrace{\Phi_{sol}}_{\substack{\text{term of} \\ \text{interest}}} + \underbrace{\Phi_{tr} + \Phi_{inf}}_{\text{HTC}} + \underbrace{\Phi_{int} + \Phi_{vent}}_{\substack{\text{not} \\ \text{included}}} \quad (6.1)$$

In the next section, we will compare the different approaches presented in Section 4.1. to incorporate solar gains in the heat balance equation. We will apply these approaches to each case study separately and discuss the results.

#### 6.1.1. Twin Test Houses

In Figure 19 several patterns can be seen. First, the estimated heat loss coefficient is, in general, lower for approach 1 (entirely omitting solar gains) than for the remaining approaches (which include solar gains in one way or another). Excluding solar gains indeed reduces the heat gains accounted for in the building, thus reducing the estimate for HTC.

The linear regression (LR) models considered here do not include an intercept. Including an intercept in the linear regression model accounts for constant unmodelled thermal effects. However, with an intercept the HTC, i.e. the slope of the fit, can more freely adapt to data, which consequently results in a higher uncertainty. For buildings with an unmodelled surplus of heat gains the intercept of the regression model will be positive. Hence, by forcing the intercept to be zero, generally a steeper regression slope and thus higher HTC is obtained.

Overall, the ARX models seem to perform most consistently (Figure 19). In general, the fitted state space models (rightmost column in Figure 19) have estimated a higher HTC than the ARX and to some extent the linear regression models. On top of that, most of the state space models have obtained extremely small standard deviations of the HTC

estimates. This might be related to the fact the standard deviation is a purely statistical measure. But one also has to consider the measurements errors and the physical interpretation of the model.

Based on the results obtained for the Twin Houses it seems most feasible to model solar gains as a constant fraction of the solar irradiation (Approach 2). Including it in the modelling has a significant impact on HTC (65% and 19% increase for Twin N2 and Twin O5, respectively, in the case of ARX models). Moreover, based on unseen data, these models provide the most accurate predictions of the heat consumption. This exercise, however, has not been retained in this report.

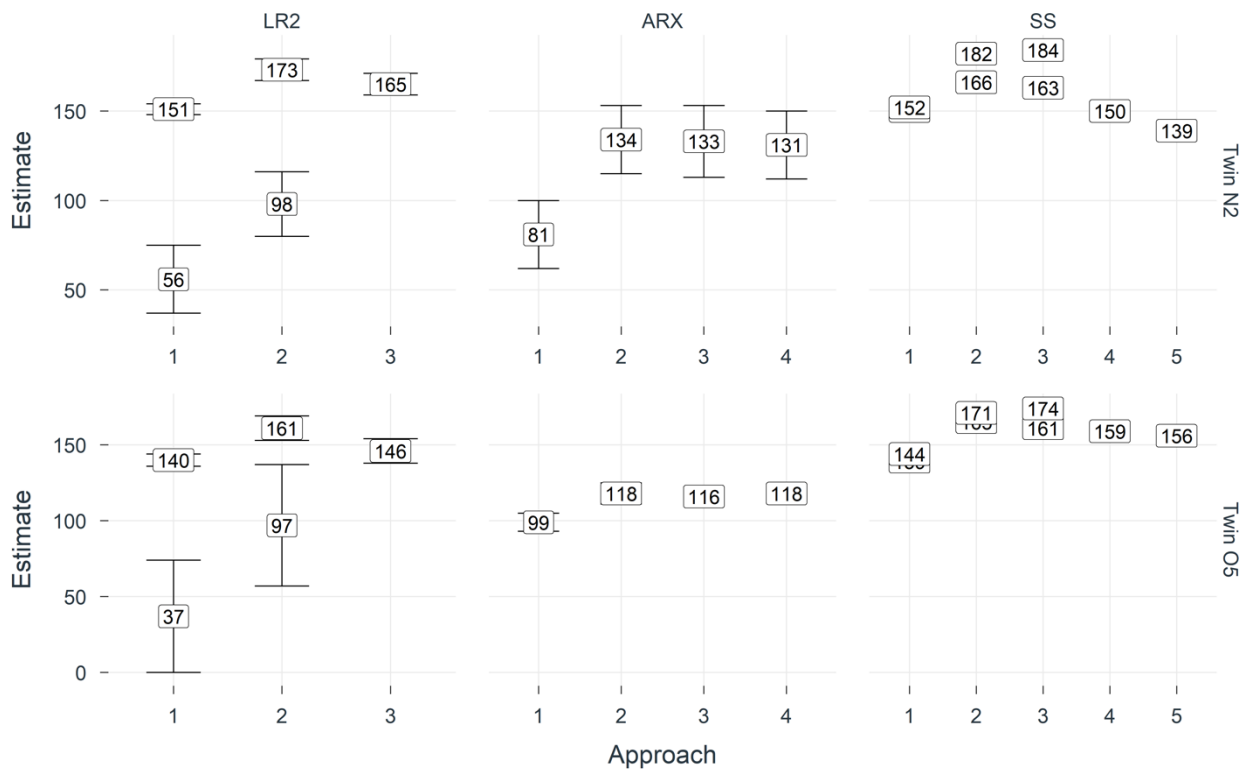


Figure 19. Multi-panel plot investigating solar gains input for the Twin test houses with the model type in separate columns and the Twin Test Houses N2 and O5 in separate rows. Modelling approaches are grouped side-by-side, numbered as they are in Chapter 4. The estimated heat loss coefficients are shown in W/K and the standard deviation is represented with error bars.

### 6.1.2. Gainsborough

In Figure 20 the estimated HTC of the Gainsborough house show a significant variation in the standard deviations. Linear regression models exhibit the largest uncertainty and the state space model the smallest. The wide confidence bands of the regression models are a consequence of two things. First, the model relies on daily average data, and second the sample comprises only 30 such data points.

On one hand, the results obtained by applying linear regression models and state space models seem to be rather consistent. On the other hand, the ARX models seem to overestimate HTC, especially when solar gains are neglected. As more detailed modelling approaches are applied, the results descend down towards the LR2 and SS results. Hence, the inclusion of a detailed model of the solar gains in the ARX models can be recommended. Also the state space model with a detailed description of both diffuse and direct irradiation seems to estimate the HTC rather accurately.

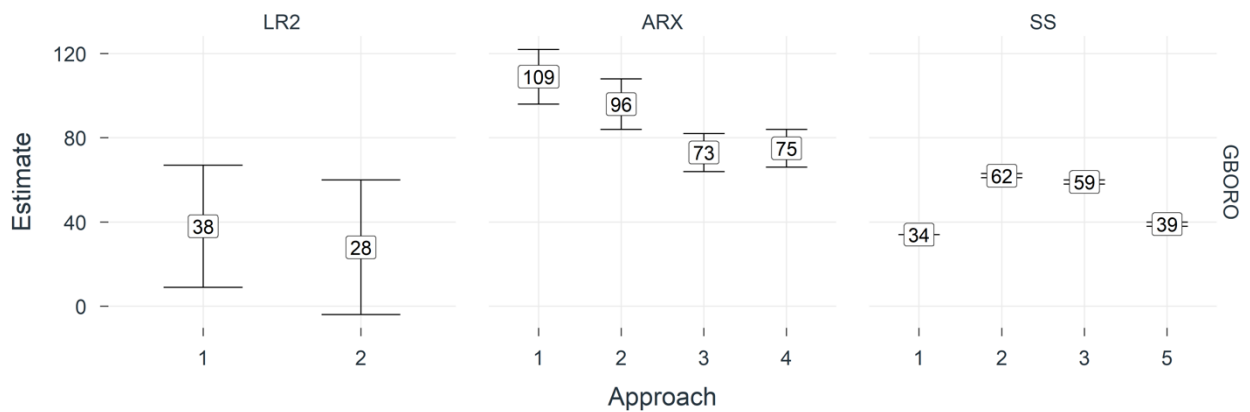


Figure 20. Estimated heat loss coefficients by different model types and formulations of the solar gain for Gainsborough. The error bar represents the standard deviation of the estimated heat loss coefficient.

### 6.1.3. Loughborough

Each of the models (linear regression, ARX, and state space models) show very consistent results, albeit in their own little corner (Figure 21). The ARX and SS models yield very different estimates, both with regard to uncertainty around HTC and its mean value. The ARX models are associated with high uncertainty, whereas the state space models with low uncertainty. Despite the consistent estimates for each of the models, a spline based solar transmittance (Approach 4) proved to result in better predictions than other approaches.

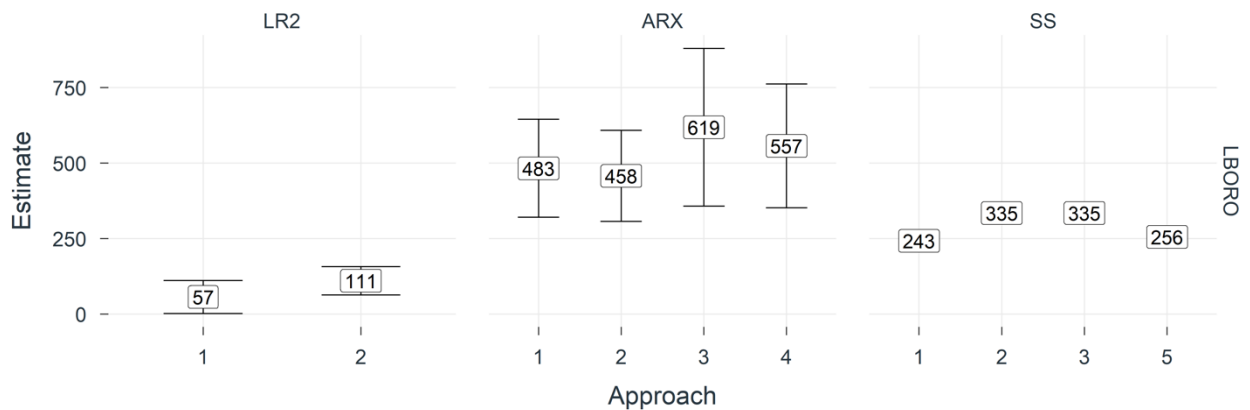


Figure 21. Estimated heat loss coefficients by different model types and formulations of the solar gain for Loughborough. The error bar represents the standard deviation of the estimated heat loss coefficient.

### 6.1.4. Uccle

As it was the case for the Loughborough house the obtained HTC's are consistent within the scope of the three models (LR, ARX and SS). However, there is a pronounced difference in the estimated mean HTC between the three model types. The modelling approaches that include solar gains in one or other form (going for Approach 1 to Approach 2, 3 or 4) yields very consistent results. But the impact is almost negligible. For ARX models, including solar gains (Approach 1 to Approach 2) yields a 5% change in the estimate of HTC. For SS models, this is only 2-3%. Moreover, the inclusion of advanced solar gain modelling approach (Approach 4) does not show any significant improvement in the overall model predictability.

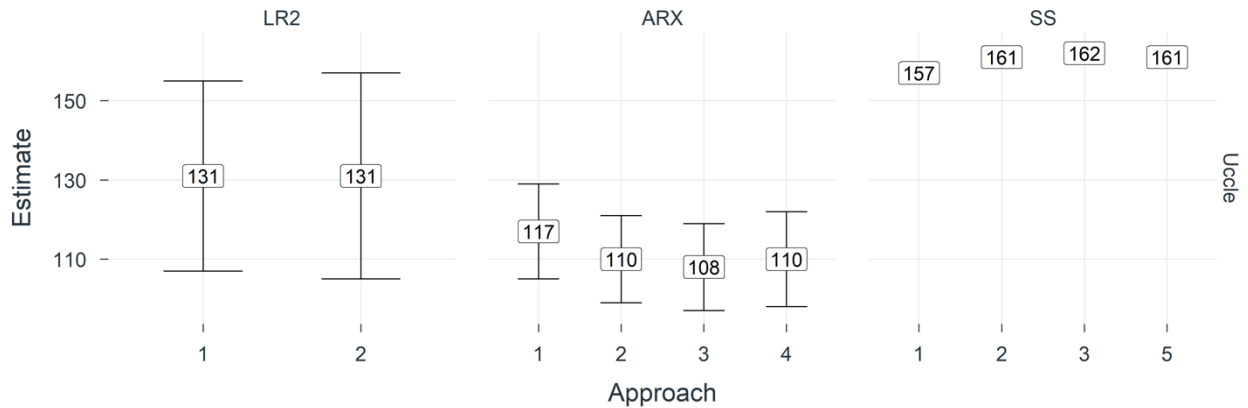


Figure 22. Estimated heat loss coefficients by different model types and formulations of the solar gain for Uccle. The error bar represents the standard deviation of the estimated heat loss coefficient.

### 6.1.5. Conclusion

From most cases there is no clear evidence of an increased accuracy of the obtained HTC by modelling the solar gain in a more advanced manner as in approach 4 (spline based solar transmittance). And as illustrated in Figure 19 there is in many cases a clear improvement in including the solar gain in one way or the other, compared to neglecting it entirely as done in approach 1.

As seen in Section 6.1.4 the steady state linear regression models, the ARX models, and the state space models are all very consistent when investigated separately. However, between the three models a large difference in the estimated HTC is observed, indicating that the models need to be interpreted differently, i.e. the HTCs obtained from the linear regression model, the ARX model and the state space model do not necessarily represent the same thing.

It is, however, important to note that a static value as the HTC is only one part of the equation when dealing with dynamical models — another important part are the thermal capacities which have not been discussed here. When investigating the models' capabilities of predicting future observations, the spline-based gA function (approach 4) generally offer a more accurate representation of the solar transmittance than a constant gA value. With that in mind, the Gainsborough and the Loughborough house seem to benefit from the spline base gA function, whereas a constant gA values is sufficient for the Twin Houses and the Uccle house.

## 6.2. Heat input

In this section, we discuss the results obtained by applying different modelling approaches for the heat input. To investigate the impact on the determination of the HTC, we make the following simplifications:

$$\underbrace{C_{i,eff} \frac{\partial \theta_i}{\partial t}}_{\text{only in dynamic models}} = \underbrace{\Phi_j}_{\text{term of interest}} + \underbrace{\Phi_{sol}}_{\text{set for LR}} + \underbrace{\Phi_{tr} + \Phi_{inf}}_{\text{HTC}} + \underbrace{\Phi_{int} + \Phi_{vent}}_{\text{neglected except for cases with exact input}} \quad (6.2)$$

Before diving into the results, we briefly introduce, for each test case, the heating system and the available heat input data.

### 6.2.1. Twin Test Houses

In the Twin N2, the heat input is generated with seven electrical heaters installed in all rooms of the house except the doorway and the staircase. The power consumption in every room is measured separately, and the heat delivered to each room is given as a measurement output. The losses of the energy conversion in the electrical heaters are negligible, therefore only one case with the exact heat input delivered to the house is analyzed, corresponding to approach 4 in Section 4.2.

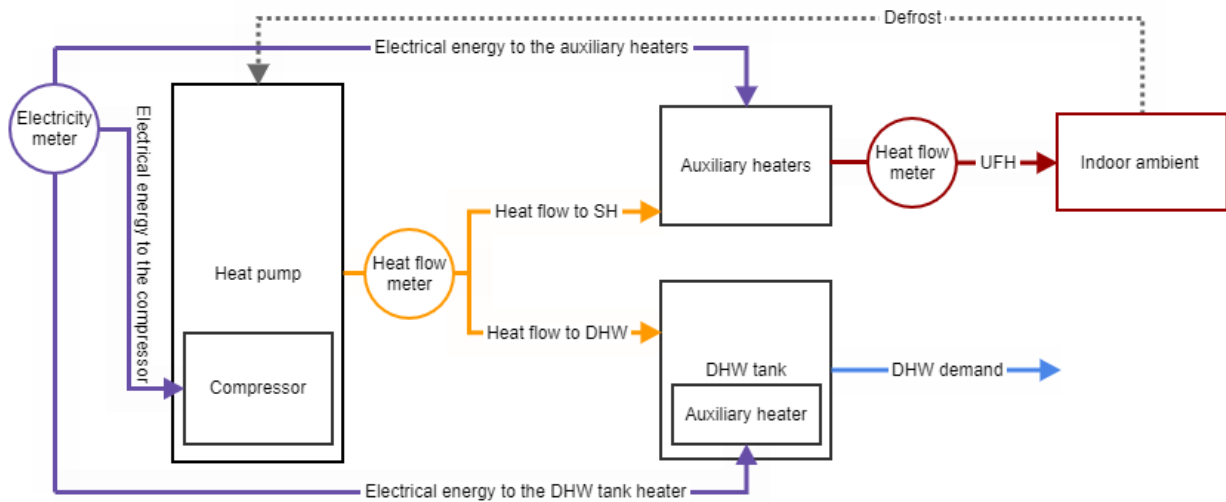


Figure 23. Simplified energy flows in the heat pump system of Twin O5

In the Twin O5, a heat pump (HP) generates heat for both space heating (SH) and domestic hot water (DHW). In addition to the heat pump, there are auxiliary electrical heaters installed between the HP and the underfloor heating (UFH) system and also an additional heater in the DHW tank. A simplified representation of the energy flows in the HP system and installed energy meters is shown in Figure 23. The detailed description of this heating system can be found in the experimental specifications [Kersken and Strachan, 2021].

In the defrosting cycle, the heat is subtracted from the indoor space and delivered to the external unit. The conversion losses on the auxiliary heaters in the UFH and DHW are negligible. As the DHW is drained out of the building, it can be expected that it does not affect the heat balance of the indoor space. Moreover, since the energy produced by the HP is split between the UFH and DHW subsystems, the exact split is known only by measurement. In the case of Twin O5 detailed measurements are available and exact energy flows are known. For this study, three measurement scenarios were assumed. The first scenario assumes that only the electrical energy consumed by the whole system is measured, without separating the energy consumed by the HP itself from the energy consumed by auxiliary heaters. Here it is assumed that the overall energy is fed to the HP and converted to thermal energy by a constant COP of 2.4. In this case, two versions of the HTC are calculated, one assuming there is no DHW split (1b), and the other with a theoretical DHW split (1c) of 20%. In the second scenario, it is assumed that the total thermal energy produced by the HP is known. Again, two cases, without (3a) and with (3b) theoretical separation of DHW use are assumed. The third scenario corresponds to the most accurate heat input, where the exact heat flow through the UFH is measured, and it corresponds to Approach 4 in Section 4.2. In Table 4 assumptions linked with different accuracy levels are presented.

In addition to the main heat source, there are electrical heaters used to simulate internal heat gains. Since these artificial internal gains are measured separately on every device, it is possible to exclude them from the overall heat input.

Table 4. Approaches applied on the heat input of Twin O5

Approach	What is measured?	DHW split
1b	El. energy used by the heating system	No
1c	El. energy used by the heating system	Theoretical: 80% SH/ 20% DHW
3a	Energy produced by the HP	No
3b	Energy produced by the HP	Theoretical: 80% SH/ 20% DHW
4	Heat delivered to UFH	Exact

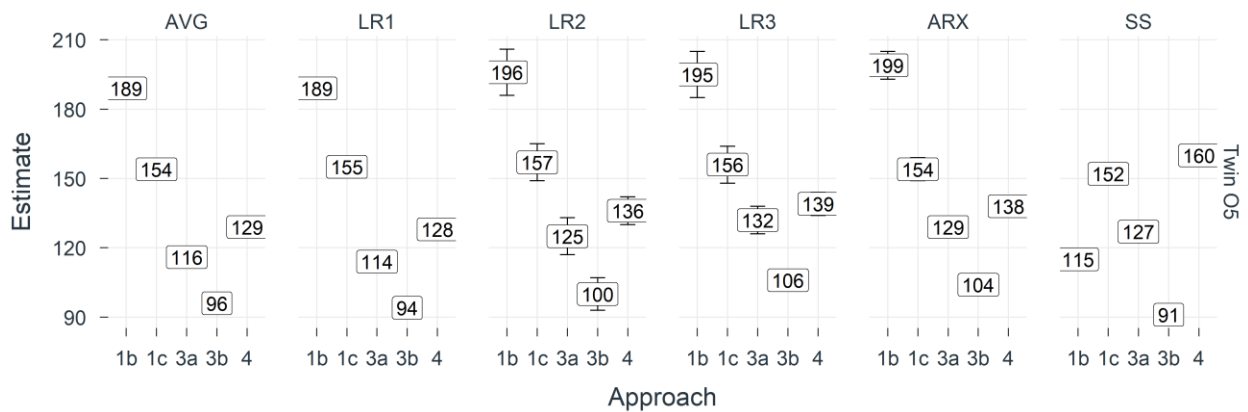


Figure 24. Estimates of the heat transfer coefficient calculated using different methods (see Chapter 3) and approaches (see Section 4.2) of the accuracy on the heat input for Twin O5. The error bar represents the standard deviation of the estimate.

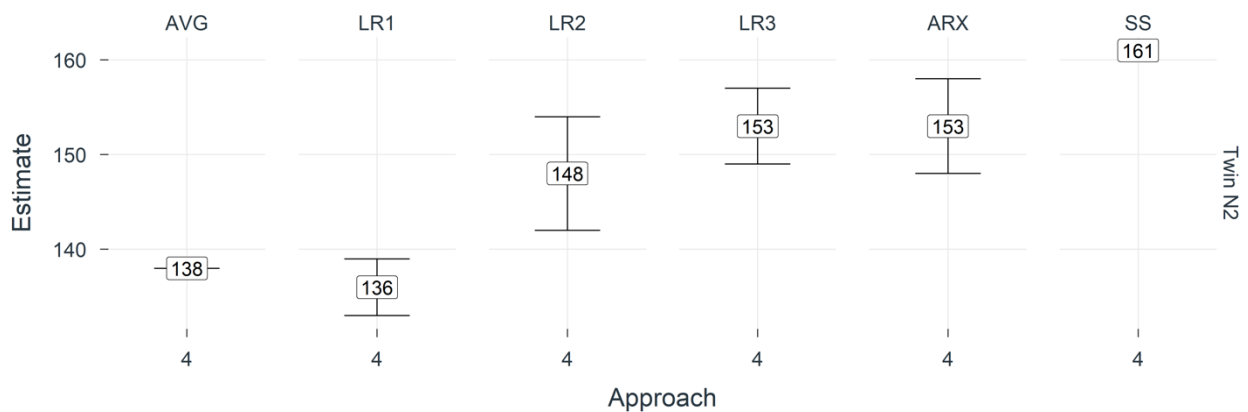


Figure 25. Estimates of the heat transfer coefficient calculated using different methods (see Chapter 3) and approaches (see Section 4.2) of the accuracy on the heat input for Twin N2. The error bar represents the standard deviation of the estimate.

From the results for the Twin O5 it is possible to notice that when the measurements of the heat input are taken closer to the emission system, thus representing the exact SH demand more precisely, the estimated HTC is significantly lower. However, in this case, the SH demand is not entirely produced by the HP and additional auxiliary electrical heaters are often turned on. Therefore, measurements of the HP output only, do not reflect the total SH demand. Another factor in this system is the DHW production which, without additional measurements, can only be assumed. Arbitrary assumptions, similar to 1c and 3b, could lead to the underestimation of the HTC. To avoid mistakes when assessing complex systems, additional measurements (Approach 4) should be considered.

### 6.2.2. Gainsborough

The heating source in the Gainsborough test case is a condensing combi boiler, with a manufacturer's quoted efficiency of 91% and a nominal power of 23.8 kW. The central radiator heating is controlled by two Honeywell room thermostats, one in the hall and one in the master bedroom. For this test case, the gas consumptions was measured in m<sup>3</sup> and has been converted to kWh using the average gas calorific value. The domestic hot water is produced by the same generator and there was no separate measurement of the DHW consumption. The scarcity of measurements inside the heating system in this test case reflects the usual set-up available in reality, where only gas-meter readings are available. Therefore, in this case, only three scenarios can be assumed. In the first scenario (1a) it is supposed that all heat released from the gas combustion in the boiler is delivered to the heated space, in 1b that assumption is corrected by adding the manufacturer's boiler efficiency. In approach 1c also a theoretical DHW split is assumed.

Table 5. Approaches applied on the heat input of the Gainsborough test case

Approach	What is measured?	DHW split
1a	Gas consumption	No
1b	Gas consumption (theoretical efficiency)	No
1c	Gas consumption (theoretical efficiency)	Theoretical (see below)

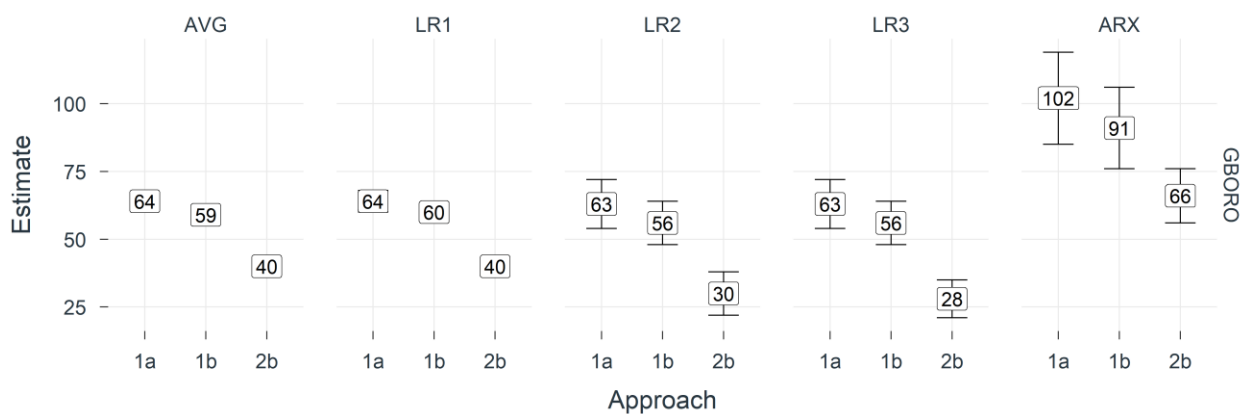


Figure 26. Estimates of the heat transfer coefficient calculated using different methods (see Chapter 3) and approaches (see Section 4.2) of the accuracy on the heat input for Gainsborough. The error bar represents the standard deviation of the estimate.

Figure 26 shows that with the increase of the heat input accuracy, for all statistical modelling methods, the value of the estimate decreases. While Approach 1b assumes a constant efficiency of the gas boiler only, in Approach 1c a more extensive analysis of the theoretical efficiency and DHW split is investigated. A detailed explanation of the performed analysis follows.

#### Uncertainty analysis

For this test case, an uncertainty analysis is performed for the boiler efficiency and the domestic hot water use, corresponding to Approach 1c. In a first step of the uncertainty analysis, a variation is chosen for the two assessed parameters. On the one hand, the boiler efficiency is chosen to be normally distributed with a standard deviation of 10 % of the mean efficiency. Figure 27a illustrates the density function for a boiler with an average efficiency of 89 %.

On the other hand, the distribution of the domestic hot water use (in liter per person per day) is based on two sources of data: data of seven Flemish Pilot Projects for Renovation (64 cases – research supported by the regional agency 'Flanders Innovation & Entrepreneurship' VLAIO) and data of the Annex 42 Project of the International Energy Agency [Knight I. et.al. 2007]. Figure 27b illustrates the density of these two data sets in four density curves:

- the density curve of the Pilot Project data calculated with a Kernel smoother (maximum at 33.5 liter per person)
- the density curve of the Pilot Project data approached as a normal distribution (mean  $42.8 \pm$  standard deviation of 15.3)
- the normal distribution of the Annex 42 data ( $51.7 \pm 21.2$ )
- the normal distribution of the average both data sets ( $47.2 \pm 18.2$ ).

The first density curve shows that the Pilot Project data is not completely normally distributed, but slightly skewed to the left. Since, however, six out of seven Pilot Projects were social housing projects, this divergence can be ascribed to the target group: the majority of the cases (48 out of 64) is inhabited by economically-minded, socially vulnerable people. Therefore, the normal distribution (second curve), of which the mean value is 9.3 liter per person higher than the peak value of the first curve, can be accepted as an input of the average domestic hot water use. The third curve, also normally distributed, is based on the Annex 42 data, where the domestic hot water use was monitored in nine

different countries. Finally, the fourth (purple) curve, which is the average of the second and third density curve, is used to calculate the distribution of the domestic hot water energy demand for each case, as a function of the number of inhabitants per dwelling.

In a second step of the uncertainty analysis the Sobol' sequence, a pseudo-random number sequence, is used to define 1000 combinations of the boiler efficiency and the DHW use, which leads to 100 variations of the heating power. The 1000 variations of the two parameters are illustrated in Figure 28. In a third step, the heat losses are calculated for all values of the heating power using the linear regression model. Finally, the resulting heat losses are compared to the heat losses for the original values of the boiler efficiency and the DHW use. This research was conducted in the framework of the dissertation of Evi Lambie [Lambie E., 2021]

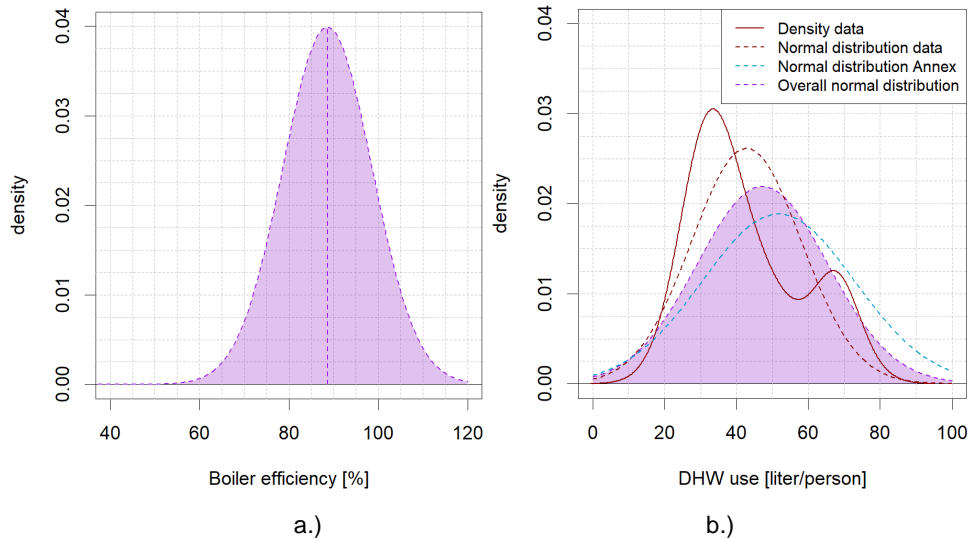


Figure 27. Illustration of a.) the normal distribution of the boiler efficiency b.) the uniform distribution of the domestic hot water use

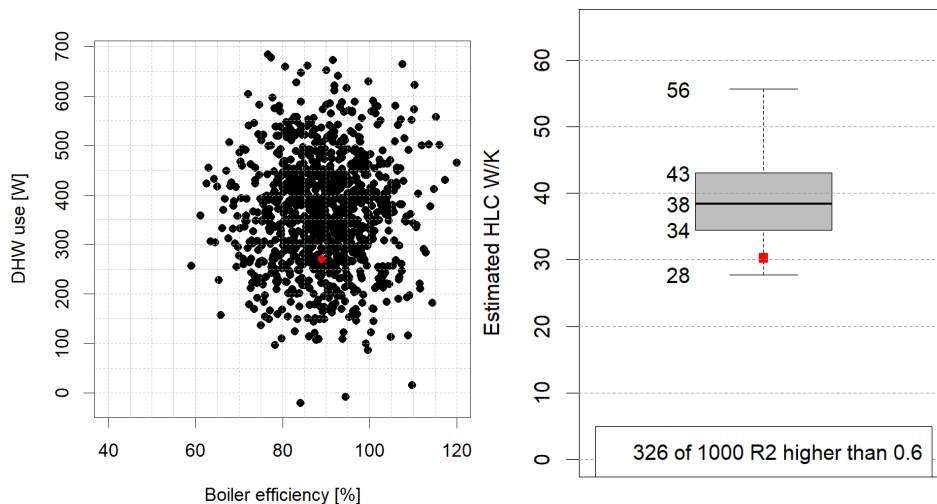


Figure 28. Illustration of the second and third step of the uncertainty analysis performed on the boiler efficiency and the domestic hot water use in the Gainsborough test case.

### 6.2.3. Loughborough

The Loughborough test house uses a 30 kW gas-fired condensing combi-boiler as heating source and the central heating system consists of radiators controlled by a programmable room thermostat located in the hallway. Since the synthetic occupancy did not include DHW consumption, the heat generator was used only to supply the required SH demand. In this case, both gas usage and boiler output were monitored. When only the gas consumption is measured two input approaches are considered. In 2a, it is assumed that all heat released from the gas combustion is delivered to the heated space, while in 2b a theoretical boiler efficiency of 89% is included. The Approach 4 corresponds to the case when the exact heat flow delivered by the boiler is measured, thus in this case, the most accurate heat input scenario.

Table 6. Approaches applied on the heat input of the Loughborough test case

Approach	What is measured?	DHW split
2a	Gas consumption	Yes (no DHW production)
2b	Gas consumption (theoretical efficiency)	Yes (no DHW production)
4	Heat output of the boiler	Yes (no DHW production)

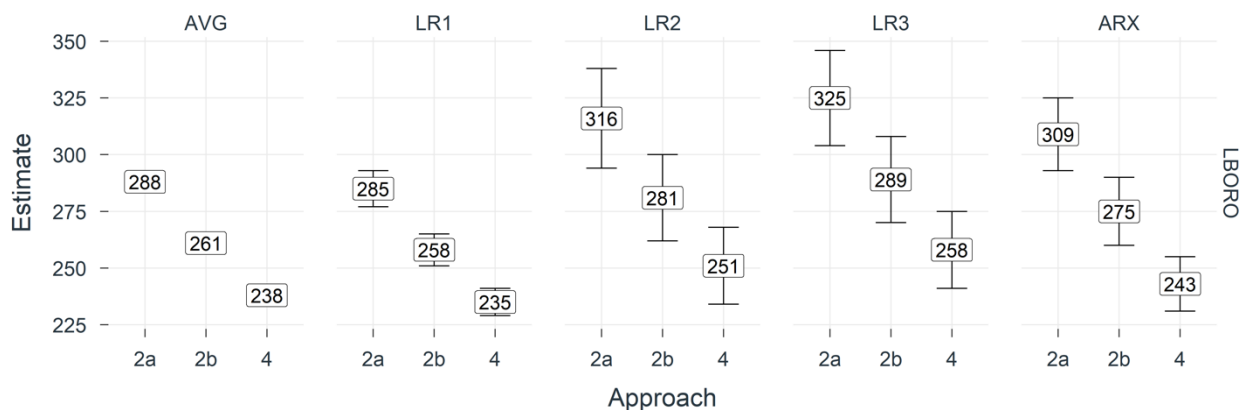


Figure 29. Estimates of the heat transfer coefficient calculated using different methods (see Chapter 3) and approaches (see Section 4.2) of the accuracy on the heat input for Loughborough. The error bar represents the standard deviation of the estimate.

From Figure 29 it is noticeable that the estimated HTC decreases, with the improvement of the heat input measurement accuracy. When comparing Accuracy 2b to 4, it can be deduced that the theoretical efficiency overestimates the real efficiency of the boiler. One of the reasons is that in reality, the efficiency is load-dependent and it often decreases significantly on low loads.

### 6.2.4. Uccle

In the Uccle test house, the heat generator is a gas insert, located in the living room, with a maximum power of 9 kW and theoretical efficiency of 85%. Domestic hot water is provided by an instant gas water heater combined with a thermal solar panel for the bathroom and an electric storage water heater of 10 litres located in the garage, used for the kitchen and the washbasin in the toilet at the first floor. For this test case two gas consumption recordings are available, the overall gas consumption and the gas consumption of the gas insert alone. When the overall consumption measurements are available it is possible to calculate the HTC with three different approaches. First, for 1a it is assumed that the gas was all consumed to heat the indoor space, while for 1b a theoretical efficiency of the gas insert is implemented. In Accuracy 1c both the efficiency of the generator and a theoretical DHW split were assumed. In case when the exact gas consumption of the insert is known there are only two possible approaches: 2a, where it is assumed all consumed gas is transformed into heat and delivered to the SH, and 2b, where a theoretical efficiency of the generator is applied.

Table 7. Approaches applied on the heat input of the Uccle test case

Approach	What is measured?	DHW split
1a	Overall gas consumption	No
1b	Overall gas consumption (theoretical efficiency)	No
1c	Overall gas consumption (theoretical efficiency)	Yes (theoretical)
2a	Gas consumption of the SH heat source	Yes (no DHW production)
2b	Gas consumption of the SH heat source (theoretical efficiency)	Yes (no DHW production)

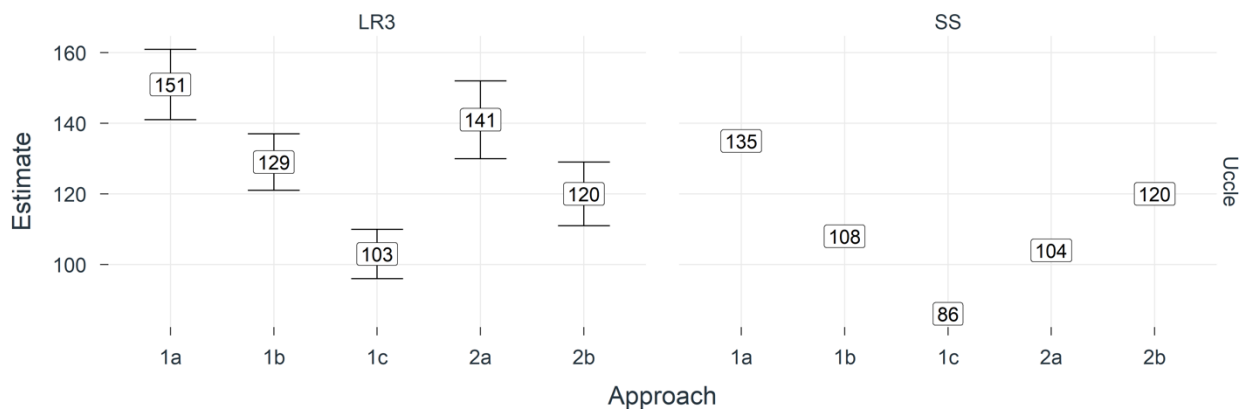


Figure 30. Estimates of the heat transfer coefficient calculated using different methods (see Chapter 3) and approaches (see Section 4.2) of the accuracy on the heat input for Uccle. The error bar represents the standard deviation of the estimate.

### 6.2.5. Conclusion

When gross energy use measurements, taken before the generator, are considered we tend to overestimate the energy demand, and thus also the HTC. In cases where a constant theoretical efficiency of the generator is implemented the produced heat is often overestimated since usually the nominal efficiency of the unit is known, rather than the average. If the same generator provides for both SH and DHW demand, DHW demand should be excluded from the heat input since its inclusion can also lead to the overestimation of the heat delivered to the indoor space. In case when assumptions are used to split the DHW demand there is the tendency to either overestimate or underestimate the HTC depending on the assumption.

The best results are obtained when energy measurements after the generator and after the split for DHW distribution are considered. Thus, when possible, installation of measurement equipment after the generator and additional data gathering to separate SH and DHW demand are recommended.

The robustness of the model types, e.g. linear regression or ARX, is dependent on the investigated case. Overall, state-space models seem to be the most robust.

## 6.3. Infiltration heat loss and ventilation heat loss

As introduced in Section 4.3, this Section investigates the impact of modelling in detail the heat transfer that arises due to mechanical ventilation and infiltration/exfiltration. We will assess the impact on the estimation of HTC of explicitly modeling heat transfer due to mechanical ventilation (Section 4.3.2). Moreover, we will investigate whether we can split HTC into  $HTC_{tr}$  and  $HTC_{inf}$ , and if so, how (Section 4.3.3).

$$\underbrace{C_{i,eff} \frac{\partial \theta_i}{\partial t}}_{\text{only in dynamic models}} = \underbrace{\Phi_h}_{\text{always included}} + \underbrace{\Phi_{sol}}_{\text{set for LR}} + \underbrace{\Phi_{tr} + \Phi_{inf}}_{\text{HTC (question 2)}} + \underbrace{\Phi_{int}}_{\text{neglected}} + \underbrace{\Phi_{vent}}_{\text{term of interest (question 1)}} \quad (6.3)$$

Approach 0 neglects ventilation heat loss. Approach 1 first estimates the ventilation heating/cooling power from measurements (supply temperature and flow rate, the latter obtained through direct measurement or estimated based on MVHR power). Approach 2 includes ventilation in the models and also attempts to include infiltration explicitly so HTC can be split into  $HTC_{tr}$  and  $HTC_{inf}$ .

### 6.3.1. Twin Test Houses

The twin houses feature mechanical ventilation with heat recovery. Air is supplied to the living room and two bedrooms. The ventilation supply rate and supply temperature are measured, which allows including the ventilation heat supply in all models, be they linear regression or grey-box.

The infiltration mass flow rate, however, remains unknown. But wind speed is measured and we might be able to build a model that correlates wind speed and air infiltration.

$$\Phi_{inf} = a_{inf} V (\theta_e - \theta_i) \quad (6.4)$$

Table 8 collects the results obtained for the infiltration heat loss separately, based on linear regression analysis (Eq. 4.36), the AIM-2 model and the rule of thumb constant infiltration based on n50 (DIN 4108), assuming a moderately exposed building. The latter two effectively estimate the infiltration flow rate prior to the regression.

Table 8. Estimates infiltration heat loss in W/K for Twin Test Houses, based on linear regression method 2 (LR2), AIM-2 and DIN 4108.

	LR2	AIM-2	DIN 4108
Twin N2	26.5 (7.1)	7.52	6.91
Twin O5	17.8 (7.1)	9.45	8.73

### 6.3.2. Gainsborough

The Gainsborough house also features mechanical ventilation with heat recovery. The ventilation mass flow rate is unknown and therefore needs to be included as an additional explanatory variable.

$$\Phi = HTC(\theta_e - \theta_i) - gAI_{sol} + \frac{\alpha_v P_v^{\frac{1}{3}} (\theta_i - \theta_s)}{\Phi_{vent}} + \frac{c_a \cdot \dot{m}_{inf} (\theta_i - \theta_e)}{\Phi_{inf}} \quad (6.5)$$

Where  $P_v$  is the power consumption of the fan. The MVHR meter (kWh) is provided in the data file.

Table 9 collects the results obtained for the infiltration heat loss separately, based on linear regression analysis (Eq. 4.36), the AIM-2 and DIN 4108 models.

Table 9. Estimates infiltration heat loss in W/K for Gainsborough, based on linear regression method 2 (LR2), AIM-2 and DIN 4108.

	LR2	AIM-2	DIN 4108
GBORO	8.1 (7.6)	7.27	4.58

Figure 31 collects the results obtained separately by two participants. For the Gainsborough case (GBORO) the impact of the person performing the analysis outweighs the impact of the modelling approach they apply. Very consistent results are obtained for the Twin Test Houses (Twin N2 and Twin O5). With a reduction of about 30%, including ventilation heating power clearly has a significant impact on the HTC estimate. Approach 1 and 2 yield very similar results, with a maximum deviation of 5% between them.

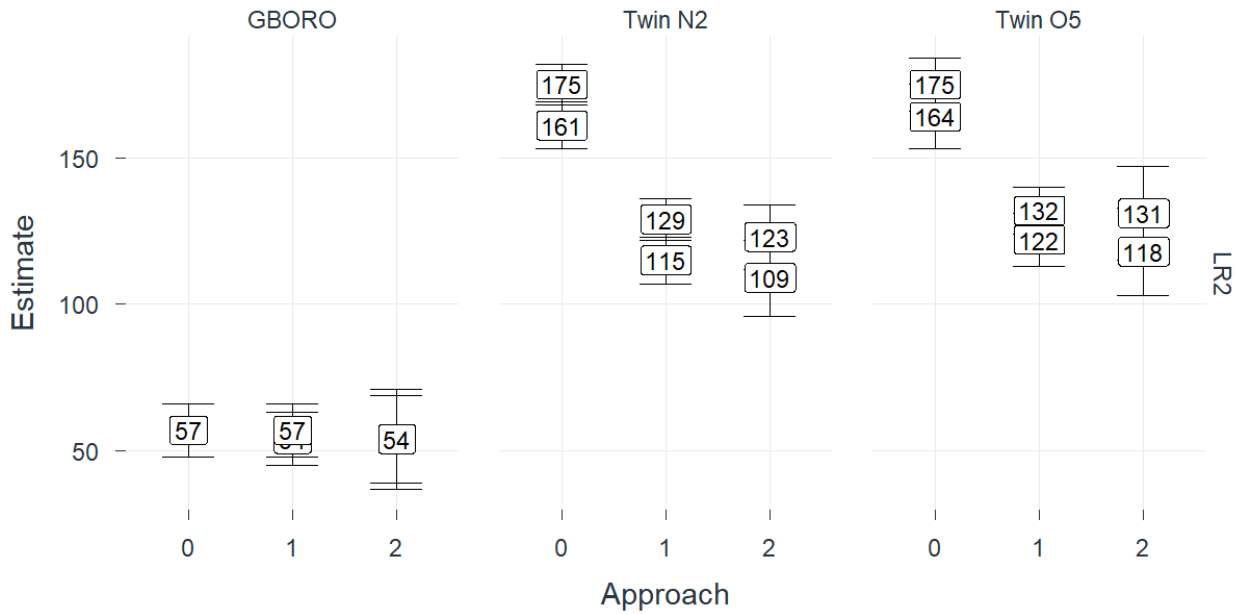


Figure 31. Estimate of the heat transfer coefficients by using different approaches to model ventilation and infiltration heat loss for the Twin Test Houses and Gainsborough.

## 6.4. Occupant and appliance heat gain

To investigate the impact on the determination of the HTC, we make the following simplifications:

$$\underbrace{C_{i,eff} \frac{\partial \theta_i}{\partial t}}_{\text{only in dynamic models}} = \underbrace{\Phi_h}_{\text{always included}} + \underbrace{\Phi_{sol}}_{\text{set for LR}} + \underbrace{\Phi_{tr} + \Phi_{inf}}_{\text{HTC}} + \underbrace{\Phi_{int}}_{\text{term of interest}} + \underbrace{\Phi_{vent}}_{\text{neglected}} \quad (6.6)$$

Figure 32 and Figure 33 visualize the internal heat gains for both the Gainsborough and Uccle test cases, as estimated based on the modelling approaches introduced in Section 4.4.1 to 4.4.4. When applying the ISO method (Approach 1, Section 4.4.1) to the two test cases under consideration (Uccle and Gainsborough), the input parameters and usage schedule for residential, detached houses were assumed.

### 6.4.1. Gainsborough

The occupant presence based on RH measurements was considered for two rooms (lounge and bedroom), whilst the occupant presence based on CO<sub>2</sub> measurements was considered only for the lounge. As a result, the application of the RH method (Approach 3) results in higher metabolic heat inputs than for the CO<sub>2</sub> method (Approaches 4 and 5). However, this has little impact on the HTC estimate. When comparing the results obtained when occupant heat gains are not considered (Approach 1) with the results obtained when they are, applying the ISO method (Approach 2) seems to overestimate HTC (by up to 7%). Moreover, comparing approaches 1 and approaches 3-5, the impact of including occupant heat gains (on top of appliance heat gains) is negligible.

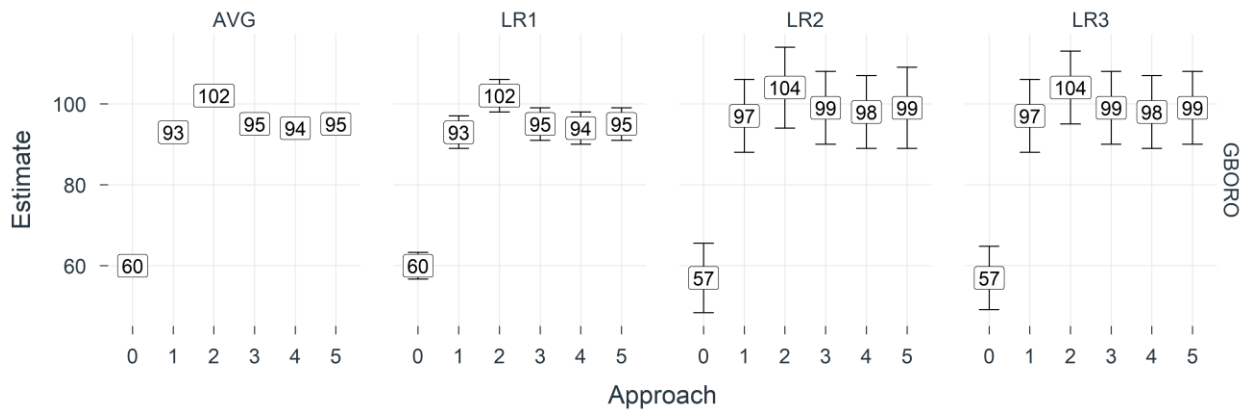


Figure 32. Multi-panel plot with the model type in separate columns. Modelling approaches are grouped side-by-side, numbered as they are in Chapter 4. The estimated heat transfer coefficients and the standard deviation are represented as points and error bars, respectively.

#### 6.4.2. Uccle

Both RH and CO<sub>2</sub> measurements were taken in the living room, bathroom and guest room. Also here, Approach 2 seems to slightly overestimate HTC, by up to 12%. In the case of the Averaging method (AVG) and linear regression model 1 (LR1), considering a CO<sub>2</sub> mass balance (Approach 5) yields slightly lower estimates than estimating metabolic heat inputs based on RH and CO<sub>2</sub> measurements (Approaches 3 and 4). This trend, however, is not confirmed by the other methods.

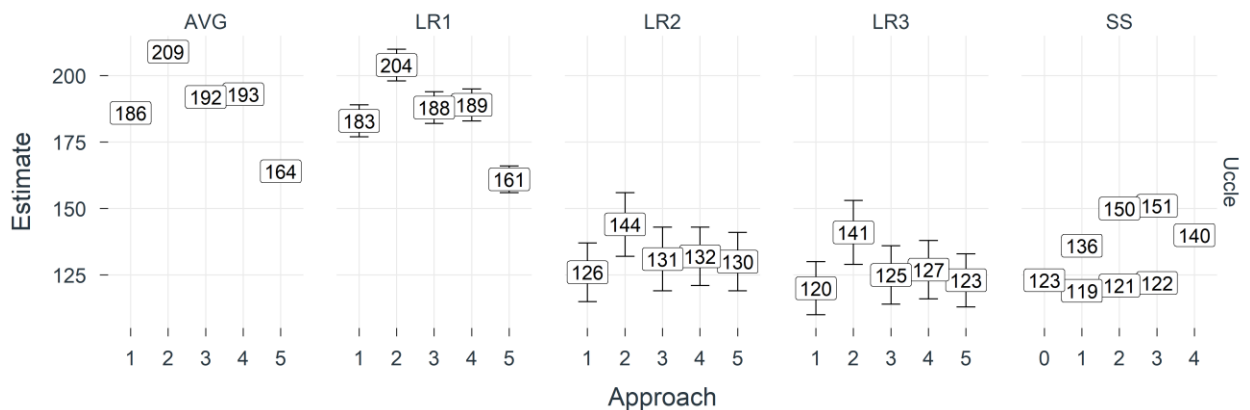


Figure 33. Estimates of the heat transfer coefficient estimated by using different modelling approaches (as outlined in Chapter 4) for occupant and appliance gains.

#### 6.4.3. Conclusion

Compared to gas and electricity consumption, the obtained metabolic heat inputs are low. The ISO method results in the highest metabolic heat input. With the exception of the LR2 method in the Uccle case object, the HTCs obtained through different methods and approaches seem to be overestimated. This must at least partially be attributed to the fact that inaccurate figures for some parameters (e.g. heat input and indoor temperatures) have been used. The difference in obtained HTCs through the approaches 0 and 1 in the Gainsborough case show that the inclusion of electricity consumption in the internal heat gains has a large impact on the derived HTC.

Compared to the RH and CO<sub>2</sub> methods, the CO<sub>2</sub> balance method results in slightly higher metabolic heat input rates for the Gainsborough case object, and slightly lower metabolic heat input rates for the Uccle case object. But as this method explicitly takes ventilation into account, it heavily relies on an accurate estimation of the ventilation rate.

Considering that CO<sub>2</sub> and RH sensors were only present in a limited number of rooms in both test cases, it is expected that the metabolic heat inputs, which are determined by methods that rely on these measurements, are underestimating

the occupant heat gains. On the other hand, the metabolic heat input is likely overestimated in some cases, due to non-human sources of moisture or CO<sub>2</sub> (e.g. cooking).

In the absence of measurements regarding occupant presence in the Gainsborough and Uccle case objects, a validation study has been done on another test case, for which measurements of temperature, relative humidity and CO<sub>2</sub> concentration were registered on a 5-minute interval, and occupant presence was registered on a 1-minute interval. Based on the results of this validation study, the CO<sub>2</sub> balance method was found to yield the most accurate results in terms of occupant presence. It must be noted, however, that this method is relatively complex in that it relies on the accurate quantification of the CO<sub>2</sub> concentration in the replacement air and the air change rate in the building (zone) under consideration.

## 6.5. Weather data

For every location, the closest meteo-stations covering the period of the experiments was identified. Hourly observations were acquired through the NOAA Integrated Surface Database (ISD) and processed using the `isdparser` package for R [CRAN]. The ISD database consists of global hourly and synoptic observations updated daily from more than 14 000 active stations worldwide, including a large number of airports, conveniently made available through web API's in various formats [NCEI, 2003]. Observed elements at each station were then identified, and the distance to the site plotted (Figure 34). For the two locations in the UK, closer-to-site hourly measurements of wind speed and direction, air temperature and global horizontal irradiance recorded by stations operated by the Met Office could be acquired through the MIDAS Open public datasets [Met Office, 2019]. In Germany, 10-minute observations and hourly data from the national network of automated stations are available online at the German climate data center (CDC) open data portal [DWD, 2020]. In Belgium, 10-minute observations and hourly data from 17 automatic weather stations around the country are being released in the RMI opendata portal in accordance with the INSPIRE directive [RMI, 2020].

ERA5 reanalysis data covering the same period was also downloaded via the Copernicus Climate Store using the `ecmwf` and `ncdf4` packages for R [CRAN]. The gridded datasets were stacked into time series and pre-processed as described in chapter 4.7, using bilinear weighting of the four grid cells closest to the location. The resolution of the ERA5 (0.25°x0.25°) and ERA5-Land (0.1°x0.1°) gridded data available in the CDS catalogue are illustrated in Figure 34. The ERA5-Land model runs at an increased resolution of 9 km over ERA5's 31 km native grid spacing, but do not include all the parameters of the atmospheric reanalysis. Consequently, both were acquired for the analysis.

Figure 34, illustrate the four nearest grid cells of the ERA5 reanalysis dataset in red, the ERA5-Land surface dataset in blue and the centre of the satellite pixels of the CAMS radiation service (orange points) surrounding the building site locations (crosses). The closest meteorological stations are also illustrated in green (triangles).

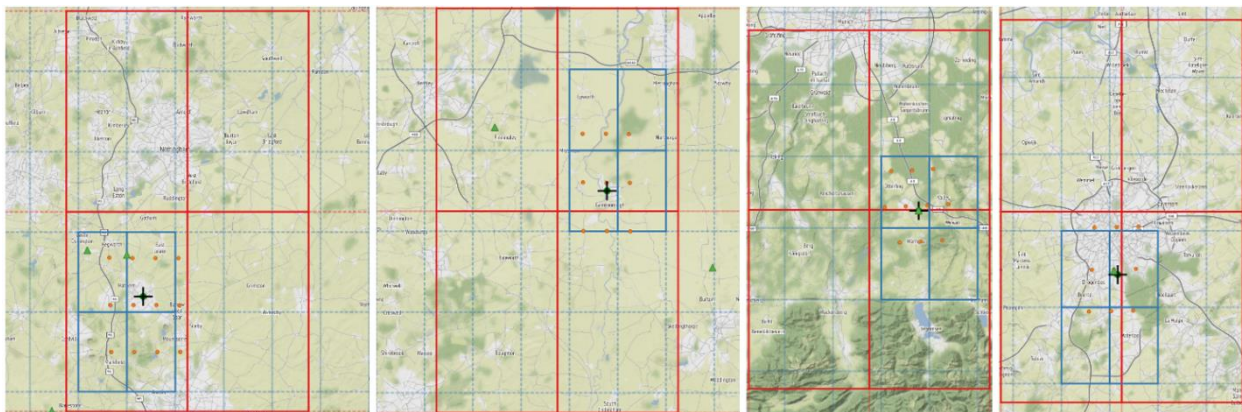


Figure 34. Illustration of the four nearest grid cells of the ERA5 reanalysis dataset in red, the ERA5-Land surface dataset in blue and the center of the satellite pixels of the CAMS radiation service (orange points) surrounding the building sites (crosses). The closest meteorological stations are also illustrated in green triangles. Map tiles by Stamen Design, under CC BY 3.0. Map data from OpenStreetMap.

For Loughborough, 6 km from the site, air temperature and 10-meter wind is measured. It is located in a village, whereas the second closest station, an airfield 9 km away, additionally records solar radiation. During the test, the exterior air temperature and relative humidity are measured on-site. For Gainsborough, the closest meteo-station only measures air temperature and is located 8 km away. Wind speed and direction is observed at two airfields both located ca. 17

km away, in opposite directions. The closest location found to measure solar radiation is located 31 km from the building site. On-site during the test the exterior air temperature is measured. For the Twin Test Houses, all the requested parameters are measured in relation to the meteo tower on-site (< 100 meter). Finally, for the Uccle test case, air temperature and wind speed is measured 1 km away at the site of the Belgian weather institute (RMI). Solar irradiance measurements were not acquired.

For all the cases (from left to right LBORO, GBORO, TWINS and UCCLE), air temperature and wind (illustrated by green triangles on the maps) is observed closer to the building than the resolution of the reanalysis datasets, except for the Gainsborough site. When available, these nearby observations are used.

Table 10. Weather data

Variable	#	LBORO	GBORO	TWINS	UCCLE
Wind speed (10m)	ws	6 km	17 km	Site	1 km
Wind direction	wdir	6 km	17 km	Site	1 km
Air temperature	te	Site	Site	Site	1 km
Global horizontal irradiance	ghi	CAMS-Rad	CAMS-Rad	Site	CAMS-Rad
Global diffuse irradiance	dhi	CAMS-Rad	CAMS-Rad	Site	CAMS-Rad
Beam horizontal irradiance	bhi	CAMS-Rad	CAMS-Rad	Derived	CAMS-Rad
Beam normal irradiance	bni	CAMS-Rad	CAMS-Rad	Derived	CAMS-Rad
Sky irradiance (LW)	strd	ERA5	ERA5	Site	ERA5
Sky temperature	tsky	Derived	Derived	Derived	Derived
Ground Albedo	albedo	ERA5/ERA5L	ERA5/ERA5L	ERA5/ERA5L	ERA5/ERA5L
Diffuse surface irradiance	isol_dif	ISO52010	ISO52010	ISO52010	ISO52010
Direct surface irradiance	isol_dir	ISO52010	ISO52010	ISO52010	ISO52010
Solar height angle	alpha_sol	ISO52010	ISO52010	ISO52010	ISO52010
Solar azimuth angle	fai_sol	ISO52010	ISO52010	ISO52010	ISO52010

Solar radiation was only measured locally at the TWINS building site in Holzkirchen: for the other cases Copernicus CAMS Solar Radiation Service provided minute estimates of global, direct and diffuse radiation. The service is based on 15-minute satellite images combined with atmospheric radiation modelling. Figure 34 show that the centre of the satellite pixels surrounding the site in orange, has a much finer spatial and temporal resolution to capture local sky conditions than hourly measurements available several km away. The 1-minute data product was downloaded using the CamsRad R-package [Lundström, 2016] and aggregated into 10-minute and 15-minute samples. For TWINS, beam normal irradiance was calculated from observed 10-minute global and diffuse horizontal irradiance using the solar positioning algorithm in the R-package solarCalcISO52010 available on Github [Lundström, 2018]. The same tool was used to calculate direct unshaded vertical irradiance for every building orientation (Table 10).

## 6.6. Indoor temperature

In this section the possible ways to account for the indoor temperature described in Chapter 4.6. are explored on the four test cases. Following the description of approaches, a systematic way to present and compare the results is shown in Table 11. It is important to note that the Approach 1 for all test cases assumes a uniform indoor temperature of 18°C. Even though the temperature in the main living space is usually higher, a temperature reduction factor is taken into account for temperature variations within the house in accordance to the Belgian method [BS, 2019]. For approaches under number 3 where the house is divided into two zones, it is assumed that the living room temperature is applied to the day zone while the master bedroom temperature is applied for the night zone.

An additional limitation of the assumed approaches is that the ARX modelling cannot be performed for Approach 1. The reason is that the temperature is constant and therefore correlated with itself, thus the model works only for the 1<sup>st</sup> order which does not produce reliable results in this case. Given different measurement set-ups, it is not feasible to apply all approaches to each test case, thus a discussion of the results follows.

Table 11. Description and nomenclature of the approaches applied to the indoor temperature.

Approach	Description
1	Uniform $\theta_i$ according to standard
2	Uniform $\theta_i$ according to one sensor in the main living room
2a	$\theta_i$ according to one sensor in the main living room, night zone $\theta_i$ -2°C, arithmetic mean
2b	$\theta_i$ according to one sensor in the main living room, night zone $\theta_i$ -2°C, volume-weighted
2c	$\theta_i$ according to one sensor in the main living room, night zone $\theta_i$ -2°C, façade area-weighted
3a	$\theta_i$ according to sensors in each zone, arithmetic mean
3b	$\theta_i$ according to sensors in each zone, volume-weighted
3c	$\theta_i$ according to sensors in each zone, façade area-weighted
4a	$\theta_i$ according to detailed measurements in each room, arithmetic mean
4b	$\theta_i$ according to detailed measurements in each room, volume-weighted
4c	$\theta_i$ according to detailed measurements in each room, façade area-weighted

### 6.6.1. Twin Test Houses

Since the Twin Test houses were extensively monitored during the experiment, it was possible to perform all approaches described in Table 11. HTC estimates obtained while performing the calculation with different indoor temperature assumptions are presented in Figure 35. In this test case, the occupancy was synthetic, therefore no significant variations in the indoor temperature set point and achieved temperatures were introduced. Also, there was no difference in the set-points in the day and night zone, which produced a relatively uniform temperature inside the whole house. For the purpose of this study, it is assumed that the day zone consists of the kitchen, living and dining room, all other rooms are assumed to be the night zone.

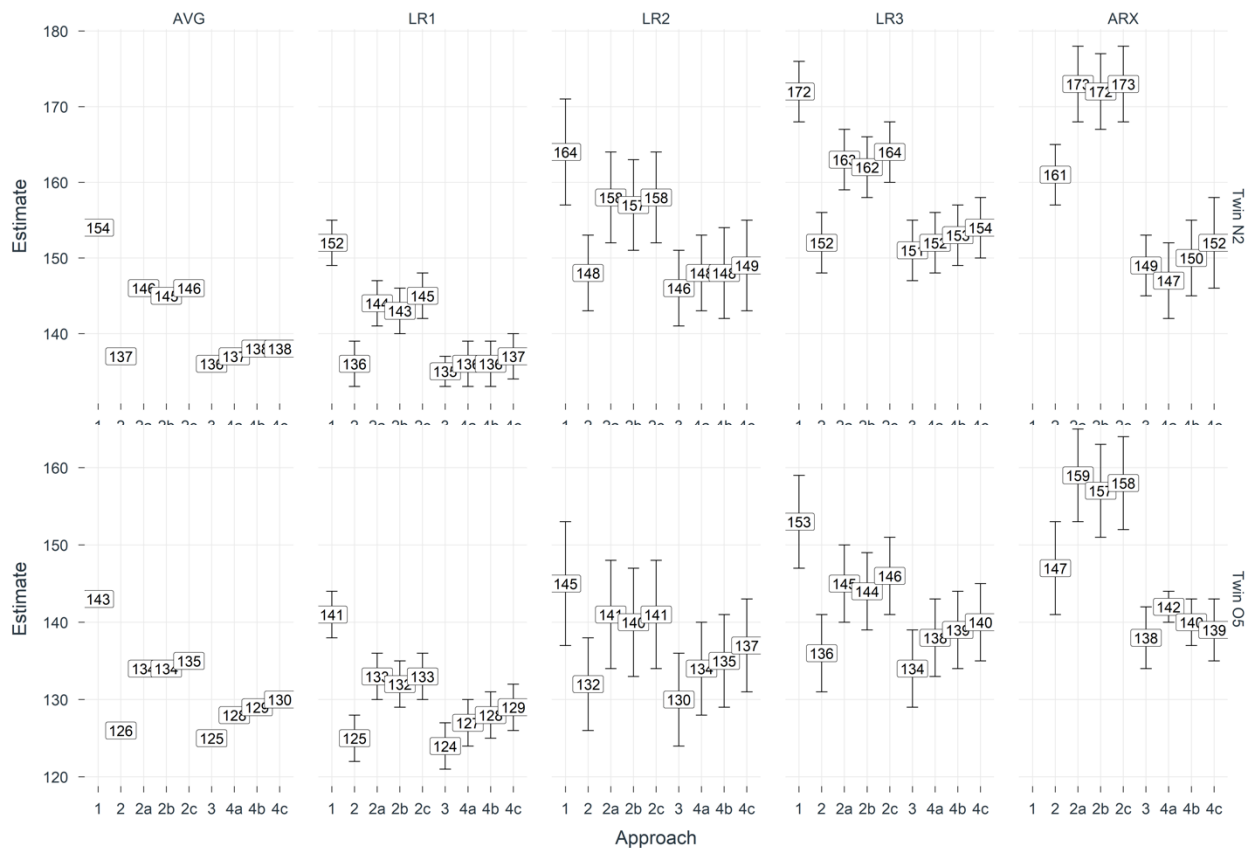


Figure 35. Estimates of the heat transfer coefficient calculated using different methods (see Chapter 3) and approaches (see Section 4.6) on the assumption of indoor temperature for the Twin Test Houses. The error bar represents the standard deviation of the estimate.

Now, results will be commented from ones calculated with the “worst” assumptions to the best assumptions for this test case. The largest discrepancy in the estimate can be noticed in Approach 1 because the assumed temperature is significantly lower compared to other approaches. In Approaches 2a, 2b and 2c again the assumption of a lower temperature achieved in the night zone leads to a larger deviation. Because of the assumed greater temperature difference in the four mentioned approaches the heat losses are overestimated. Given the setup of this experiment, all other approaches produce similar results. For example, when the living room temperature is assumed to be achieved in the whole house, Approach 2, the estimate is equally good as the temperatures were measured in all rooms, which in practice would often not be the case. Moreover, due to the compact geometry and the room layout of the observed house, averaging by façade or by volume gives similar results. In the plots approaches denominated by 3 gave similar results therefore just one estimate is shown. It can be also noticed that those approaches give slightly lower results than approaches under number 4. Approaches under 4 which in practice require the most accurate measurements, according to our expert knowledge, should produce the most exact estimates.

When observing the results, the same relations between different approaches are noticed regardless of the statistical modelling methods. On the other hand, it is possible to notice a slight increment in the estimate as the complexity of the statistical modelling method increases (AVG to ARX).

### Impact of the stratification effect

To investigate the impact of enhanced stratification occurring in Twin N2 which is heated by electric radiators, additional approaches are adopted to define the room indoor temperatures and their impact on the HTC-estimates has been investigated for state-space modelling. Assumptions made for the analysis are listed in Table 12. The additional state-space model used in this analysis is shown in Figure 36.

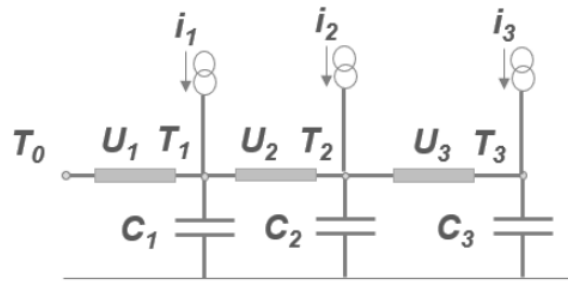


Figure 36. State Space Model used for dynamic analysis of the Twin Test Houses.

Where  $T_0$  represents the ambient temperature,  $T_1$  the external wall temperature,  $T_2$  the indoor temperature and  $T_3$  the indoor mass temperature. Moreover,  $i_2$  represents the solar heat gains, electric heating power and a proportion of the underfloor heating power,  $i_3$  the remaining proportion of the underfloor heating power, while  $i_1$  remains unused ( $i_1=0$ ).

Table 12. Assumptions adopted while performing an additional investigation on the indoor temperature inputs for the Twin Test Houses

Input	Assumptions
Solar irradiation	Fixed $g_A$ , south facade solar radiation
Heat input	Includes net heating energy, excludes internal heat gains
Ventilation	Supply air heating energy excluded
Indoor temperature	Volume weighted average between zone, temperatures considered according to different hypotheses
Timestep	Hourly data
Analysis Period	42 days
State Space Modelling	3 State Space variables

The different room indoor temperatures hypotheses considered in grey-box modelling:

1.  $t_{in,vol,avg}$ : room temperatures are measured at 1.10 m height
2.  $t_{in,vah,avg}$ : room temperatures are averaged over the room height from values recorded at 0.10 m, 1.10 m, 1.70 m heights and at 0.10 m below the ceiling.
3.  $t_{in,str,wv}$ : ground floor rooms temperatures are averaged over the room height ( $t_{in,vah,avg}$ ) while first-floor rooms temperatures are averaged between  $t_{in,vah,avg}$  and the temperature recorded at 0.10 m below the ceiling, according to the proportion of external wall area versus roof area.

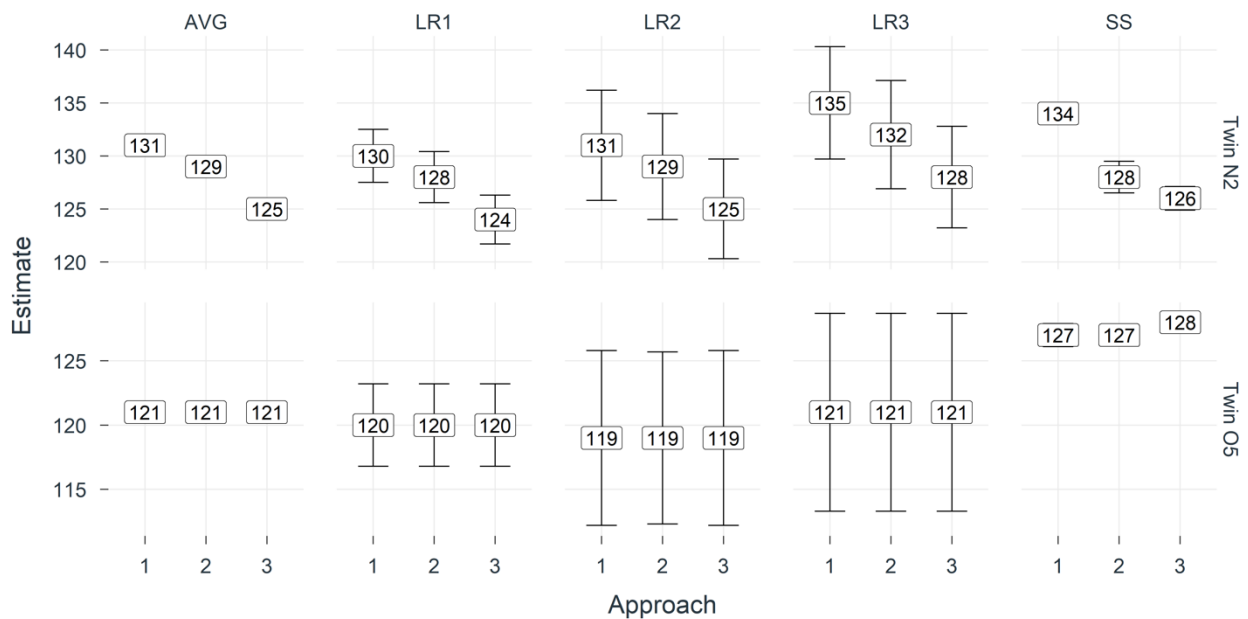


Figure 37. HTC estimates calculated for additional indoor temperature assumptions on the example of the Twin Test Houses.

For the Twin O5, no significant improvement in the estimated HTC can be noticed, that is because the indoor air was uniformly heated. However, for Twin N2 a significant improvement is achieved when the air stratification is taken into account.

### 6.6.2. Gainsborough

For the Gainsborough test case, the possibilities for the investigation of the indoor temperature are limited because only two temperatures were measured: in the living room and master bedroom. Therefore, approaches under number 4 could not be applied. Moreover, the geometry and the layout of the house are quite simple, thus it is assumed that the ground floor is the day zone and the first floor is the night zone. Since both floors have the same area and volume there is no difference between the arithmetic mean average, volume-weighted average and façade weighted average. Consequently, in the plotted results  $2a=2b=2c$ , and  $3a=3b=3c$ . HTC estimates obtained while performing the calculation with different indoor temperature assumptions are shown in Figure 38.

In this case, the temperature assumed by Approach 1 produces the highest estimated value. It indicates that the assumed temperature is significantly lower than in other cases where the temperature is actually measured, and therefore losses are largely overestimated. While approaches numbered as 2 and 3 present better assumptions of the indoor temperature. When comparing the results 2 and 3a, it can be concluded that for this test case the temperatures in the day and night zone do not differ significantly. On the other hand, when looking at the ARX modelling, it is possible to notice a significant improvement between the two assumptions when the indoor temperature is calculated according to Approach 3a.

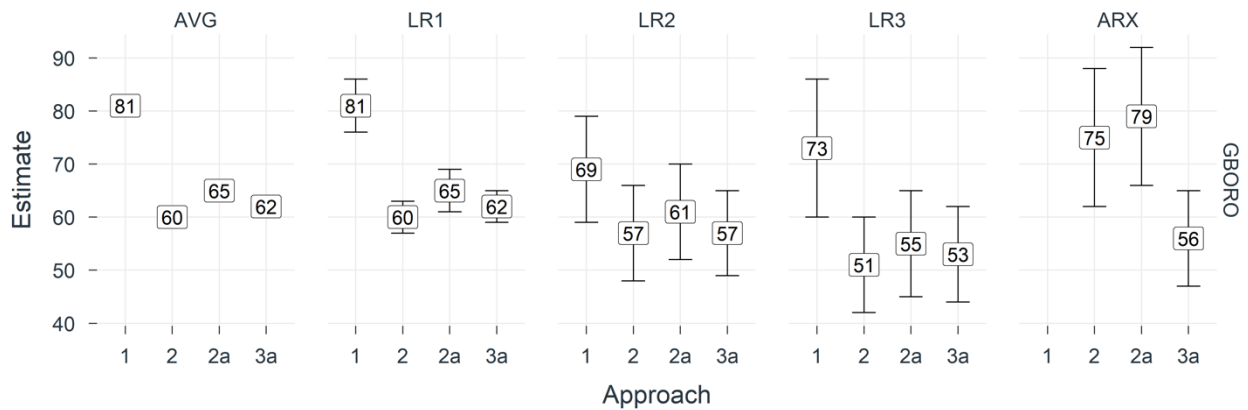


Figure 38. Estimates of the heat transfer coefficient calculated using different methods (see Chapter 3) and approaches (see Section 4.6) on the assumption of indoor temperature for Gainsborough. The error bar represents the standard deviation of the estimate.

### 6.6.3. Loughborough

In the Loughborough test house, the temperatures were monitored in every room. Knowing that the kitchen, living room and dining room are located on the ground floor, the whole floor is considered as the day zone. The first floor is considered to be the night zone. Since the floor areas and volumes of the ground and first floor are equal it is assumed that there is no difference between the arithmetic mean average and volume-weighted average in approaches under number 2 and 3, 2a=2b and 3a=3b. HTC estimates obtained while performing the calculation with different indoor temperature assumptions are shown in Figure 39.

For this test case, it is noticeable that with the increase of the statistical model complexity the calculated estimates increase in value. If comparing Approach 1 with all approaches, up to 4b which presents the most accurate assumption, it is not possible to notice a significant improvement in the estimates for all modelling approaches. Thus, it is safe to conclude that the achieved indoor temperatures did not significantly differ from the assumed uniform temperature of 18°C.

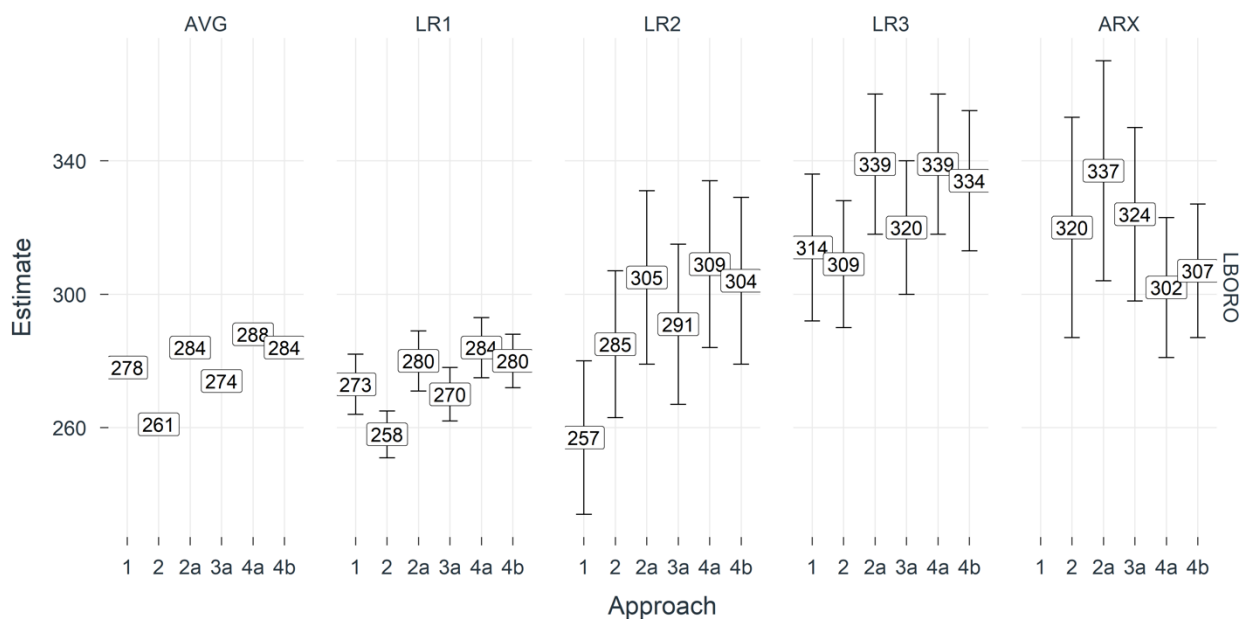


Figure 39. Estimates of the heat transfer coefficient calculated using different methods (see Chapter 3) and approaches (see Section 4.6) on the assumption of indoor temperature for Loughborough. The error bar represents the standard deviation of the estimate.

#### 6.6.4. Conclusion

When no temperature measurements are available the assumed temperature according to a standard can produce a large difference of the estimate from the actual value. It is suggested to have at least one temperature measurement in the dwelling. Moreover, knowledge about the heating preferences in different zones of the house can improve the assumption. Comparing the impact of the assumptions on the HTC-estimates, the deviations show to be case dependent. For the Twin Test Houses and the Loughborough dwelling variations up to 15 and 18% are noted, while for the Gainsborough test case they raise to 33%.

#### 6.7. Conclusions

In this chapter we learned that the estimate for HTC often benefits from including solar gains. Approach 2 should in most cases be sufficient. In those case where the models need to provide accurate predictions of the building's behaviour, more detailed modelling approaches for solar gains might be considered. Evidently, the heat input is the most important term to get right. Ideally, measurements behind the generator and data to separate SH and DHW are available. Discrepancies of up to 100% need to be taken into account when simplified modelling approaches are considered. Also, ventilation heating power was shown to have a significant impact, with HTC changing up to 30% when modelling it explicitly. With regard to internal heat gains, the impact of including lighting and appliance heat gains is significant, with HTC changing up to 55%. Internal heat gains due to occupancy was shown to only have a negligible impact. Finally, it is advisable to at least have one temperature measurement in the dwelling, as it significantly impacts the estimate of HTC.



## 7. Discussion of results

We can now confidently apply modelling approaches that have proven reliable in earlier chapters. In this Chapter, our focus shifts from the modelling approaches to the case studies themselves. In Table 13, an overview of the inputs investigated in Chapter 6 for each test case is presented. Here, instead of focusing on the impact of one aspect, e.g. solar gains, we now combine the best approaches for different terms in the building's heat balance. In this stage "best" means most precisely measured, or most advanced method, according to our expert knowledge. Note that this often might not correspond to the approach that gives the result closest to the reference value in our previous exploration of the results. The main reason is that in our previous exploration we only vary one of the modelling approaches at a time, keeping the basic approach for all the others. Hence, it is hard to predict which combination of all approaches would give the closest overall fit to the reference HTC. In this chapter, a detailed explanation of the optimal combination of modelling approaches per test case will be given.

Table 13. Case studies and heat balance terms that have been investigated in detail during the Annex 71 work

	Solar gains	Heat input	Ventilation and infiltration	Occupant and heat gains	Weather data	Temperature input
LBORO	✓	✓			✓	✓
GBORO	✓	✓	✓	✓	✓	✓
Twin N2	✓	✓	✓		✓	✓
Twin O5	✓	✓	✓		✓	✓
Uccle	✓	✓		✓		

### 7.1. Twin Test Houses

Given that during the measurement period the Twin Test Houses were extensively monitored it was possible to investigate the majority of the proposed modelling techniques and approaches. The selected period to apply the combination of best approaches for the Twin Test Houses is 30 days, from 01.01.2019. 00:00 to 30.01.2019. 23:50, and the data is provided with 10 minutes frequency. For the Twin O5 case, several heat flow meters were installed along the heating system, therefore, a detailed differentiation between the energy use of the generator, heat output and exact heat delivered to the ambient is available. In Twin N2 only the exact heat input is measured (more in 6.2.1.). The parameters of the ventilation systems were accurately monitored during the experimental period (see Section 6.3.1.). Since the houses were inhabited by synthetic occupants, occupant and appliance heat gains were recreated by heaters located in the indoor space, and the exact internal gains were measured. All the weather data was collected at the exact location. Detailed measurements of the indoor temperature in every room at different heights are available for both houses (see Section 6.6.2.). Despite the different heating systems, the same approaches are applied in the assessment of both Twin N2 and O5. For the solar heat gains the most advanced approach, Approach 4, which implies a Spline based solar transmittance calculation is adopted in grey-box modelling (details can be found in Section 4.1.4.). In static and ARX modelling a constant gA value is adopted. In the Twin N2, only one approach to calculate the heat delivered by the heating system, Approach 4, is possible. This approach proposes to use the exact heat delivered by electrical heaters. For the Twin O5 the exact heat delivered by the underfloor heating is measured by a separate heat flow meter, here again, Approach 4 is selected (more in 4.2.4.). The ventilation losses are calculated in both houses according to the most accurate measurements of ventilation air flow and temperature (more in 4.3.1.). The losses are provided as additional input to the overall heat balance. The only input that cannot be further explored in this test case are the occupant and appliances heat gains, since there were no disturbances introduced by occupants. The estimation of the internal gains cannot be improved as the exact heat input, simulating the occupancy, is measured. Next, the weather data cannot be improved because the measurements are already taken at the exact location. In the end, the indoor temperature is calculated based on the height-averaged values per each room, subsequently volume averaged. This way the stratification effect, enhanced due electrical heating present in the house N2, is better captured. The chosen accuracy is the extension of Approach 4b (more in 4.6.4.), which in practice requires the measurement of the

room indoor temperatures at different heights. Even if the stratification is not pronounced in Twin O5 the same approach is implemented.

Figure 40 and Figure 41 compares the HTC-estimates as obtained by the different statistical models for the optimal approaches described above with the reference value measured by a co-heating test. In both cases the average method (AVG) and simplest linear regression method (LR1) show similar results. When optimising the solar aperture with the statistical model (LR2, LR3, ARX or SS) more variation in the results is found. Surprisingly, estimating the solar aperture within the statistical analysis does not seem to enhance the HTC-estimate. Both for LR2, LR3 and ARX the estimates are deviating more from the reference value than it is the case for the AVG and LR1-method. State space modelling gives for the current case the best results.

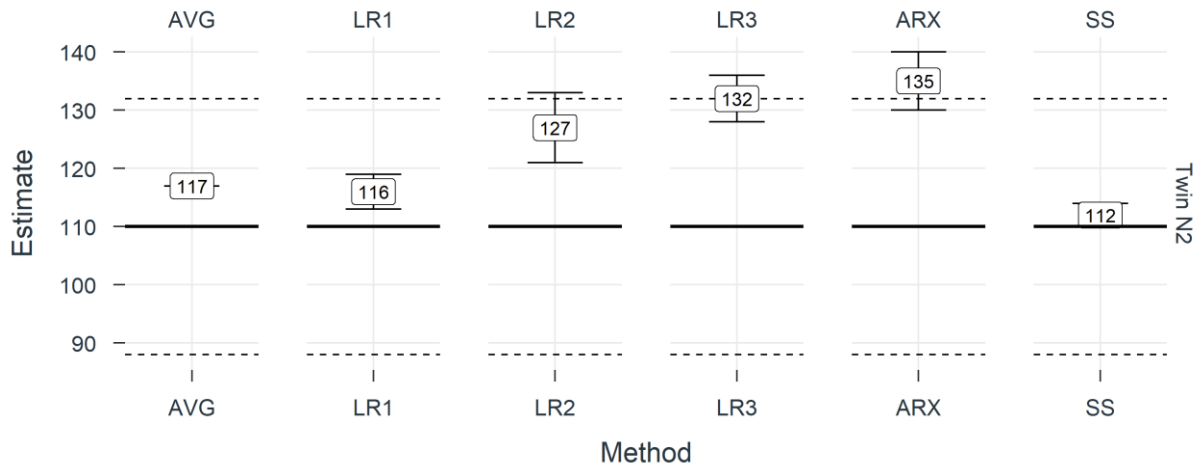


Figure 40. Results for optimal combination of approaches for the Twin Test House N2. The calculated reference value for HTC is indicated as a horizontal thick line, and a 20% deviation above and below as dashed lines.

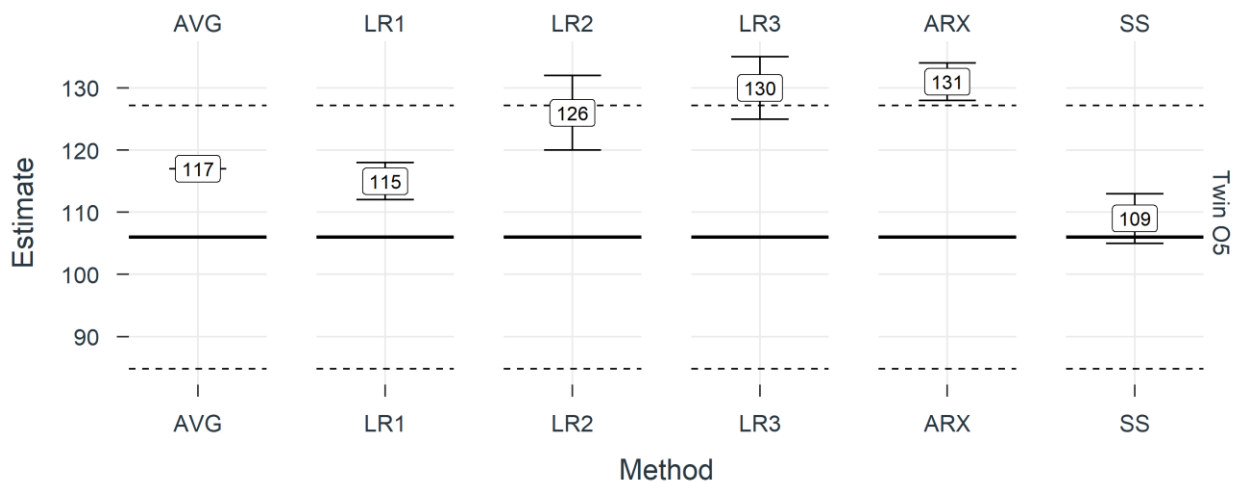


Figure 41. Results for optimal combination of approaches for the Twin Test House O5. The calculated reference value for HTC is indicated as a horizontal thick line, and a 20% deviation above and below as dashed lines.

## 7.2. Loughborough

The Loughborough test house was synthetically occupied during data collection, and as such internal gains and ventilation were not investigated. The original weather data collected nearby the dwelling was used in this best approach. Solar gains, indoor temperature, and the heat input were explored for this house. As for other test cases, a constant solar aperture was found to be most appropriate for static methods, with splines best for the dynamic state-space and ARX models. The boiler heat output was measured directly for this test case and was found to be the best approach for characterising the heat input in the analysis methods. Finally, the volume-weighted average internal temperature was selected as the best approach for this variable.

The data prepared for the optimal approach was from 17/2/14 00:00 to 15/3/14 23:00, with hourly intervals. The additional weather data was used to calculate solar splines for use in the dynamic analyses. The results of the best approaches are shown in Figure 42. Whereas for the Twin Test Houses all methods overestimated the HTC compared to the reference value, for the Loughborough case all methods calculate a lower HTC than the reference value, which was again measured by a co-heating test. Part of these deviations might be attributed to the period of analysis which in both cases deviated from the moment to co-heating test was performed. We will further dig into this in Chapter 8. For the Loughborough case, only the dynamic methods estimate the HTC within a 20% accuracy of the reference value. For the static methods, an underestimation of up to 30% is found.

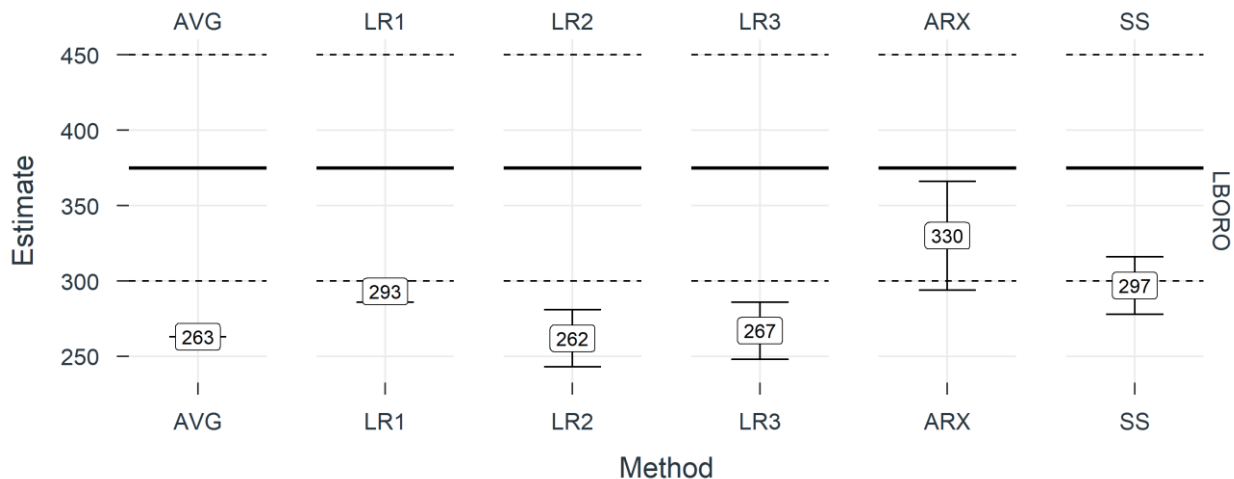


Figure 42. Results for optimal combination of approaches for the Loughborough case. The calculated reference value for HTC is indicated as a horizontal thick line, and a 20% deviation above and below as dashed lines.

## 7.3. Gainsborough

The apartment end unit in Gainsborough that was selected for analysis is in the south-facing part of the building. One month in 2014 from February 17<sup>th</sup> 00:00 to March 15<sup>th</sup> 23:50, is selected to apply the combination of best approaches (28 days). The original measurement data provided in 5-minute frequency was resampled to 10-minute mean values. From the five-minute data, gas and water meter readings were used to make a simple deterministic split between domestic hot water and space heating under the assumption that the boiler cannot operate in heating mode and domestic hot water mode at the same time. The other fundamental assumption is that gas use for domestic hot water perfectly coincides with water consumption. This is implying the absence of domestic hot water storage but could not be verified based on the available technical specifications of the system. Furthermore, a fixed boiler efficiency was assumed (see 6.2.2.) 5-minute CO<sub>2</sub> measurements were also used to estimate occupancy before converting the occupancy model output to 10-minute internal heat gain. Recorded electricity consumption was also included in the internal heat gains. Electricity and occupancy model gains constitute about half of the internal gains each (Table 14). Note that by including the estimated internal gains, the HTC estimates increase as the internal gains are more than four times of the energy derived for space heating (Table 14) and two times the energy for space heating and domestic hot water (without separating out domestic hot water from boiler gas consumption). Hence, a high degree of uncertainty can be attributed to the assumptions used in the gas splitting method.

Table 14. Mean specific heat gains per floor area over the period.  $I_{sol}$  multiplied by a fixed  $gA$  of  $3.6$  was used in some of the basic approaches.

	$Q_{h,sh}$ gas split	$Q_{h,dhw}$ gas split	$Q_{i,el}$ meter	$Q_{i,occ}$ model	$I_{sol} * 3.6 \text{ m}^2$
Heat gain	$2.9 \text{ W/m}^2$	$3.9 \text{ W/m}^2$	$7.2 \text{ W/m}^2$	$6.6 \text{ W/m}^2$	$5.0 \text{ W/m}^2$

The indoor temperature was recorded in the lounge (ground floor) and main bedroom (first floor). Envelope transmission and infiltration heat loss of each floor was calculated from U-values, surface areas and air volume. The indoor temperature was weighted according to the calculated heat loss, assuming that the temperature of the lounge equals the temperature of the whole ground floor (lounge, kitchen and staircase) and that the temperature of the main bedroom is the temperature of the first floor (staircase, two bedrooms and bathroom). This division leads to a 50 % weighting of either and represents the new dataset's indoor temperature. An alternative separation according to room functions, where the main bedroom's temperature is considered representative of the two bedrooms only would lead to a 27%/73% allocation. The bedroom's measured temperature is one degree colder on average than what was measured in the lounge, Figure 43. In addition to the room temperatures, the ventilation supply air temperature in the balanced ventilation unit was measured after heat recovery. The supply temperature was higher than the weighted bedroom and lounge temperature at times, even though the outdoor air is not pre-heated by a coil. This finding indicates that the ventilation extract air temperature is warmer than in the lounge and bedroom (at least in the room air measurement position) and results in a positive ventilation heat gain during part of the period. With balanced ventilation, it is common to extract air from the bathroom and kitchen, and supply fresh air to other rooms. Neither bathroom nor kitchen room temperatures were measured. In a ventilation scheme relying on overflow between rooms, the mean indoor temperature used to assess the envelope heat losses may not be the same as the that should be used in assessing the building ventilation heat losses. Nevertheless, we used the weighted 50% lounge and 50% bedroom temperature for both assessments.

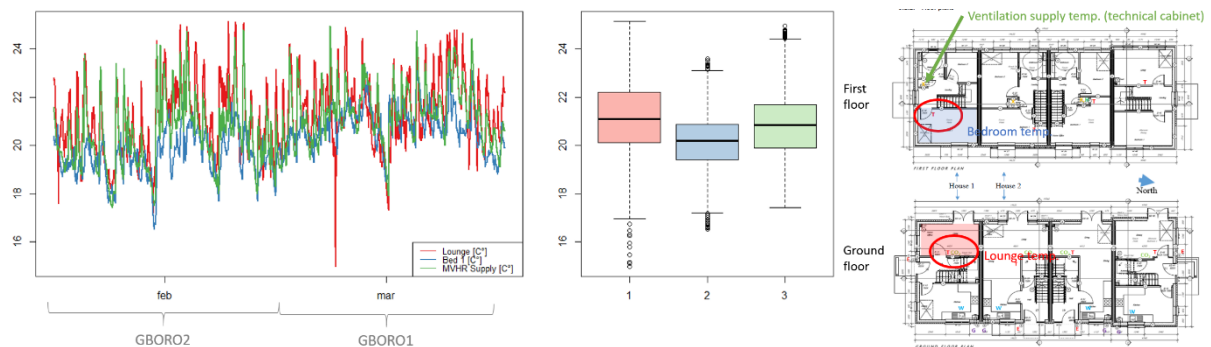


Figure 43. Measured indoor temperature and supply temperature during the full period of analysis.

A comparison of building roof PV production to the hourly global horizontal radiation recorded at Waddington 31 km away, revealed that solar irradiance was shifted by one hour in the basic dataset. This error had no implications in the static approaches where daily data was used but was corrected for the dynamic approaches using hourly data, and the extended ten-minute dataset. The PV electricity meter also made it possible to compare the global horizontal irradiance observed 31 km away to the satellite irradiance product. First, the hourly observations from Waddington were resampled from hourly to 10-minute data, and a diffuse separation method was applied (see 6.5.). The resulting global, direct and diffuse irradiance from both the observations and the satellite irradiance product was compared to the on-site PV installations measured output. By applying simple linear regression, the satellite product achieved an  $R^2$  of 0.75 compared to an  $R^2$  of 0.69 for the observational dataset. On this basis, the global horizontal irradiance observations from Waddington was replaced for the satellite irradiance model downloaded from CAMS-Rad.

A constant  $gA$ -value was adopted for the static methods and for the ARX models. Splines were tested, having greater impact on the months before March, where the solar elevation angle was lower and the nearby buildings obstruct solar irradiance (especially on the south façade).

Ventilation mass flow rate was estimated from the air handling unit electricity use sub-meter, assuming a fixed specific fan power. The derived flow rate was used in the ventilation loss calculations. Infiltration was not separated out as an individual effect in the final approach.

Note that for this case study, the reference value is calculated based on designed parameters. The actual estimated result is likely to be higher, among others due to workmanship issues. This is indeed confirmed in Figure 45: all methods show a significantly higher HTC-estimate than the design value. Furthermore, all results are consistent around 80 W/K (double the design value), only the state space modelling results in a lower estimate.

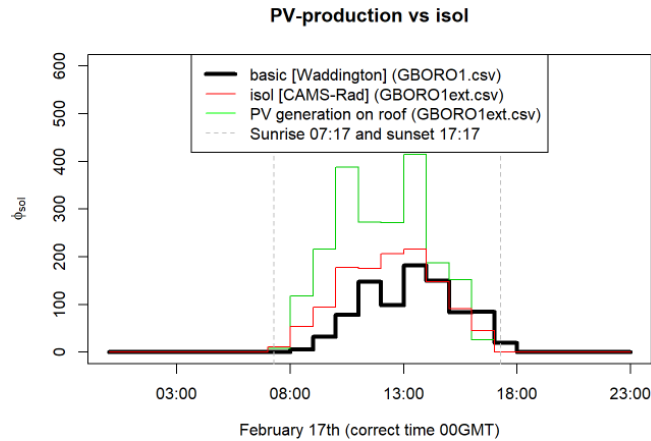


Figure 44. Measured PV generation and solar irradiance sourced from CAMS-Rad and observations at Waddington. Some of the difference at mid-day between PV generation and solar irradiance stems from shading effects due to a nearby building blocking part of the sun at this time of year.

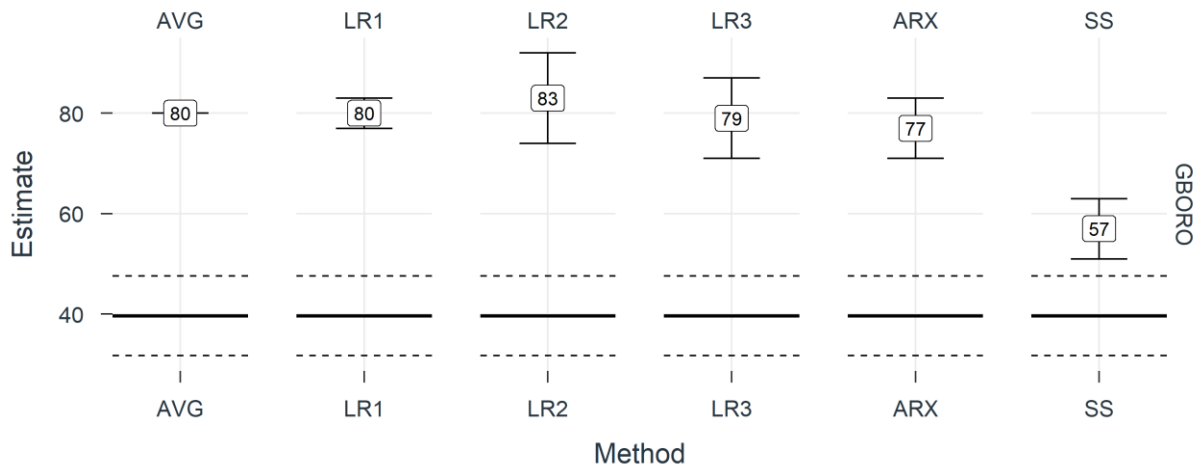


Figure 45. Results for optimal combination of approaches for Gainsborough. The calculated reference value for HTC is indicated as a horizontal thick line, and a 20% deviation above and below as dashed lines.

## 7.4. Uccle

Finally Figure 46 compares the results for the Uccle test case. Only results of the static methods are shown. The most optimal approach uses as indoor temperature, the weighted average temperature over the loss surfaces. For the outdoor temperature, the temperature from a weather station nearby and the Soda-pro website are used. The global solar radiation is also from the Soda-pro website and is multiplied with a fixed solar aperture (AVG and LR1) or estimated as part of the modelling (LR2 and LR3).  $\Phi_n$  comprises the gas use for space heating, the total electricity use and the metabolic heat gains derived from the CO<sub>2</sub> balance method. All static methods seem to overestimate the reference value, but the overestimation is much less pronounced for the methods that estimate both HTC and solar aperture.

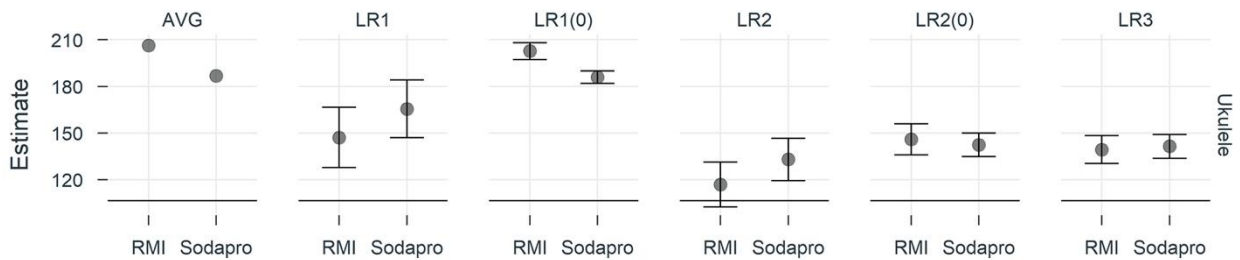


Figure 46. Results for the optimal combination of approaches for the Uccle Test House.

## 7.5. Guidelines

To conclude this chapter, this section presents a set of general guidelines, subdivided for different inputs, built on our expert knowledge and results gathered while working on the explored five test cases. The first step towards a reliable HTC calculation is the collection of information about the building in focus. For the presented test cases this can be found in Chapter 5. Since the main aim is to assess the performance of the building envelope, knowledge about the construction materials, insulation quality or even construction year can give a first perception of the expected outcome. Next, the inputs explored in Chapter 6 should be investigated for the observed building. The guidelines presented below could serve that purpose.

### Solar gains

- Knowledge about the orientation, glazed area and external shading can give a first indication of the expected solar gains magnitude in the overall heat balance.
- Overall, solar heat gains turn out to significantly contribute to the building's heat balance. Ignoring them will result in an underestimation of the HTC.
- The lower the expected HTC (newly erected and well-insulated buildings) and/or the larger the glazed area, the more important is to include solar gains precisely in the heat balance equation
- If the windows are rather evenly distributed over the different facades, estimating a constant solar aperture will mostly suffice
- Only for buildings with windows particularly orientated to one direction, a more precise, orientation-dependent estimation of the solar aperture seems beneficial. This can be done by fitting a gA-value for each principle orientation or by implementing a spline-based estimation.

### Heat input

- In order to identify the possibilities of the heat input measurement, it is important to know which heat generator is installed in the dwelling.
- If we consider gross energy use measurements, taken before the generator, we tend to overestimate the HTC.
- Another important factor is the information about the DHW production, to understand which demand is reflected in the collected measurements. If there is no separate measurement of the DHW demand we tend to overestimate the HTC. On the other hand, if theoretical splitting is assumed it is possible to either overestimate or underestimate the HTC, depending on the assumption.
- Best results are obtained when the heat delivered to the indoor space is individually measured.
- When assessing buildings with complex systems (i.e. heat pumps), to avoid arbitrary assumptions of the efficiency and DHW split, additional measurements of the SH supply should be considered.

### Infiltration and ventilation

- Losses due to air exchanged through installed mechanical ventilation (with or without heat recovery units) should not be included in the HTC.
- Often mechanical ventilation systems are equipped with sensors e.g. in the heat recovery systems which can be used to determine this heat gain/loss more precisely
- It is often hard to separate infiltration (which is included in the HTC) and natural ventilation (not included in the HTC). Simplified models can be used to estimate the ventilation rates. Alternatively, sometimes both are combined in an equivalent HTC.

#### Occupant and appliances gains

- As for solar gains, internal heat gains can be an important additional heat gain in the building's heat balance. Ignoring internal heat gains will always result in a too low HTC.
- A first idea of the importance of appliances gains can be made by calculating the share of electricity use by lighting and appliances over the total energy consumption of the dwelling. The higher this share, the more important it will be to characterise the internal heat gains precisely.
- Typically, a correct assumption of the internal heat gains will be more important for well-insulated buildings.
- Appliances gains can be estimated based on a survey or site visit by listing appliances and lighting.
- For occupant heat gains, given the stochastic nature of this input, most of the explored approaches (Chapter 4.4.) rely on additional measurements, such as CO<sub>2</sub> or RH-data.
- If no additional measurements are available, standardised occupancy profiles can be used to estimate occupant and appliances heat gains.

#### Indoor temperature

- When no temperature measurements are available the assumed temperature according to a standard can produce a large difference of the estimate from the target value. It is suggested to have at least one temperature measurement in the dwelling (when possible even one sensor per zone).
- The averaged indoor temperature is determined by the heating preferences of the occupant, but also by the house layout and rooms' purposes. Knowledge about the heating preferences in different zones of the house can improve the assumption.
- Temperature stratification highly depends on the installed emission system. If the emission system (i.e. electric heaters) is suspected to cause enhanced stratification, sensors at different heights should be considered.

#### Additional comments and suggestions

- The basic setup for any of the proposed statistical modelling approaches in Chapter 3 should include the following measurements: indoor temperature, heat input, external temperature and global horizontal irradiance. This setup was the starting point in the exploration of inputs, Chapter 6. Depending on the building it should be taken into consideration to perform additional measurements. When possible, the most detailed measurements should always be taken into account.
- After conducting the measurement campaign and collecting the recordings it is important to identify which measurements will be used and inspect them for missing values. Selecting a period with incomplete measurements can result in erroneous calculations. Another aspect of data pre-processing includes resampling and creation of organized datasets which will be used in the next steps.
- Depending on the characteristics of the observed building and available measurements it is possible to select from Chapter 4 which approaches will be applied. For all presented inputs approaches range from the simplest to the most complex in ascending number order.
- The choice of the modelling method depends on the expertise of the assessor to correctly apply the methods, validate and understand the outcome. On the other hand, the available dataset (measured inputs, frequency, length, etc.) also introduces limitations. Detailed instructions for applying the approaches presented in Chapter 3 can be found in Annex 58: Report of Subtask 3, part 2: Thermal performance characterisation using time series data – statistical guidelines.

#### Duration and frequency of data collection/data pre-processing

- To investigate cases presented in Chapter 5 only one length of the dataset was selected and all participants used the same, previously pre-processed, data to carry out their research. Because of this reason, the impact of the data length and start date on the estimates was not investigated. A short investigation of the period impact was carried out in section 8.5.1.
- Since the chosen period of 30 days is too short, the Energy Signature method could not display reasonable results, thus was not included in graphs.
- The frequency of the data used to perform different statistical modelling techniques was not prescribed. Therefore, for dynamic modelling, the choice was made individually by the participants.



## 8. Towards real-life applications

*The work presented in this chapter is conducted in collaboration with the Loughborough University, UK and the datasets used were created for the Technical Evaluation of SMETER Technologies (TEST) Project (Phase 2), which was funded by the Department for Business Energy and Industrial Strategy via the Smart Meter Enabled Thermal Efficiency Ratings (SMETER) Innovation Competition: Phase 2.*

In this chapter, we turn our attention from “ideal” and extensively monitored test cases towards dwellings with limited information and measurements available. The introduced dwellings reflect realistic measurements setups with no additional energy usage monitoring other than smart meters, already available on site. Another difference from the previous work is that the target, reference value of the HTC, is unknown to the participants at the beginning of this exercise. This offer the possibility to perform a blind test and validate the assumptions and guidelines presented in previous chapters.

### 8.1. SMETER test cases

All test cases presented in this chapter, named HH07, HH18, HH20, HH21 and HH25, are located in North West England in two neighbouring towns. The dwellings are all semi-detached but differ mainly in size and occupancy. All dwellings are equipped with smart meters which monitor gas and electricity usage. The main heating source in all cases is a combi boiler, which means it provides for both SH and DHW demand and individual measurements of delivered heat flows are not available. Moreover, it is important to note that all appliances in the house are electric, including the stove. Apart from the boiler, no additional thermotechnical services are installed in the dwellings and the dwellings are naturally ventilated. Additional details about the dwellings can be found in Table 15. Along with the additional information, floor plans of all dwellings are presented in Figure 47.

Table 15 Additional information about the SMETER dwellings.

House ID	Type	Floor Area (m <sup>2</sup> )	Number of bedrooms	Number of occupants	Boiler model
HH07	End terrace bungalow	43.18	1	1	Vaillant ecoTEC pro 28
HH18	End terrace bungalow	39.4	1	1	Vaillant ecoTEC pro 28
HH20	Semi-detached house	64.97	3	3	Vaillant ecoTEC pro 28
HH21	Semi-detached house	78.08	4	6	Vaillant ecoTEC pro 28
HH25	Semi-detached house	64.97	2	4	Vaillant ecoTEC pro 28



Figure 47. Layouts of the SMETER test cases. For each dwelling, the living room is shown in red and the main bedroom in blue.

## 8.2. Datasets

### 8.2.1. Measurements

For each of the five dwellings, measurements were provided for gas consumption ( $\text{m}^3$ ) and electricity consumption (kWh), both collected at the meter for the whole dwelling. Indoor air temperature ( $^{\circ}\text{C}$ ) and relative humidity (%) data were measured with sensors located in individual rooms. Datasets have a 30-minute frequency and the start dates for the data collection vary and in some cases commenced prior to occupants moving in. The total lengths of the datasets are up to 7 months and all measurement campaigns were conducted from the end of 2019 to the summer of 2020.

Outdoor weather data measured at a single location within 6 km of all the homes is also available. Weather data comprise wind direction (degrees from N), wind speed (m/s), rainfall (mm), air temperature, relative humidity, air pressure (hPa), and global solar irradiance ( $\text{W}/\text{m}^2$ ), but mounted vertically and facing south. The exact location of the station is also known to the participants, thus it is possible to explore also additional weather inputs, as described in Section 4.5.

The dwellings were vacated by the occupants for one month, during which time a co-heating test, fan pressurisations tests, and other surveys were conducted. The co-heating test and fan pressurisation results have been omitted in the framework of this project to allow for blind prediction of heat transfer coefficient.

### 8.2.2. Preprocessing

Because of individual sensors failure, the temperature and humidity measurements collected in the dwellings show gaps of different lengths. Those data were preprocessed to fill the gaps which are not longer than 3h. The 3h period was selected because, according to our expert knowledge, no significant change in temperature or humidity would be present in the observed time. The gaps were filled in with a simple interpolation between the last and next known measurement. Gaps longer than 3h were not corrected. Since the indoor sensors are located in each room, most of the times only one of the sensors fails, so there is a possibility to calculate the averaged indoor temperature from other

sensors in the dwelling. In cases where gaps are attributed to problems in the acquisition unit (failure for multiple dwellings at the same and longer time) preprocessing could not fill the gaps. Thus for some cases, there are still some gaps present, as can be seen in Figure 48.

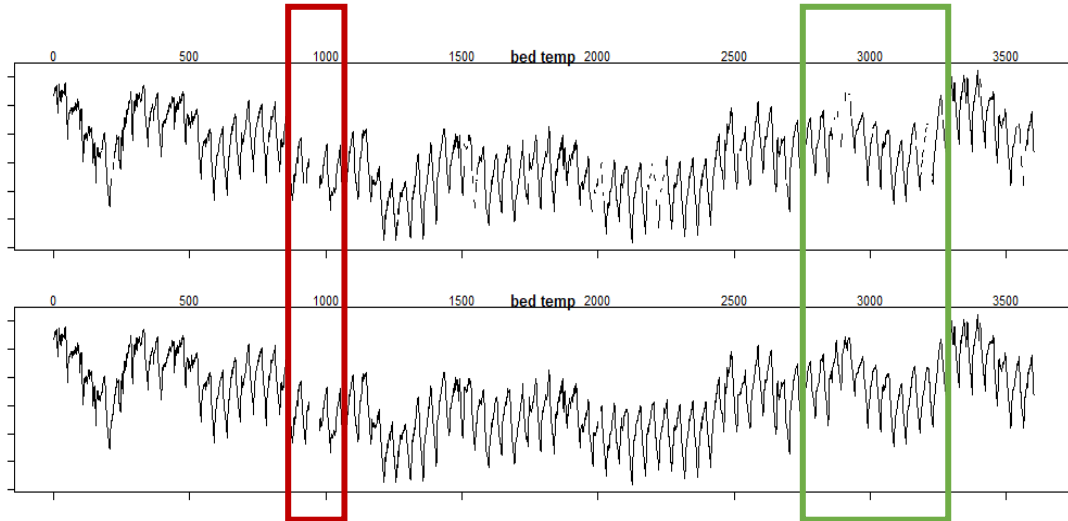


Figure 48. Example of successful (green) and unsuccessful (red) data preprocessing on indoor temperature measurements. Only data gaps shorter than 3h were corrected via linear interpolation.

All weather data were measured at 10-minute intervals and pre-processed to match the dwellings' measurements of 30 min. For each dwelling, a dataset of 60 days containing all available inputs was created. The selected 60 days contain measurements from January, February and March, depending on the dwelling. This period was selected because all inhabitants previously moved into the dwellings and the indoor temperature and gas usage were stable. This might have not been the case in the first days after moving in due to the elevated heat demand needed to bring the indoor temperature to an operational average. On the other hand, it was noticed that the external temperature starts increasing by the end of March, which can be reflected in lower heat demand.

### 8.3. Assumptions

Given the available data and information the following assumptions and approaches were adopted following the guidelines presented in Chapter 7:

**Solar gains:** All statistical methods were computed using the given global radiation on the vertical south façade. Moreover, the  $g_A$  was estimated individually by each participant, and not beforehand as in previous test cases. Thus, only methods which do not require  $g_A$  as input were performed.

**Heat input:** The raw datasets had gaps in the measurements, thus only the periods where electricity and gas meter data are continuous and inhabitants moved in the dwellings are selected. Electricity measurements were not manipulated and are in the original form. However, the gas measurements were preprocessed. In order to transform the heat input to W the calorific value of the gas and an average seasonal efficiency of the boiler were used. An average gas calorific value was calculated from the data provided by the energy distributor for the observed period and location ( $39.72 \text{ MJ/m}^3$ ). The efficiency of the boiler was assumed to be constant, according to the seasonal boiler efficiency of 89.3%, as provided by the manufacturer. In addition to this transformation, DHW decoupling, see Figure 49, was performed according to [Bacher P. et al., 2016]. The DHW decoupling will be further elaborated in Section 8.2.

**Infiltration and ventilation:** Since the natural ventilation rate cannot be monitored it was not possible to separate ventilation losses from the HTC. Thus, it was decided to compare the results to the co-heating estimate [Allinson D. et al., 2020] which includes ventilation losses. Note that a similar approach was also applied in the SMETER-project.

**Occupant and appliances gains:** Inhabitant gains were neglected and part of the electricity measurements, precisely 50 %, was included as appliances gains.

**Indoor temperature:** Temperature measurements from all rooms were area-averaged.

**Period:** To avoid deviation in estimates due to different conditions present in different periods, it was decided that all participants use the same 30 days (7<sup>th</sup> February – 8<sup>th</sup> March).

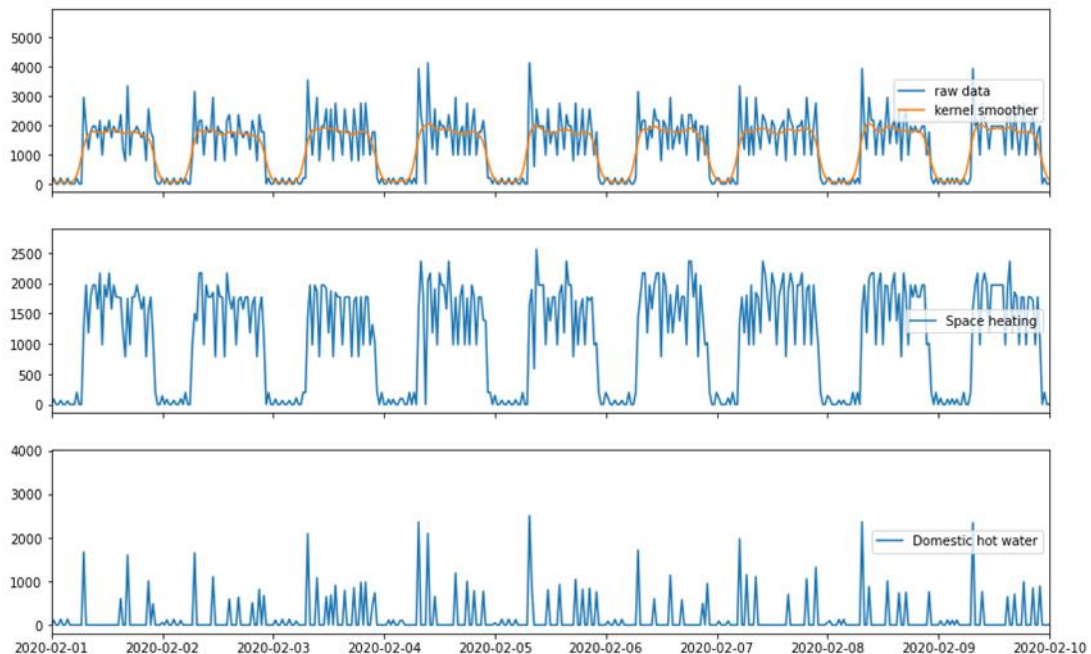


Figure 49. DHW decoupling procedure according to Bacher et al. Performed on SMETER gas measurements. The first plot shows the total energy delivered by the boiler in blue, while the resulting kernel smoother is indicated in yellow. The second and third plot show the separated SH and DHW respectively.

## 8.4. Results

Eight participants of the ST3 participated in the presented blind exercise and performed different statistical modelling techniques. First, all participants received the preprocessed datasets of 60-days length and the choice of the period used for the estimation was individual. After comparing the first results, large deviations in estimates were noticed between different statistical modelling techniques, but also between the results provided by different participants and the same modelling. Therefore, in the next step, the unique period of 30 days was prescribed (see also Section 8.3.). Here, the results are presented only for the 30 days. Moreover, three additional causes of discrepancy in the results were identified and further explored in section 8.5.

The results in this section are presented for each house and subdivided per statistical method and participant. The validation procedure for different modelling techniques was performed according to guidelines collected in Annex 58 ST3 statistical guidelines [IEA EBC Annex 58, 2016], and it is not presented in this work.

It is important to mention that the target value was added to the plots even though at the moment of calculation it was unknown. The target, reference value of the HTC as determined in the SMETER-project, is shown in the plots as the continuous horizontal line, together with the lower and upper confidence bound (shown as dashed lines). The lower and upper bounds include an estimate of the measurement uncertainty (95% CI) plus an additional uncertainty to account for the HTC changes through the season due to ground temperature and average wind speed. The reference HTC and the confidence bounds were obtained from the SMETER project. The results for all test cases are presented in Figure 50 to Figure 54.

Static methods performed by all participants give consistent results, while in dynamic modelling there is a discrepancy in the results between different participants. This deviation can be attributed to the freedom modellers have in choosing the inputs for the models and variant of the model (state-space modelling). Moreover, different setups for ARX and SS modelling require also different frequencies. All parameters of dynamic models are selected and tuned in order to pass the model validation (more in [IEA EBC Annex 58, 2016]). Different results among participants can also be caused by the use of different programming languages and respectively also optimizers.

For all test cases the estimates obtained for the observed period, given the adopted assumptions, resulted to be significantly lower than the results obtained from a co-heating test (target value). The underestimation of the heat losses is equally noticeable for smaller test cases, with lower energy demand, and the larger ones, with higher demand. This leads to the conclusion that the assumptions presented in Section 8.3. can be improved and further investigation is presented in Section 8.6.

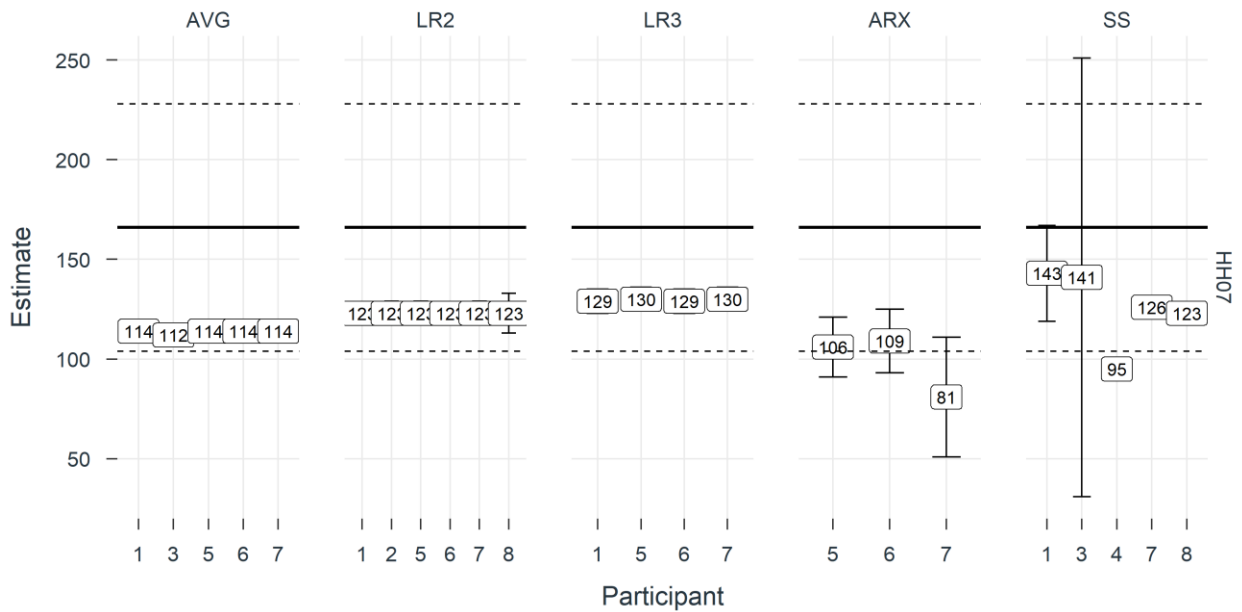


Figure 50. Resulting HTC estimates subdivided per modelling method and compared to the reference value for the test case HH07 of the SMETER project.

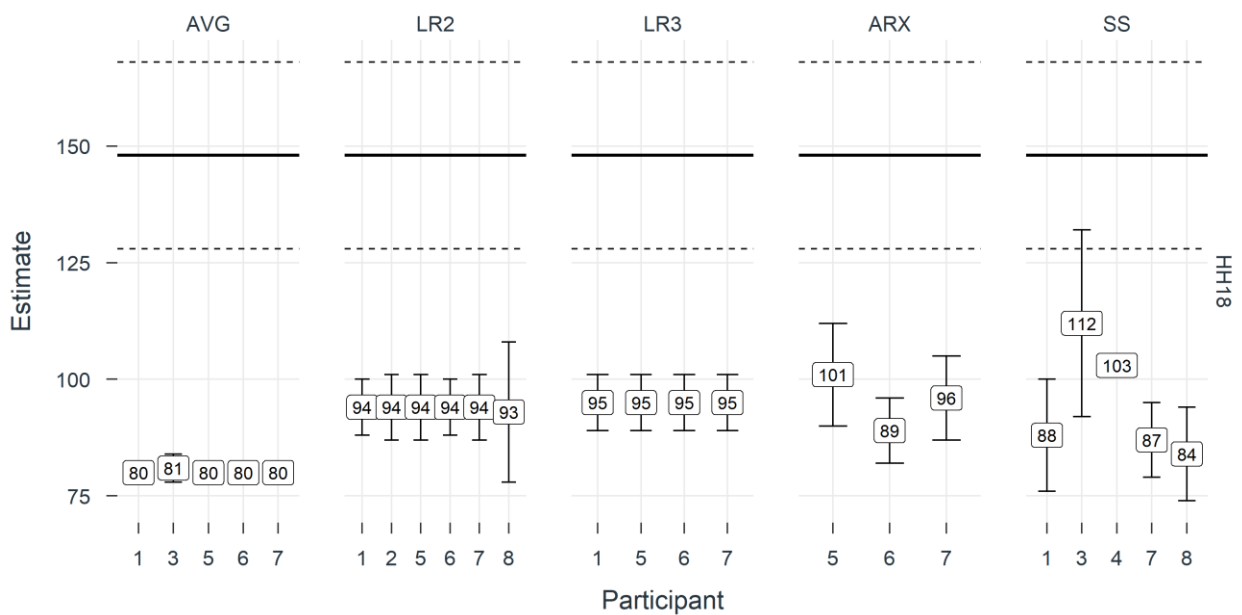


Figure 51. Resulting HTC estimates subdivided per modelling method and compared to the reference value for the test case HH18 of the SMETER project.

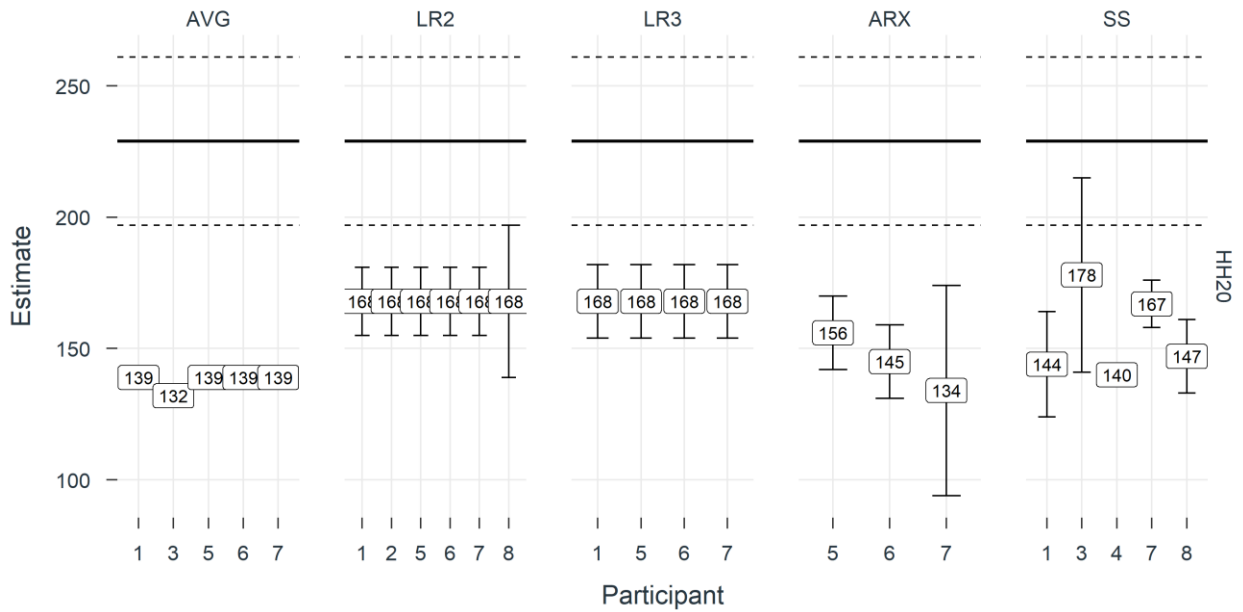


Figure 52. Resulting HTC estimates subdivided per modelling method, and compared to the reference value for the test case HH20 of the SMETER project.

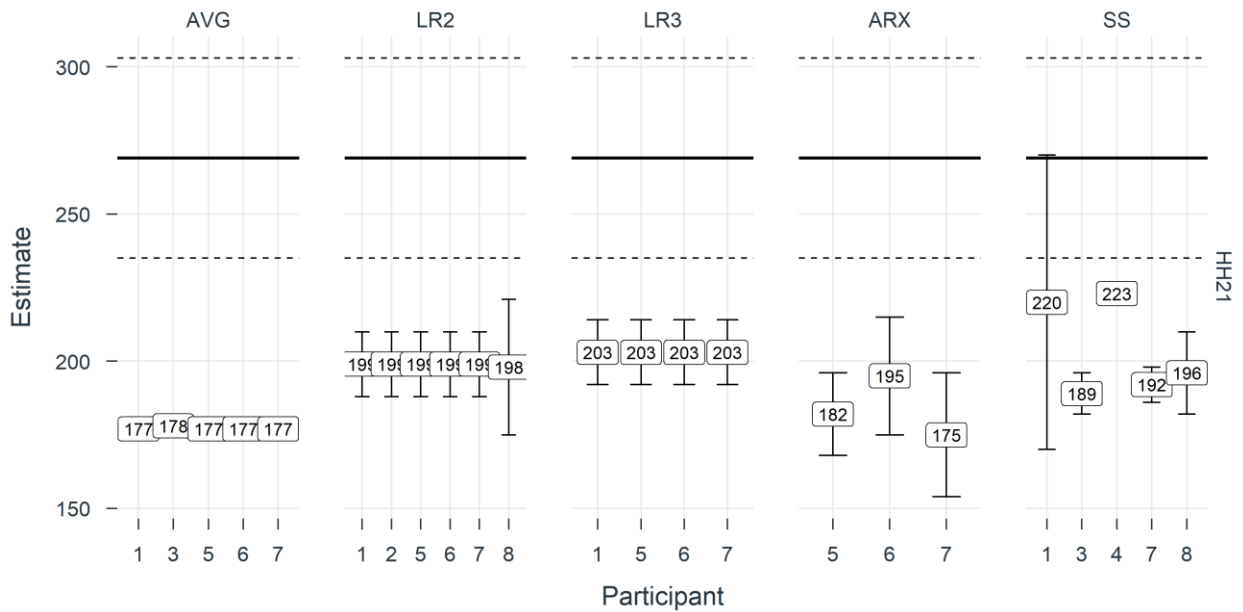


Figure 53. Resulting HTC estimates subdivided per modelling method and compared to the reference value for the test case HH21 of the SMETER project.

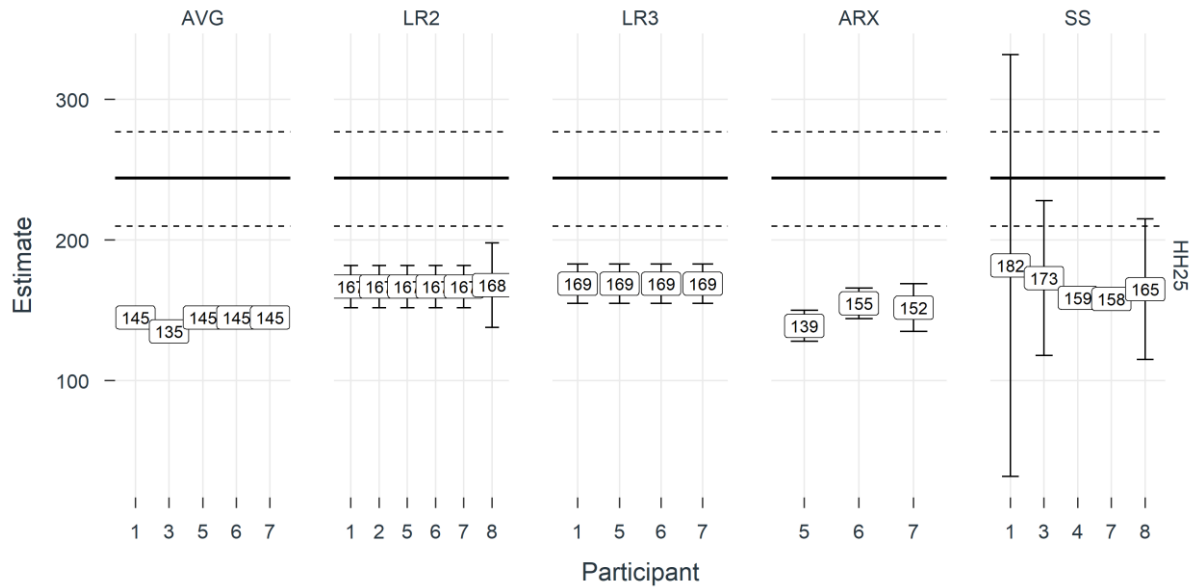


Figure 54. Resulting HTC estimates subdivided per modelling method and compared to the reference value for the test case HH25 of the SMETER project.

For the presented test cases static (AVG, LR2 and LR3) and dynamic (ARX, and SS) modelling techniques were used in HTC and gA assessment. Given the available datasets and information, LR1 could not be performed because it requires the gA value computed beforehand, thus only methods which can estimate the gA alone were used. The estimated gA values are presented in Figure 55, however, there are no references available for comparison

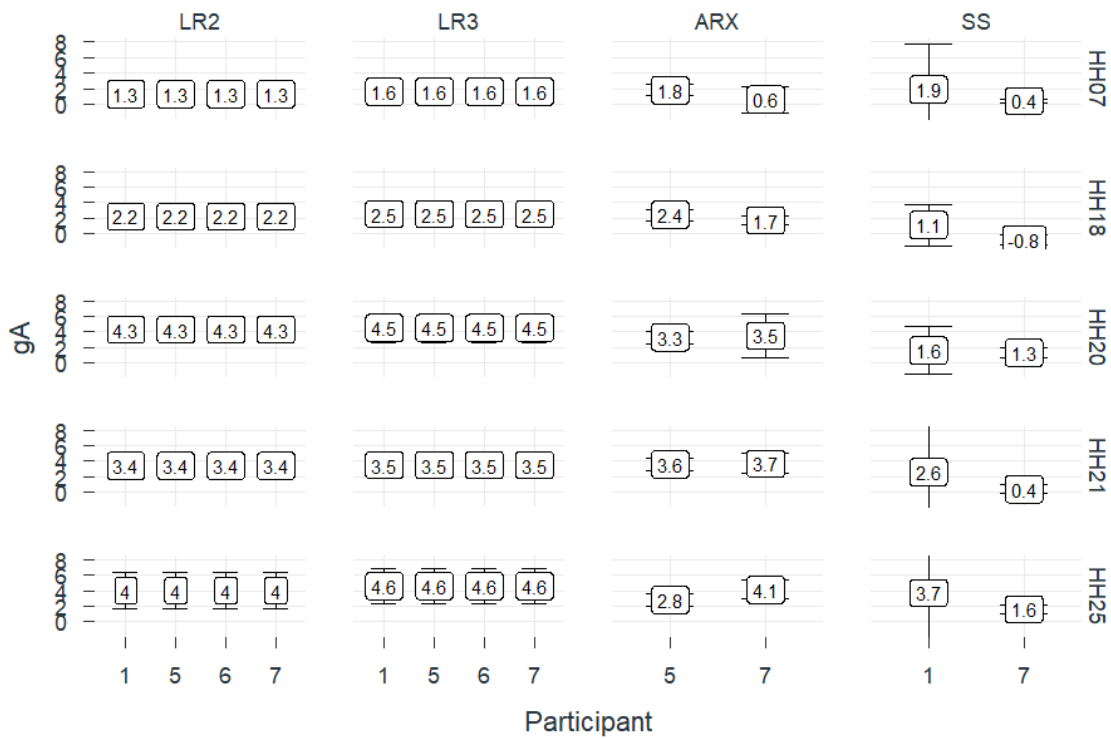


Figure 55. Resulting gA estimates subdivided per modelling method and test case of the SMETER project.

Same as in the HTC estimation, all participants got consistent results when performing LR2 and LR3 modelling. On the other hand, for dynamic modelling, the results vary between participants and there are not enough results to identify a relation between results obtained with different modelling techniques. The impact of the solar gains, thus the calculation of the gA value, is questionable for all cases because the assessment was carried out using global solar irradiation on a vertical plane facing south while the orientation of the houses is unknown. Despite the fact that the solar radiation in winter months comes predominantly from the south, solar gains from other orientations could not be properly taken into account.

## 8.5. Investigation of the assumptions

After noticing significant deviation in estimated HTCs between participants, in total five assumptions were additionally investigated: the impact of the choice of the period, the impact of the assumption adopted for the appliance gains, the impact of the selected DHW splitting method, the impact of the choice of the indoor temperature average and the Impact of weather data availability on HTC estimation. These effects were explored by four different participants and now presented more in detail.

### 8.5.1. Impact of the choice of period

The main aim of this investigation was to observe if, for different periods and lengths, the estimate would converge to different values. To investigate the effect of the period length and starting point on the HTC estimate an algorithm for period selection was created. The algorithm starts at the length of two days and continues up to the length of the whole 60 days dataset, along with the duration the starting point of the dataset is also changed. Here, the HTC is estimated based on a moving time window, by means of three static modelling methods (AVG, LR2, LR3). For each subset of the dataset, a new HTC estimate and its standard deviation are calculated. In Figure 56 to Figure 58 each marker represents one estimate.

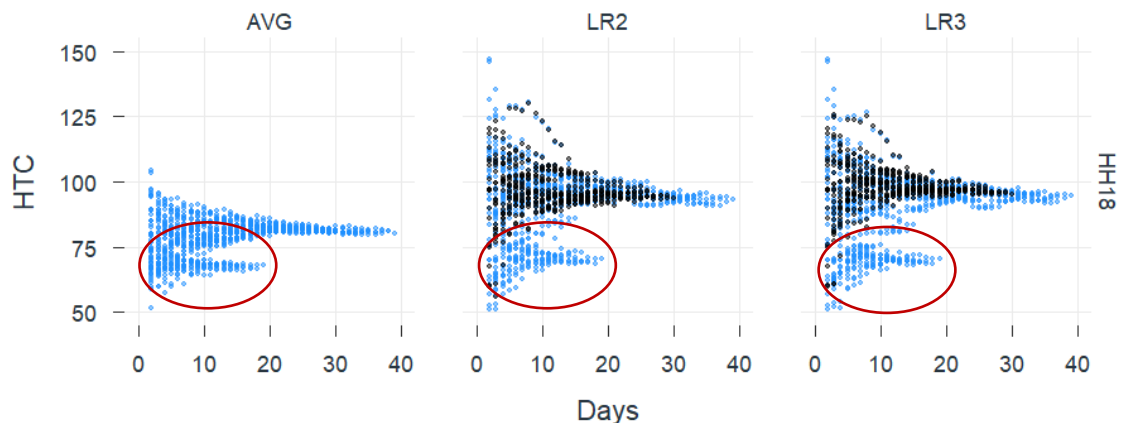


Figure 56. Impact of the period length and starting point on the HTC estimate for the example of the test case HH18.

Estimates shown in blue colour are obtained when the whole 60 days (January to March) dataset was observed, while the black ones are obtained when only 30 days (February) from the dataset are taken into account. It is important to note that for this test case there was a failure in data collection on day 20 of the long dataset and the data is not continuous, thus broken into two parts. This gives the opportunity to single out the cloud of estimates related to the first 19 days, marked in red. It is possible to conclude that the difference in the period selection, even if the datasets are only a month apart, can significantly influence the assessment and lead to a different result. Moreover, looking at the longest available period, it is arguable what is the minimum required dataset length to get a stable estimate. For the work conducted in this chapter, the minimum of 30 days, shown in black, was chosen.

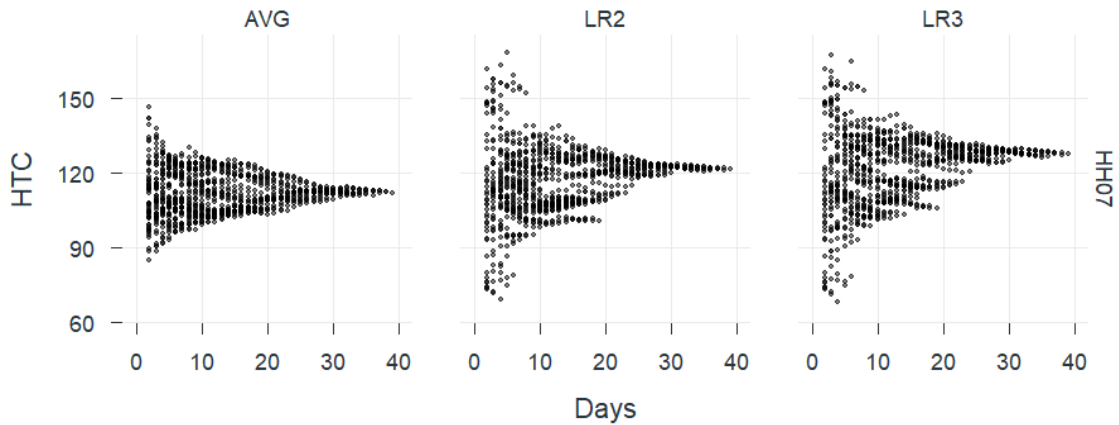


Figure 57. Impact of the period length and starting point on the HTC estimate for the example of the test case HH07.

However, the impact of the period selection is not significant in all explored test cases. Estimates obtained for test cases HH18 and HH20 present a higher sensitivity on the period choice, while for cases HH07, HH21 and HH25 the impact is not noticeable, Figure 57.

In Figure 58, the corresponding standard deviation is shown for the estimates presented in Figure 56. Here, no significant difference can be attributed to the different starting point of the observed period. Also, it can be noticed that the standard deviation stabilizes after the length of 25 days.

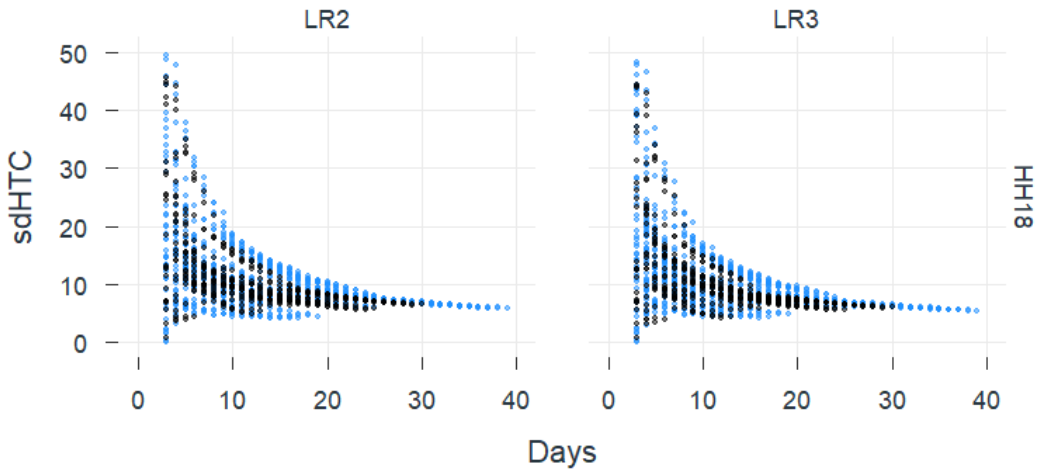


Figure 58. Impact of the period length and starting point on the standard deviation of estimate for the example of the test case HH18.

Given the complexity of the automatization of the period choice for the dynamic methods, only a comparison between the estimation using state-space models for 15, 30 and 60 days is presented. Based on limited tests, as shown in Figure 59, some preliminary conclusions can be drawn: 1) For the five real cases, it is not easy to converge to parameter estimates with physically reasonable values and a model that passes the statistical validation (e.g. parameter significance and white-noise residuals). The complexity of the datasets results in multiple 'optimal solutions', where one 'solution' refers to a set of values for parameter estimations. The grey-box model fitting outcome was found to be sensitive to the initial and boundary values. 2) In general, a longer period of the dataset leads to a better estimation (i.e. smaller standard error) and an easier model fitting. It is noticeable that for all cases when moving towards a longer dataset the 95CIs are narrowed and the stable HTC-determination is kept. However, for some cases, there was no significant difference between 30 and 60 days confidence bounds. The only exception is the case HH21 which had a valid estimation for all three lengths. 3) Model validation, such as the assumption of white-noise residuals and statistical significance, is very important for the HTC-determination, especially the statistical significance for thermal resistances.

Generally, if one parameter (e.g. thermal resistance) is not statistically significant in the grey-box model, it leads to unstable estimation for this parameter and relatively large standard error value.

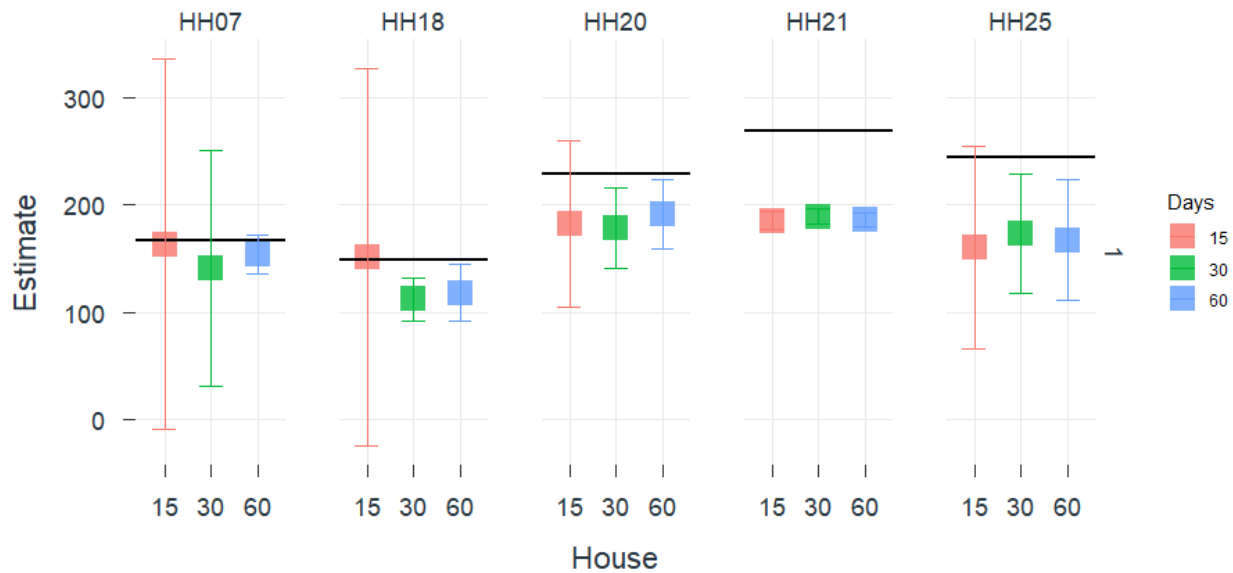


Figure 59. Impact of the period length on the HTC estimation for the SMETER test cases when SS modelling is performed.

### 8.5.2. Impact of electrical appliances gains

It is known that part of the energy consumed by appliances is dissipated in the internal environment of a building as heat gains, which mainly contributes to the raising of the indoor temperature. However, it is difficult to estimate which percentage of this energy is being released to the indoor volume as it depends on the appliances type and efficiency. To test how sensitive the HTC estimate is to the assumption made on the appliances gains the HTC was calculated considering that either 100%, 50% or 0% of the appliances consumed energy is converted to heat. This way it is possible to assess the maximum error this term can introduce. Multiple linear regression, LR2, was used in this study, and the resulting estimates are shown in Figure 60.

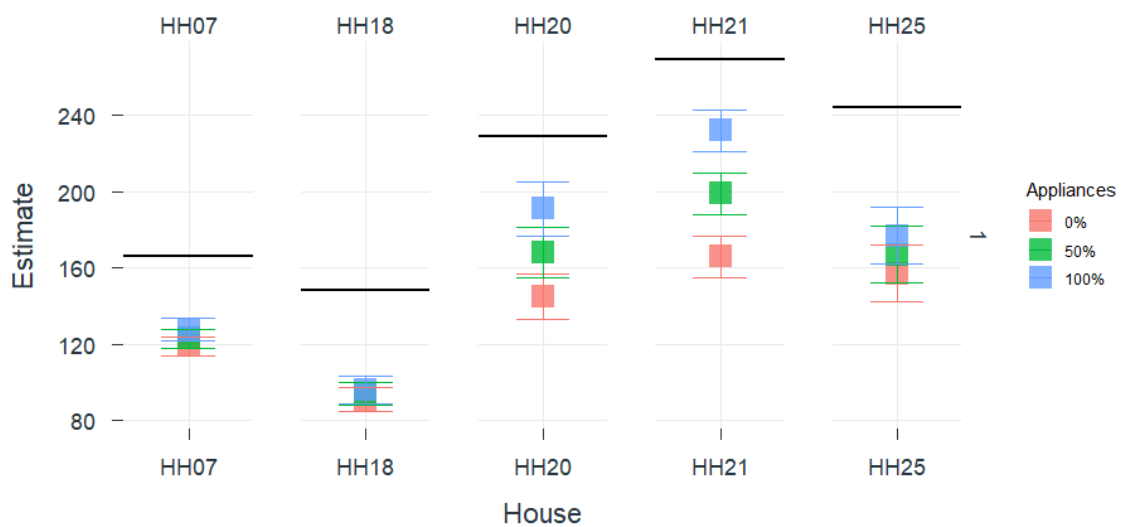


Figure 60. Impact of electrical appliances gains on SMETER test cases

The results show that there exists a significant difference between the HTC estimates in houses HH20, HH21 and HH25, which can be around 30% in the worst cases. On the other hand, houses HH07 and HH18 presented a smaller difference, which was below 10%. A higher dispersion between the HTC estimates is noticed in houses having more occupants since the electrical consumption in respect to the gas demand was higher. This is confirmed by Figure 61, which plots the relative deviation of the HTC-estimates when assuming 50% or 100% electrical gains compared to 0% gains as a function of the electricity use over total energy use. As can be expected, if the share of electricity use in the total energy use is higher, the deviation (and hence the uncertainty on HTC-estimate) is higher. This brief study points out that the assumption we make on the appliances gains can have a big impact on the HTC estimate. Evaluating the share in electricity use for appliances in the total energy use can help to estimate the uncertainty.

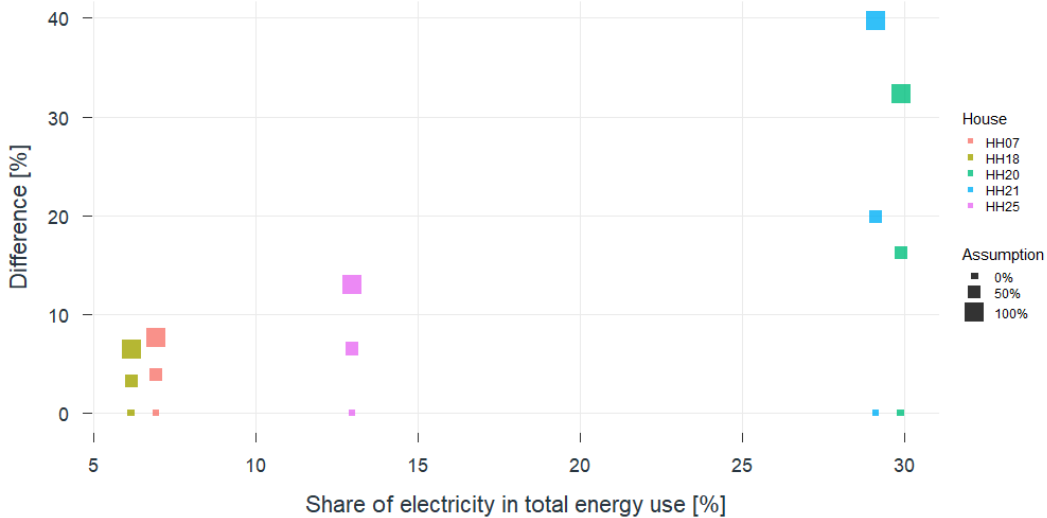


Figure 61. Difference in the HTC estimates from the estimates when no appliance gains are considered, shown as function of the share of electricity consumption in overall energy usage.

### 8.5.3. Impact of DHW splitting

All five houses have combi boilers without storage tanks which means they provide both DHW and space heating on demand. The heat delivered to the indoor space is not measured, only gross measurements of gas consumption ( $m^3$ ) at 30-minute intervals were available. In order to separate between DHW heating spikes and space heating, decoupling was done according to the non-parametric kernel smoothing method by Bacher et al. [2016]. This approach is extended to detect periods when occupants are not using domestic hot water, reallocating the spike in gas consumption from DHW to space heating. During the daytime, measurements of absolute humidity from living spaces, kitchen and bathroom were used to identify time steps where the absolute humidity above outdoor air decreased in all rooms. At these time-steps and night (from 01:00 to 05:00), it is assumed that all heat production is attributed to space heating. Other possible conditional statements that consider additional measurements like room temperature increase or the number of occupants per household were not tested.

Figure 62 compares the extended allocation based on assumptions of presence to the base kernel smoothing method and an alternative where no attempts are made to separate between DHW and space heating. Shown in red are the estimates calculated using the kernel smoothing decoupling method to split DHW from gas meter consumption, while for estimates in green the additional conditions were applied. Presented in blue are the estimates calculated without decoupling of DHW and space heating (all gas consumption is space heating).

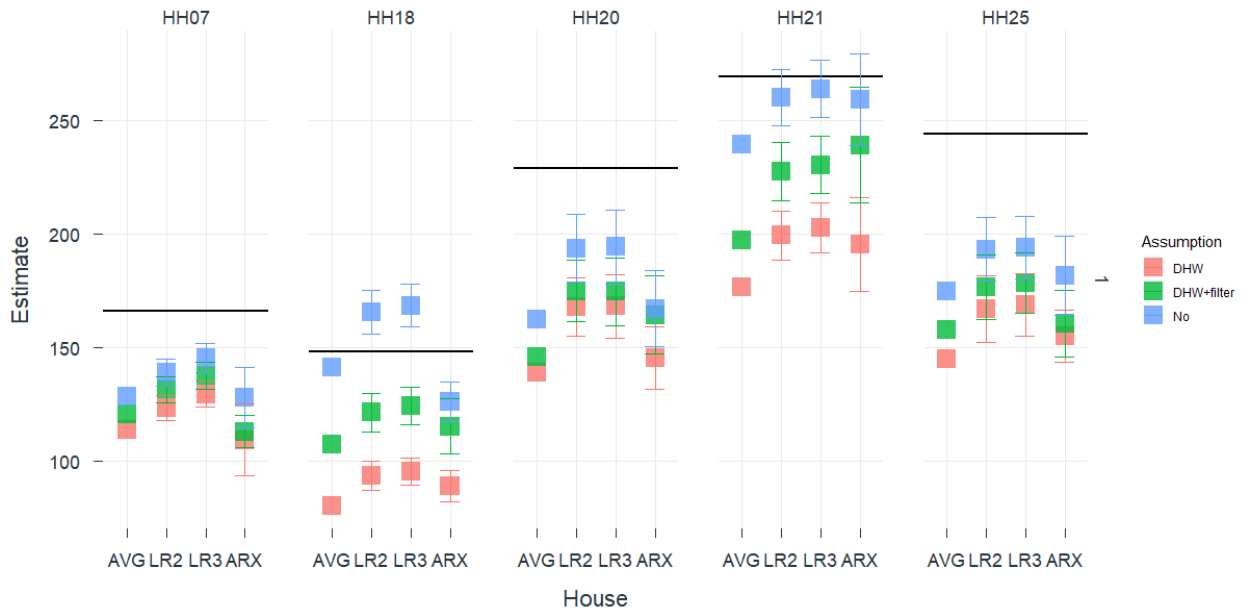


Figure 62. Impact of the different assumptions applied in DHW and SH splitting for SMETER test cases.

It is expected that not attempting to decouple DHW use from gas leads to overestimations of HTC. Splitting may lead to either underestimation or overestimation of the HTC. The smallest influence on HTC is seen in household 7, which is known to be a one-person household. The largest difference can be seen in household 21 with six occupants, followed by HH20 and HH25 (3 and 5 person households). Household 18, known to have one occupant, more unexpectedly show the largest relative difference between HTC estimates. These results indicate the importance of knowing details about the heat generator installed in the building and information about the DHW production. Data availability at a higher resolution (30-minute) than what was used in the HTC estimations (24-hour sampling for non-dynamic methods and 3-hour for ARX) makes it possible to investigate different decoupling methods.

#### 8.5.4. Impact of temperature averaging

Section 6.6. showed that the assumption regarding the indoor temperature can have a significant effect on the resulting HTC estimate. Here, the impact of three assumptions is compared. First, it is assumed that only the living zone temperature is known. Next, an average between the living zone temperature and the temperature of one bedroom is calculated. Finally, an average between the temperatures of all the zones is considered. For the second and third assumption, the indoor temperatures are averaged according to the floor areas.

The implementation of the second approach requires choosing one bedroom for the calculation of the average indoor temperature. For the dwellings HH07, HH18, HH21 and HH25, the master bedroom (which is often the only bedroom) is chosen. For HH20, the master bedroom temperature was not available, so the front bedroom is chosen. The chosen rooms are marked blue in Figure 47.

The indoor temperature profiles of the living zone and bedroom are found to be close to each other when located on the same (ground) floor, while those temperature profiles are more distant from each other when the bedroom is located on the first floor (Figure 63).

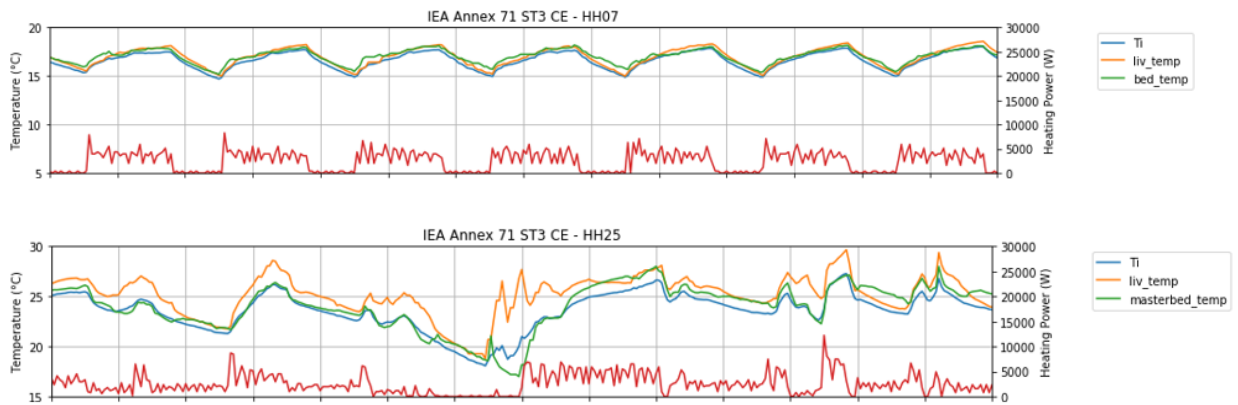


Figure 63. Indoor temperature profiles of the living zone (orange), of the bedroom (green) and average indoor temperature profile including all the zones (blue) for the case HH07, where the bedroom is and living zone are on the same floor, and the case HH25 where the bedroom is on the first floor and the living zone is on the ground floor.

Since the temperature of the living zone is typically higher than the temperature of the other rooms, the average indoor temperature decreases as soon as more zones are involved. Hence, also the indoor-outdoor temperature difference decreases, resulting in a higher HTC. The results are presented in Figure 64. The difference in the calculated HTC depending on using an average temperature measurement across all the sensors or just the reading from one is up to 11 %. Similar results were found in the analysis of the SMETER Project. [R. Jack et al, 2021] reported differences of up to 15% in the calculated HTC between an averaged temperature across all sensors or just the reading from one.

Only dwelling HH07 show a different pattern because the temperature of the bedroom in this house is slightly higher than in the living zone. For all other cases, the bedroom temperatures are lower than in the living spaces. It can be noticed for all cases that, with including all rooms in the averaging, thus improving the assumed indoor temperature, the estimates are closer to the references.

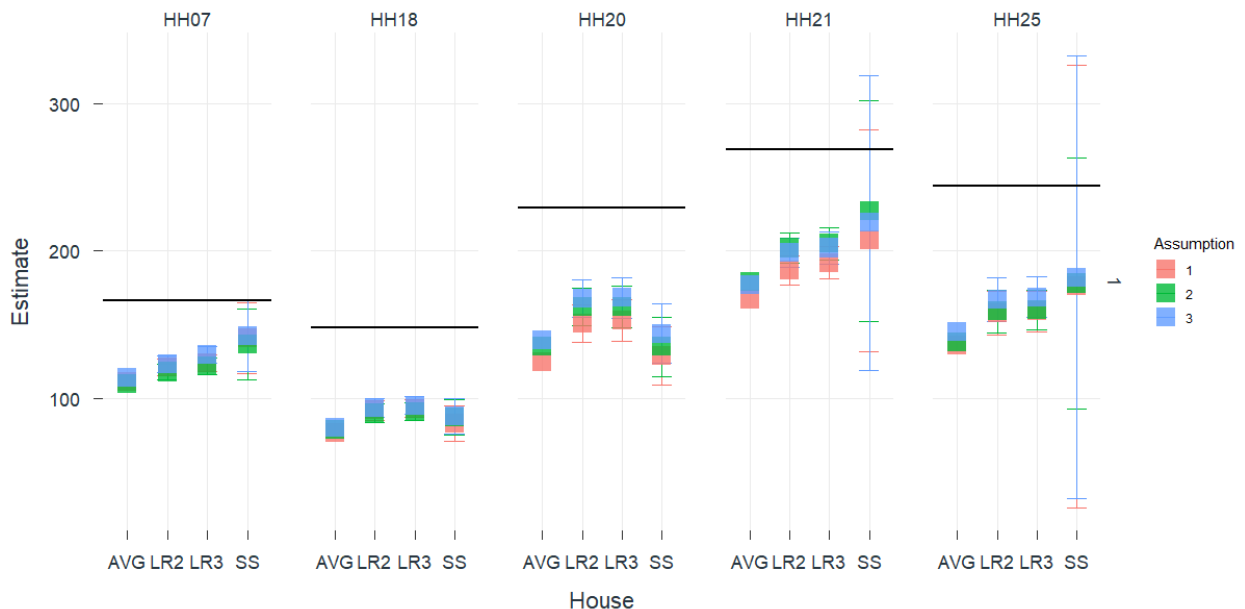


Figure 64. Impact of the different assumptions applied on indoor temperature averaging for SMETER test cases.

### 8.5.5. Impact of weather data availability on HTC estimation

The weather station was within approximately 6 km of all homes, measuring all the main weather variables, including outdoor air temperature and vertical global solar irradiance facing south. Data were collected at 10-minute intervals and pre-processed to match the dwellings' measurements (30 min). Not knowing the exact location of the dwellings, the weather station's location was used to compare HTC estimates to a situation where local measurements are not available.

We followed a similar procedure to the case study buildings in Chapter 7 and downloaded ERA5 reanalysis data via Copernicus Climate Store and CAMS solar radiation time-series via Copernicus Atmosphere Data Store. The outdoor temperature from ERA5 was interpolated from 30 km gridded hourly values to the location of the weather station and in time from hourly instantaneous values into 30-min averages over the past half hour. The Copernicus CAMS Solar Radiation Service provided estimates of global, direct and diffuse radiation based on 15-minute satellite images combined with radiation modelling. The acquired time series was processed to calculate direct unshaded vertical irradiance for the south-facing façade (using the R-package solarCalcISO52010). It was assumed that only diffuse irradiance hits the building facades when the solar elevation angle is below 9°. This assumption was made to account for shading of direct irradiance from nearby obstacles without knowing the exact situation around the buildings. Finally, the 15-minute averages of vertical irradiance were converted to 30-minute averages to match the local measurements.

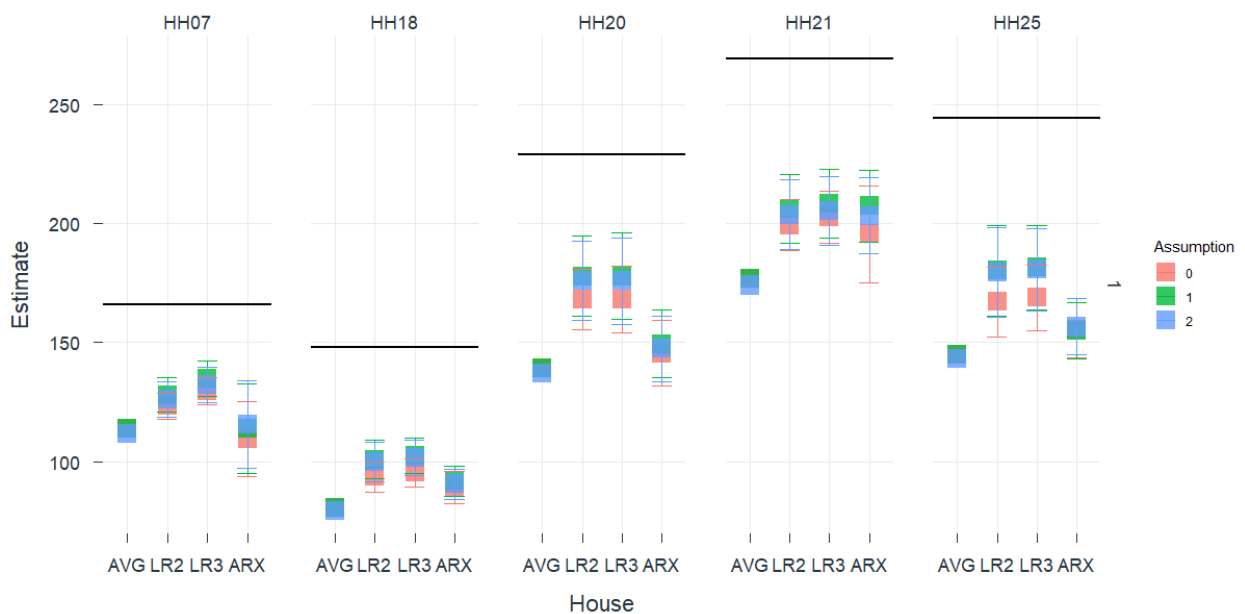


Figure 65. Impact of the different weather data on the HTC estimation for SMETER test cases. Assumption 0 (red) corresponds to measured air temperature and vertical irradiance sourced < 6 km from the building site, assumption 1 (green) same, but with calculated vertical irradiance from satellite irradiance product, and assumption 2 (blue) to vertical irradiance from satellite and outdoor air temperature from reanalysis.

Figure 65 shows the impact on HTC estimates when substituting weather observations with other datasets. Shown in red are the estimates calculated using measured air temperature and vertical irradiance sourced < 6 km from the building site. Estimates when the irradiance is swapped with calculated vertical irradiance from satellite irradiance product, are shown in green, while estimates calculated with the vertical irradiance from satellite and outdoor air temperature from reanalysis are shown in blue.

The results indicate that compared to solar irradiance measurements taken close to the site (< 6 km), data from remote-sensing satellite irradiance products may provide a viable alternative. Using the calculated vertical irradiance seemed to provide better results than using the global horizontal irradiance from the satellite product directly (not shown). This result is in line with previous literature, indicating that estimating solar gains from global horizontal measurements may overestimate HTC in co-heating experiments [Stamp et al. 2017]. According to this study, the best results are obtained vertical south-facing or weighting each façade irradiance by their respective glazing proportions, depending on the orientation of the dwellings and local shading effects. Since we do not know the exact orientation of the dwellings, it is impossible to verify the results. However, we found that HTC estimates were closer to the results obtained with

measured irradiance from the weather station when assuming that direct (and circumsolar) irradiance is blocked at lower sun elevation angles ( $< 9^\circ$ ).

By replacing both irradiance and outdoor temperature with model data, results display the significance of outdoor temperature on HTC estimates. The influence on HTC of not having measurements of air temperature from a nearby station is greater than for solar irradiance, but this may be due to the relatively coarse spatial resolution of the reanalysis used. New regional surface reanalysis products are expected to take better advantage of Europe's observation stations density, and observations closer to the site than 30 km could easily be acquired through the MIDAS Open public datasets [Met Office, 2019]. Another reason for the differences is that the reanalysis does not always fully capture the lows found in the measured outdoor temperatures [Skeie et al., 2021]. On the other hand, local measurements are sometimes under the influence of solar irradiance, which can mask diurnal differences. For the selected 30 day period, the mean bias difference ( $-0.20^\circ\text{C}$ ) between the reanalysis and local weather station is low. The root mean square error ( $0.68^\circ\text{C}$ ) and mean absolute difference ( $0.53^\circ\text{C}$ ) is also better than for the other cases investigated in Chapter 6. Consequently, the result from the averaging approach is almost unchanged. The other methods used to estimate HTC above may indicate more difference in the dynamic approaches, which utilizes a shorter time step, but overall the differences are small.

## 8.6. Conclusions

In this Chapter, a blind test was performed on five real dwellings for which only smart meter readings were available. Based on the guidelines developed in Chapter 7, basic assumptions were made to perform the analysis. In the next step, the impact of these assumptions was investigated. For all houses, a significant underestimation of the HTC was observed compared to the reference value. The static methods showed to be very consistent when comparing the results of different participants, while larger variations were found for the dynamic methods. This can be attributed to the freedom in the dynamic methods, such as choice of data frequency, model selection procedure, etc. When exploring the impact of the assumptions on the HTC-estimates, the time and duration of the measurement period, the occupants and appliance gains and the splitting of DHW and SH were found to be the most important parameters influencing the outcome.



## 9. Conclusion

This document reported the work performed within Subtask 3 'Physical Parameter Identification' of the IEA EBC Annex 71 project. In this subtask, we investigated methodologies to identify the thermal performance of the fabric of residential buildings that are in use, and for which we have only limited monitoring data available. We started with deducing the full heat balance equation of a building to highlight the assumptions that are made in simplified models to determine the building's Heat Transfer Coefficient (HTC). We then, step by step, analysed the impact of different approaches to determine the input parameters to solve the heat balance equation with simple statistical tools. Both static (averaging and single and multiple linear regression) and dynamic (ARX and state space modelling) methods were investigated. This explorative study was performed on five case studies, and for each input parameters (solar gains, the net heat input, infiltration and ventilation heat losses, occupant and appliance heat gains, weather data and indoor temperature) the impact of a modelling approach on the HTC-estimates was evaluated. Based on this information, the optimal approach was determined for each case study building and applied to determine the HTC as precise as possible. Since for all case study buildings, reference values were available, we could compare the different modelling outcomes with the target values. The results of the different static and dynamic statistical methods showed to be rather consistent, but deviated often significantly (20% or more) from the target value. This analysis allowed us to deduce general guidelines on how to deal with the different input parameters for specific cases.

In a final step, a blind exercise was performed on five inhabited dwellings in the UK for which indoor temperature measurements and smart meter readings were available. Based on the guidelines, an optimal approach was selected and applied to all five dwellings. Different participants participated in this blind test. It was found that the outcomes of the static methods were very consistent, while for the dynamic methods, which allow more freedom to the user, larger deviations were observed between the HTC's as estimated by the different participants. Hence, the static methods can be considered more robust in application, but overall both static and dynamic measurements resulted in similar estimates, which for some of the buildings were in close agreement with the target values (co-heating test results), while for other buildings deviations up to almost 50% were found. Analysis of the impact of the assumptions on the predicted outcomes revealed that assumptions on almost all parameters (measurement time and period, internal heat gains, temperature averaging,...) significantly impact the outcome.

Overall, it can be concluded that the statistical tools investigated in this work show promise to determine the building's HTC based on limited on-site monitored data. Care has to be taken, however, on the assumptions made with regard to the input parameters in the heat balance equation. A further in-depth analysis on more case studies is advisable to turn the methods into reliable tools to be used in actual performance assessment. In doing so, specific attention should go to an in-depth analysis of the uncertainty and repeatability before moving to large scale applications.



## 10. References

- Allinson D, Crawley J, Elwell C, Farmer D, Fylan F, Glew D, Gorse C, Hardy A, Hollick F, Johnston, D, Lomas K, Loveday DL, Miles-Shenton D, Parker J, Reeve L, Roberts BM, Roberts G, Thomas F and Wingfield J. (2021). Technical Evaluation of SMETER Technologies Project Phase 2 Data: Temperature, Relative Humidity, Dwelling Information, and Local Weather, 2019-2020. [Data Collection]. Colchester, Essex: UK Data Service. 10.5255/UKDA-SN-854701
- ASTM STP 885, Bales, E., Bomberg, M., Courville, G.E., (eds.); Philadelphia: American Society for Testing and Materials, 1985, pp. 203-219.
- Babar B, Graversen R, Boström T. Solar radiation estimation at high latitudes: Assessment of the CMSAF databases, ASR and ERA5. *Sol Energy* 2019;182:397–411. <https://doi.org/https://doi.org/10.1016/j.solener.2019.02.058>.
- Bacher, Peder & Saint-Aubain, Philip & Christiansen, Lasse & Madsen, Henrik. (2016). Non-parametric method for separating domestic hot water heating spikes and space heating. *Energy and Buildings*. 130. 107-112. 10.1016/j.enbuild.2016.08.037.
- Batterman, S. (2017). Review and extension of CO<sub>2</sub>-based methods to determine ventilation rates with application to school classrooms. *International Journal of Environmental Research and Public Health*, 14(2), 1–22. <https://doi.org/10.3390/ijerph14020145>
- Beizaee A, Allinson D, Lomas K, Foda E, Loveday D, 2015. Measuring the potential of zonal space heating controls to reduce energy use in UK homes: The case of un-furbished 1930s dwellings. *Energy and Buildings* 92: 29-44. Available online at <https://doi.org/10.1016/j.enbuild.2015.01.040>
- Beizaee A, 2016. Measuring and modelling the energy demand reduction potential of using zonal space heating control in a UK home. PhD thesis, Loughborough University. Available online at [https://repository.lboro.ac.uk/articles/thesis/Measuring\\_and\\_modelling\\_the\\_energy\\_demand\\_reduction\\_potential\\_of\\_using\\_zonal\\_space\\_heating\\_control\\_in\\_a\\_UK\\_home/9455939](https://repository.lboro.ac.uk/articles/thesis/Measuring_and_modelling_the_energy_demand_reduction_potential_of_using_zonal_space_heating_control_in_a_UK_home/9455939)
- Belgisch Staatsblad (Belgian Official Journal): Bijlage 5 bij het energiebesluit: Bepalingsmethode EPW: Bepalingsmethode van het peil van primair energieverbruik van residentiële eenheden., (2019). [https://energiesparen.login.kanooh.be/sites/default/files/atoms/files/Bijlage EPW 20181130 vergunningenNA2019.pdf](https://energiesparen.login.kanooh.be/sites/default/files/atoms/files/Bijlage_EPW_20181130_vergunningenNA2019.pdf) (accessed June 9, 2019).
- Copernicus Climate Change Service (C3S) (2017): ERA5: Fifth generation of ECMWF atmospheric reanalyses of the global climate . Copernicus Climate Change Service Climate Data Store (CDS), (Accessed: 17.11.2020) <https://cds.climate.copernicus.eu/cdsapp#!/home>
- Crawley D. B., Lawrie L., 2019, Should We Be Using Just 'Typical' Weather Data in Building Performance Simulation?, *Building Simulation Conference 2019* DOI: [10.26868/25222708.2019.210594](https://doi.org/10.26868/25222708.2019.210594)
- Deltour J, Assessing the building envelope performance during occupancy, E3S Web Conf. 172 22004 (2020)
- DWD (2020) Deutscher Wetterdienst <https://www.dwd.de/EN/ourservices/opendata/opendata.html>
- Hayati A, Mattsson M, Sandberg M. Evaluation of the Ibl and aim-2 air infiltration models on large single zones: Three historical churches. *Building and Environment* 2014;81:365–79. <https://doi.org/https://doi.org/10.1016/j.buildenv.2014.07.013>
- Hersbach, H, Bell, B, Berrisford, P, et al. The ERA5 global reanalysis. *Q J R Meteorol Soc.* 2020; 146: 1999– 2049. <https://doi.org/10.1002/qj.3803>
- Hurel N, Sherman MH, Walker IS. Sub-additivity in combining infiltration with mechanical ventilation for single zone buildings. *Building and Environment* 2016; 98:89–97. <https://doi.org/https://doi.org/10.1016/j.buildenv.2015.12.020>.
- Hurel N. Impact of air infiltration on buildings' performance : Focus on the experimental study within timber-frame walls. PhD Thesis. Université Grenoble Alpes, 2016.
- ISO 8996 (2004). ISO 8996: Ergonomics of the thermal environment - Determination of metabolic rate.

- ISO 9869 (2014) Thermal insulation - Building elements - In-situ measurement of thermal resistance and thermal transmittance
- ISO 17772-1 (2017) Energy performance of buildings - Indoor environmental quality - Part 1: Indoor environmental input parameters for the design and assessment of energy performance of buildings.
- Janssens A. (2016) IEA EBC Annex 58 Reliable building energy performance characterisation based on full scale dynamic measurements. Report of Subtask 1b: Overview of methods to analyse dynamic data.
- Jimenez MJ, Heras MR. (2005). Application of multi-output ARX models for estimation of the u and g values of building components in outdoor testing. *Solar Energy*, 79(3):302–310
- Jiménez MJ, Madsen H. Models for describing the thermal characteristics of building components. *Build Environ* 2008;43:152–62
- Kersken M, Strachan P. (2021) IEA EBC Annex 71 Building energy performance assessment based on in-situ measurements. Design, description and results of the validation of building energy performance simulation programs.
- Kiel DE, Wilson DJ. Influence of natural infiltration on total building ventilation dominated by strong fan exhaust. *ASHRAE Transactions* 1987;93.
- Lambie E. Evaluation of the impact of energy renovation measures: Experimental study of residential buildings. PhD thesis KU Leuven, 2021.
- Lundström L, Akander J, Zambrano J. Development of a space heating model suitable for the automated model generation of existing multifamily buildings—a case study in nordic climate. *Energies* 2019;12:485.
- Lundström, L. CamSrad: Client for CAMS Radiation Service, version 0.3. 0; R package; R Core Team: Vienna, Austria, 2016.
- Lundström, L. Total Solar Irradiance According to ISO 52010-1:2017; GitHub: San Francisco, CA, USA, 2018; Available online: <https://github.com/lukas-rokka/solarCalcISO52010/> (accessed on 16 July 2019).
- Madsen, H. 2008. Time Series Analysis, Chapman and Hall.
- Madsen H., Holst J. 1995. Estimation of continuous-time models for the heat dynamics of buildings. *Energy and Buildings*, 22, pp. 67-79.
- Madsen H, Bacher P, Bauwens G, Deconinck AH, Reynders G, Roels S, Himpe E, Lethé G. (2016). IEA EBC Annex 58 Reliable building energy performance characterisation based on full scale dynamic measurements. Report of Subtask 3, part 2: Thermal performance characterisation using time series data – statistical guidelines. KU Leuven, Belgium
- Met Office (2019): Met Office MIDAS Open: UK Land Surface Stations Data (1853-current). Centre for Environmental Data Analysis, date of citation. (Accessed: 17.11.2020) <http://catalogue.ceda.ac.uk/uuid/dbd451271eb04662beade68da43546e1>
- Modera M.P., Sherman M.H., Sounderegger R.C. Determining the U-Value of a Wall from Field Measurements of Heat Flux and Surface Temperatures. In *Building Applications of Heat Flux Transducers*
- Muñoz Sabater, J., (2019): ERA5-Land hourly data from 1981 to present. Copernicus Climate Change Service (C3S) Climate Data Store (CDS). (Accessed: 17.11.2020), <https://doi.org/10.24381/cds.e2161bac>
- NCEI (2003) Integrated Surface Database (ISD), Asheville, North Carolina: National Centers for Environmental Information, U. S. Department of Commerce. <https://www.ncdc.noaa.gov/isd>
- Norlén U. (1994). Determining the Thermal Resistance from In-Situ Measurements. In: *Workshop on Application of System Identification in Energy Savings in Buildings* (Edited by Bloem, J.J.), 402-429. Published by the Commission of The European Communities DG XIII, Luxembourg.
- Persily, A., & de Jonge, L. (2017). Carbon dioxide generation rates for building occupants. *Indoor Air*, 27(5), 868–879. <https://doi.org/10.1111/ina.12383>
- Rasmussen C, Frölke L, Bacher P, Madsen H, Rode C. Semi-parametric modelling of sun position dependent solar gain using B-splines in grey-box models. *Solar Energy* 2020 (195)249-258. <https://doi.org/10.1016/J.SOLENER.2019.11.023>

- Richard Jack, Luke Smith, Richard England, Adam Low, "SmartHTC Validation Report: Data collection and analysis", Version 5.1, January 2021. [www.buildtestsolutions.com](http://www.buildtestsolutions.com)
- RMI (2020). Royal Meteorological Institute of Belgium (2020). Open data. URL: <https://opendata.meteo.be/> (accessed: 10-2020).
- Senave M, Roels S, Verbeke S, Saelens D. Analysis of the influence of the definition of the interior dwelling temperature on the characterisation of the heat loss coefficient via on-board monitoring. *Energy and Buildings* 215, 109860. <https://doi.org/10.1016/j.enbuild.2020.109860>
- Sherman M, Grimsrud D. Measurement of infiltration using fan pressurization and weather data. NASA STI/Recon Technical Report N 1980;81.
- Skeie, K.; Gustavsen, A. Utilising Open Geospatial Data to Refine Weather Variables for Building Energy Performance Evaluation—Incident Solar Radiation and Wind-Driven Infiltration Modelling. *Energies* 2021, 14.
- Sodagar, B., & Starkey, D. (2016). The monitored performance of four social houses certified to the Code for Sustainable Homes Level 5. *Energy and Buildings*, 110, 245–256. <https://doi.org/10.1016/j.enbuild.2015.11.016>
- Stamp, S.; Altamirano-Medina, H.; Lowe, R. Measuring and accounting for solar gains in steady state whole building heat loss measurements. *Energy Build.* 2017, 153, 168–178.
- Tirfe A., Zhang J.. A novel approach to near-real time monitoring of ventilation rate and indoor air quality in residential houses. In: 2018, pp. 841–6. <https://doi.org/10.14305/ibpc.2018.ie-4.01>.
- Wang W., Beausoleil-Morrison I., Reardon J. Evaluation of the alberta air infiltration model using measurements and inter-model comparisons. *Building and Environment* 2009;44:309–18. <https://doi.org/https://doi.org/10.1016/j.buildenv.2008.03.005>
- Zhang X., Rasmussen C., Saelens D., Roels S. Dynamic solar aperture estimation: comparing data-driven and numerical approaches. Submitted to *Renewable & Sustainable Energy Reviews* (2021).



# 11. Annex: Common Exercises

- IEA EBC Annex 71: Building energy performance assessment based on in-situ measurements. First common exercise – instruction document. August 2017.
- IEA EBC Annex 71: Building energy performance assessment based on in-situ measurements. Common exercise 1bis – instruction document. January 2018.
- IEA EBC Annex 71: Building energy performance assessment based on in-situ measurements. Common exercise 2 Twins test case – instruction document. November 2019
- IEA EBC Annex 71: Building energy performance assessment based on in-situ measurements. Common exercise 3 Blind test on BEIS data – instruction document. February 2021



